A Finite Element Model of a Human Head and a Corresponding Acoustic Test Fixture to Assess the Objective Occlusion Effect Induced by Earplugs under Bone-Conducted Stimulation

by

Huiyang XU

THESIS PRESENTED TO ÉCOLE DE TECHNOLOGIE SUPÉRIEURE IN PARTIAL FULFILLMENT FOR THE DEGREE OF DOCTOR OF PHILOSOPHY
Ph.D.

MONTREAL, DECEMBER 21, 2022

ÉCOLE DE TECHNOLOGIE SUPÉRIEURE
UNIVERSITÉ DU QUÉBEC

BOARD OF EXAMINERS

THIS THESIS HAS BEEN EVALUATED

BY THE FOLLOWING BOARD OF EXAMINERS

Mr. Jacques de Guise, Thesis Supervisor
Department of System Engineering, École de Technologie Supérieure

Mr. Franck Sgard, Thesis Co-Supervisor
Research Division, Institut de recherche Robert-Sauvé en santé et en sécurité du travail

Mr. Éric Wagnac, Thesis Co-Supervisor
Department of Mechanical Engineering, École de Technologie Supérieure

Ms. Marlène Sanjosé, Chair, Board of Examiners
Department of Mechanical Engineering, École de Technologie Supérieure

Mr. Olivier Doutres, Member of the Jury
Department of Mechanical Engineering, École de Technologie Supérieure

Mr. Pascal Hamery, External Examiner
Institut franco-allemand de recherches de Saint-Louis, France

THIS THESIS WAS PRESENTED AND DEFENDED

IN THE PRESENCE OF A BOARD OF EXAMINERS AND THE PUBLIC

ON DECEMBER 15, 2022

AT ÉCOLE DE TECHNOLOGIE SUPÉRIEURE

ACKNOWLEDGEMENTS

First and foremost, this endeavor would not have been possible without my thesis supervisors Jacques de Guise, Franck Sgard and Éric Wagnac. I want to give my deepest appreciation to them for their enthusiasm for the project, for their encouragement and patience. Words cannot express my gratitude to Franck for the unconditional guidance, outstanding feedback, and unlimited support.

I would like to extend my sincere thanks to the Board of Examiners for kindly evaluating this doctoral thesis and giving their expert feedback: Marlène Sanjosé, Olivier Doutres and Pascal Hamery.

I would also like to gratefully acknowledge the financial support from the Natural Sciences and Engineering Research Council of Canada (NSERC) and the Canada Research Chair.

Many thanks to the "participant" of my project for his patience and availability. I would also like to recognize Laurence Marck who took her time to help me with the ethical documents.

I am extremely grateful to Kévin Carillo for his contribution to this project and the valuable discussions we had along the road.

Thanks should also go to Simon Benacchio and Thomas Padois who were always there for help about anything that I was unsure of.

I would always remember my fellow labmates Bastien, Simon, Hugo, Fabien, Maxime, Valentin, Louis, Saber, Alexis for the fun-time we spent together.

I would be remiss in not mentioning my friends in Montreal, Shanshan, Jiajia, Qiqi, Jenny, Bingbing, Shitou, Jiefei and their families for making the past years much more enjoyable and keeping me sane throughout the whole process.

I am deeply indebted to my beloved parents for their unconditional supports from 9,671 km away. I love you as much as you love me.

Finally, I could not have undertaken this journey without my husband Yu Luan. My time with you is full of joy and happiness. To our Chance, to our future.

Modélisation par éléments finis d'une tête humaine et une tête artificielle correspondante pour évaluer l'effect d'occlusion objectif induit par des bouchons d'oreille sous une stimulation par conduction osseuse

Huiyang XU

RÉSUMÉ

L'effet d'occlusion fait référence à la perception accrue des sons transmis par les os (par exemple, les bruits physiologiques comme la propre voix, la respiration, la mastication, le rythme cardiaque) lorsqu'un individu porte des protecteurs auditifs et constitue un inconfort acoustique majeur. Ce phénomène se manifeste principalement en basses fréquences (inférieures à 1.0 kHz) et touche plus particulièrement les protecteurs auditifs de type bouchons d'oreille.

Cette thèse s'intéresse à l'évaluation de l'effet d'occlusion des bouchons d'oreille à l'aide de testeurs virtuel et physique, tous les deux basés sur la même géométrie réelle de la tête d'un participant vivant. Le testeur virtuel consiste en un modèle numérique par éléments finis de la tête tandis que le testeur physique correspond à une tête artificielle réaliste. Le modèle numérique de la tête est évalué en comparant les résultats numériques avec des données expérimentales (i) disponibles dans la littérature qui sont obtenues sur des groupes de participants, (ii) mesurées avec la présente tête artificielle, et (iii) mesurées sur le participant dont la tête a été utilisée pour construire le modèle géométrique de la tête artificielle. La tête artificielle est évaluée en comparant l'effet d'occlusion d'un bouchon d'oreille en mousse mesuré sur celle-ci et sur le participant.

En fait, plusieurs modèles numériques qui étudient l'effet d'occlusion sont disponibles dans la littérature. Cependant, il a été constaté que les conditions aux limites et l'excitation affectent significativement les résultats de simulation obtenus par ces modèles en raison de l'utilisation des oreilles externes tronquées. Au contraire, le modèle numérique de la tête développé ici n'est sensible aux conditions aux limites définies sur les surfaces artificielles crées par la troncation (à la base de la tête dans ce cas) qu'en très basses fréquences. Par conséquent, ce modèle évite d'avoir à recaler les conditions aux limites pour que les résultats de simulation correspondent au mieux aux données expérimentales. De plus, le présent modèle numérique inclus un domaine d'air extérieur qui englobe la tête entière et sur lequel est appliquée une condition aux limites parfaitement absorbante (perfectly matched layer) simulant une condition de champ libre. Cela permet de prendre en compte le rayonnement acoustique des tissus mous de la tête dans le conduit auditif ouvert. Ainsi, le présent modèle simule un effet d'occlusion qui correspond mieux aux données expérimentales en basses fréquences. Troisièmement, le modèle de tête entière permet d'étudier l'influence de la position de la stimulation sur l'effet d'occlusion. La sensibilité de l'effet d'occlusion à la position de la stimulation pour une partie donnée de la tête (par exemple, la mastoïde ipsilatérale) suggère que ce facteur contribue à la variabilité des données expérimentales obtenues sur des groupes de participants dans la littérature. Dans cette étude, le modèle numérique de la tête est également utilisé pour étudier la variabilité de l'effet d'occlusion induite par les propriétés mécaniques des tissus environnants

du conduit auditif (c'est-à-dire les tissus mous, le cartilage et l'os). Il ressort de cette étude que les paramètres de raideur (c'est-à-dire le module de Young et le coefficient de Poisson) des tissus mous et du cartilage ont la plus grande influence sur l'effet d'occlusion. De plus, les champs acoustiques dans les conduits auditifs ouvert et occlus sous une stimulation par conduction osseuse sont explorés à l'aide du modèle de la tête. Les résultats montrent que l'effet d'occlusion calculé au tympan est similaire à celui calculé à la position de la surface médiale du bouchon d'oreille. Cette dernière position est plus sécuritaire et confortable pour les sujets humains impliqués. Finalement, l'évaluation expérimentale de la tête artificielle réaliste montre que l'effet d'occlusion des bouchons d'oreille ne décroît pas avec la fréquence contrairement aux mesures sur le participant, et ce, principalement en raison des propriétés mécaniques des matériaux utilisés pour sa fabrication.

À long terme, après une validation et calibration robuste, la tête artificielle réaliste développée durant ce projet pourrait cependant constituer un outil puissant pour évaluer la performance acoustique des bouchons d'oreille (effet d'occlusion et atténuation sonore).

Mots-clés: effet d'occlusion, modélisation par éléments finis, tête artificielle, bouchon d'oreille

A Finite Element Model of a Human Head and a Corresponding Acoustic Test Fixture to Assess the Objective Occlusion Effect Induced by Earplugs under Bone-Conducted Stimulation

Huiyang XU

ABSTRACT

The occlusion effect refers to the increased perception of bone-conducted sounds (e.g., physiological noises like one's own voice, breathing, chewing, heartbeat) when one wears hearing protection devices, and it constitutes a major acoustic discomfort factor. This phenomenon occurs mainly at low frequencies (below 1.0 kHz) and is particularly pronounced for earplug-type hearing protection devices.

This thesis is interested in assessing the occlusion effect of earplugs using virtual and physical testers both based on the same real head geometry of a living participant. The virtual tester consists of a finite-element head model whereas the physical one corresponds to an augmented acoustic test fixture (i.e., a realistic artificial head). The finite-element head model is evaluated by comparing numerical results with experimental data (i) available in the literature obtained on groups of participants, (ii) obtained on the augmented acoustic test fixture, and (iii) measured on the participant whose head is used for constructing the geometrical head model. The augmented acoustic test fixture is evaluated itself by comparing the occlusion effect of a foam earplug measured on it and on the participant.

In fact, several numerical models for studying the occlusion effect are available in the literature. However, it is found that boundary and loading conditions greatly affect the simulation results of these models due to the consideration of truncated outer ears. On the contrary, the finite-element head model developed in this thesis is found to be only sensitive to the boundary conditions on the artificial boundaries created by the truncation (at the head base in this case) at very low frequencies. It thus avoids choosing boundary conditions so that the corresponding simulation results match the experimental data at the best. Moreover, the finite-element model includes an external air domain surrounding the entire head. A perfectly absorbing condition (i.e., perfectly matched layer) is applied to the boundaries of the air domain, which simulates a free sound field. This allows for taking into account the radiation from the soft tissues of the head into the open earcanal. The present numerical model thus simulates the occlusion effect that better matches experimental data at low frequencies. Thirdly, the finite-element head model allows for investigating the effect on the occlusion effect of the stimulation position. The sensitivity of the occlusion effect to the stimulation position for a given part of the head (e.g., the ipsilateral mastoid) suggests that this factor contributes to the variability of the experimental data obtained on groups of participants in the literature. In this study, the present model is also used to investigate the variability of the occlusion effect induced by the material properties of the earcanal surrounding tissues (i.e., soft tissues, cartilage, and bone). The stiffness parameters (i.e., Young's modulus and Poisson's ratio) of the soft tissues and the cartilage are found to affect the occlusion effect the most compared with the other parameters. Besides, the sound fields

in the open and occluded earcanals under bone-conducted stimulation are explored using the finite-element head model. Results suggest that the occlusion effect measured at the eardrum position is similar to that assessed at the position of the earplug medial surface. The latter position is safer and more comfortable for the human subjects involved. Finally, the experimental evaluation of the augmented acoustic test fixture shows that in contrast to the measurement on the participant, the occlusion effect of earplugs does not decrease with frequency, which is mainly due to the mechanical properties of the materials used for its fabrication.

In the long term, after robust validation and calibration, the augmented acoustic test fixture developed during this project could serve as a powerful tool for evaluating the acoustic performance of earplugs (e.g., occlusion effect and sound attenuation).

Keywords: occlusion effect, finite-element modeling, acoustic test fixture, earplug

TABLE OF CONTENTS

Page

INTRODUCTION 1

CHAPTER 1 LITERATURE REVIEW 5
1.1 Bone-conducted sound transmission and occlusion effect 5
1.2 Brief overview of the human head and ear anatomies 6
1.3 Models of the open and occluded sound pressures in the earcanal 8
1.4 Parameters influencing the occlusion effect induced by earplugs 10
1.5 Experimental assessment of the objective occlusion effect 14
1.6 Summary 19

CHAPTER 2 RESEARCH OBJECTIVES 21

CHAPTER 3 METHODOLOGY 23
3.1 Development of the finite element model of a human head 23
3.1.1 Geometries 23
3.1.1.1 Head including the ear 23
3.1.1.2 Earplug 26
3.1.2 Material properties 27
3.1.2.1 Biological tissues 27
3.1.2.2 Earplugs 28
3.1.2.3 Air-filled earcanal cavity and external air 29
3.1.3 Boundary, coupling and loading conditions 29
3.1.4 Meshing 31
3.1.5 Finite element problem solving 32
3.1.6 Vibratory and acoustic indicators 32
3.1.6.1 Occlusion effect 32
3.1.6.2 Input mechanical impedance 33
3.2 Fabrication of the acoustic test fixture 33
3.3 Evaluations of the finite element head model and the acoustic test fixture 35
3.3.1 Experiments 35
3.3.1.1 Stimulation 35
3.3.1.2 Devices for earcanal sound pressure measurements 37
3.3.1.3 Measurements on the acoustic test fixture 38
3.3.1.4 Measurements on the participant 39
3.3.2 Simulations 40
3.3.2.1 Case of the acoustic test fixture 40
3.3.2.2 Case of the participant 40
3.3.2.3 Calculation of the occlusion effect 40
3.4 Investigations of the factors affecting the simulated occlusion effect of earplugs 40

3.4.1 Boundary condition at the head base 41
3.4.2 Modeling of the external air 41
3.4.3 Material properties of the earcanal surrounding tissues 42
3.4.3.1 Statistical analysis on the tissue material properties 42
3.4.3.2 Study on the effect of soft tissue Poisson's ratio 43
3.4.4 Influence of the position in the earcanal where the occlusion effect is evaluated 44
3.4.5 Stimulation position 44
3.5 Summary 45

CHAPTER 4 RESULTS AND DISCUSSION 47
4.1 Evaluation of the finite element model of the human head 47
4.1.1 Comparison with the experimental data in the literature 47
4.1.1.1 Input mechanical impedance of the skull 48
4.1.1.2 Occlusion effects for different earplug insertion depths 51
4.1.1.3 Occlusion effects for different stimulation positions 53
4.1.1.4 Occlusion effects for different earplug types 54
4.1.2 Comparison with the experimental data obtained on the acoustic test fixture 55
4.1.3 Comparison with the experimental data obtained on the participant 59
4.1.4 Summary 61
4.2 Evaluation of the acoustic test fixture 61
4.3 Factors affecting the simulated occlusion effect of the earplug 65
4.3.1 Boundary condition at the head base 65
4.3.2 Modeling of the external air 66
4.3.3 Material properties of the earcanal surrounding tissues 69
4.3.3.1 Statistical analysis on the tissue material properties 69
4.3.3.2 Study on the effect of the soft tissue Poisson's ratio 71
4.3.4 Influence of the position in the earcanal where the occlusion effect is evaluated 74
4.3.5 Stimulation position 78

CONCLUSION AND RECOMMENDATIONS 83
5.1 Finite element model of the human head 83
5.1.1 Contribution 84
5.1.2 Limitation and perspective 85
5.2 Acoustic test fixture 87
5.2.1 Contribution 88
5.2.2 Limitation and perspective 88

APPENDIX I MATERIAL PROPERTIES OF THE SOFT TISSUES 91

APPENDIX II ACADEMIC ACHIEVEMENTS 93

BIBLIOGRAPHY 95

LIST OF TABLES

Page

Table 3.1 Material properties for the components in the model 28

Table 3.2 Mechanical properties of the materials used in the ATF 35

Table 3.3 Tissue material property sets 43

Table 4.1 Tissue material property sets adopted for simulating the input mechanical impedance 48

Table 4.2 Upper and lower limits of each property regarding the foam earplug adopted in the 2^3 full factorial design of experiment 59

Table 4.3 Material properties of the ATF in comparison with the reference material property set of the participant 63

LIST OF FIGURES

Page

Figure 1.1 Human head and ear anatomy Image courtesy of Adobe Stock 7

Figure 1.2 SPLs measured at the eardrum L_{p_E} (respectively L'_{p_E}) and in the EC L_{p_M} (respectively L'_{p_M}) for the open ear and occluded ear cases 17

Figure 1.3 Experimental setups for the cylindrical artificial ear and parallelepiped-shaped artificial ear Adapted from Brummund (2014, p. 146) and Luan, Cyr-Desroches, Carillo, Doutres & Sgard (2022, p. 3) 18

Figure 3.1 MRI and cone-beam CT images of the participant's head, and 3D views of the scanned region in the open source software platform 3D slicer 24

Figure 3.2 Final reconstructed head with interior structures indicated 25

Figure 3.3 Final reconstructed head with boundary, coupling, and loading conditions 30

Figure 3.4 Augmented ATF fabricated based on the same geometrical model as the FE head model 34

Figure 3.5 Experimental setup for the measurements on the ATF 36

Figure 3.6 Devices for EC sound pressure measurements 38

Figure 3.7 Measurements on the participant 39

Figure 3.8 Head stimulated at three positions on the ipsilateral mastoid part of the ST 45

Figure 3.9 Simulation configurations 46

Figure 4.1 Magnitude (dB, factor 20, ref. 1 Ns/m) and phase of the input mechanical impedance simulated by the head model using different tissue material properties, compared with that simulated by Chang, Kim & Stenfelt (2016) and that measured by Stenfelt & Goode (2005b) 49

Figure 4.2 Simulated OEs of the foam earplug at different insertion depths for the forehead stimulation versus the experimental data of Stenfelt & Reinfeldt (2007) 51

Figure 4.3 Simulated OEs of the mediumly inserted foam earplug for three different stimulation positions versus the corresponding experimental data of Reinfeldt, Stenfelt & Håkansson (2013) 52

Figure 4.4 Simulated OEs of the foam and silicone earplugs at various insertion depths for the ipsilateral mastoid stimulation versus the experimental data of Brummund, Sgard, Petit, Laville & Nélisse (2015) (mean ± S.D.) in four selected third octave bands 55

Figure 4.5 Comparison between the simulated OE and the experimental OE (mean ± S.D.) for the case of the ATF 56

Figure 4.6 Comparison between the simulated OE and the experimental OE (mean ± S.D.) for the case of the participant 60

Figure 4.7 Comparison between the experimental OEs (mean ± S.D.) for the cases of the ATF and the participant 62

Figure 4.8 Ratios between the amplitudes of the volume velocities imposed on the occluded and open EC cavities ($20\log_{10}\left(|\hat{q}^{\mathrm{occl}}/\hat{q}^{\mathrm{open}}|\right)$) computed using the FE head model for the cases of the ATF and the participant 64

Figure 4.9 Simulated OEs of the foam earplug at various insertion depths, for the free and fixed head bases, and three stimulation positions 66

Figure 4.10 Simulated OEs with the fully coupled PML and radiation impedance (rad. imp.) at three different EC entrances (E1 – E3) (versus experimental data in the literature), and the corresponding SPLs at the eardrum surface in the open EC 67

Figure 4.11 Simulated OEs for various tissue material property sets compared with experimental data in the literature. The mediumly inserted foam earplug, ipsilateral mastoid stimulation and free head base are used 69

Figure 4.12 Effects on the OE of the material properties of the EC surrounding tissues in four selected third octave bands 70

Figure 4.13 SPLs in the ECs open and occluded by the mediumly inserted foam earplug for different ST Poisson's ratios 71

Figure 4.14 Volume velocity (dB, factor 20, ref. 1 m^3/s) imposed by the non-occluded part of the EC walls and the earplug medial surface for different ST Poisson's ratios 72

Figure 4.15 OEs of the mediumly inserted foam earplug for different ST Poisson's ratios 73

Figure 4.16 SPLs in the open and occluded ECs computed at the eardrum surface and at the earplug medial surface, respectively 75

Figure 4.17 OEs computed at the eardrum surface versus OEs computed at the earplug medial surface 76

Figure 4.18 SPLs (dB, factor 20, ref. 2×10^{-5} Pa for the colorbar) in the ECs open (a–c) and occluded (d–f) by a shallowly inserted earplug at frequencies of 0.125 kHz, 0.5 kHz and 1.0 kHz, respectively 77

Figure 4.19 SPLs in the open and occluded ECs for the stimulation applied to three different positions of the ipsilateral mastoid. The mean (± S.D.) of the three simulation results are also presented 78

Figure 4.20 Total mechanical energy in the ST and acoustic volume velocity on the EC walls (dB, factor 20, ref. 1 m^3/s) in the open EC case for the stimulation applied to three different positions of the ipsilateral mastoid 79

Figure 4.21 OEs for the stimulation applied to three different positions of the ipsilateral mastoid versus experimental data measured on the participant. The mean (± S.D.) of the three simulation results are also presented 80

LIST OF ABBREVIATIONS

ANSI	American National Standards Institute
ATF	Acoustic (or acoustical) test fixture
CHUM	Centre hospitalier de l'Université de Montréal
CT	Computed tomography
EC	Earcanal
ÉTS	École de technologie supérieure
FE	Finite element
HPD	Hearing protection device
MRI	Magnetic resonance imaging
OE	Occlusion effect
PML	Perfectly matched layer
SD	Standard deviation
SPL	Sound pressure level
ST	Soft tissues
STL	Standard triangle language

LIST OF SYMBOLS AND UNITS OF MEASUREMENTS

dB	decibel
Hz	hertz (with prefix k for kilohertz)
kg	kilogram
m	meter (with prefix m or c for millimeter or centimeter)
min	minute
N	newton
℃	degree Celsius
Pa	pascal (with prefix M for megapascal)
s	second
J	joule

INTRODUCTION

Worldwide, more than 5% of the population suffer from disabling hearing loss (WHO, 2021). Sixteen percent of the disabling hearing losses are caused by occupational noise exposure (Nelson, Nelson, Concha-Barrientos & Fingerhut, 2005). An estimated 11.2 million Canadians have been or are currently exposed to hazardous occupational noise according to the Canadian Health Measures Survey conducted during 2012-2015 (Statistic Canada, 2015). In the province of Quebec, the occupational hearing loss is the second occupational disease in terms of cases compensated by the commission on workplace standards, fairness, health, and safety (Réseau de santé publique en santé au travail, 2022). The commission has accepted more than 109 000 workers having occupational hearing loss between 1997 and 2019. More than 10 000 new cases have been added per year during the years 2018 and 2019 (Réseau de santé publique en santé au travail, 2022).

Hearing protection devices (HPDs), like earmuffs and earplugs, are worn by people exposed to hazardous noise in order to prevent noise induced hearing loss. However, the protection of HPDs is sometimes considered insufficient (Groenewold, Masterson, Themann & Davis, 2014) mainly due to the discomfort of HPDs according to Berger & Voix (2019). In fact, the comfort aspects of HPDs are crucial to ensure their correct and/or consistent uses. Intermittent and improper uses of the HPDs affect greatly the efficiency of HPDs (Arezes & Miguel, 2005; Berger & Voix, 2019). In 2019, Doutres *et al.* proposed a four-dimensional construct of HPD comfort, including the physical, functional, psychological, and acoustical dimensions, and identified the main comfort attributes for each dimension, for example (for the earplug-type HPDs),

- Physical: static mechanical pressure, irritation;
- Functional: unhandy, stability;
- Psychological: acceptability, got used;
- Acoustical: having difficulties in conversations (hearing and speech) and in hearing useful sounds (machinery noise and warning signals).

The acoustical dimension of the (dis)comfort of HPDs is related to two indicators: (i) the sound attenuation, which is a measure of the degree of protection that can be achieved by a HPD, and (ii) the occlusion effect (OE), which refers to the increased perception of the bone-conducted sounds when HPDs are worn and is a phenomenon the most pronounced at frequencies lower than 1.0 kHz.

This thesis focuses on the OE of earplugs. The earplug-type HPDs are chosen since they induce the most prominent OE compared with earmuffs (Berger & Voix, 2019). In fact, the OE of earplugs has been the subject of many studies in the field of hearing protection. Besides a great number of experimental studies carried out on participants (e.g., Berger & Kerivan, 1983; Stenfelt & Reinfeldt, 2007; Lee, 2011; Reinfeldt *et al.*, 2013; Surendran & Stenfelt, 2022), analytical and numerical models (Schroeter & Poesselt, 1986; Stenfelt & Reinfeldt, 2007; Tonndorf, 1966; Hansen, 1998; Zurbrügg, Stirnemannn, Kuster & Lissek, 2014; Brummund, Sgard, Petit & Laville, 2014; Brummund *et al.*, 2015; Carillo, Doutres & Sgard, 2020, 2021a) have also contributed significantly to the understanding of the OE mechanisms. In particular, the use of numerical models makes it possible to overcome several problems of experimental nature, such as (i) practical and ethical issues of direct measurement on living human participants; (ii) complexity of experimental manipulation; and (iii) issues related to the reproducibility and comparability of experiments due to individual differences of test objects. From an experimental point of view, acoustic test fixtures (ATFs) can facilitate measurements by accommodating a large variety of experimental setups, reducing the measurement time, and providing repeatable results (Berger, 1986; Schroeter & Poesselt, 1986). However, current numerical models and ATFs for assessing the OE still suffer from several limitations mainly due to the use of truncated outer ears.

In the continuation of the previous works of the research group (Brummund *et al.*, 2014, 2015; Carillo *et al.*, 2020, 2021a; Cyr-Desroches, 2021), this thesis aims at developing a finite-element

head model and an augmented artificial head for quantifying the objective OE induced by earplugs under bone-conducted stimulation. In the following, a literature review identifying the research problems is presented in Chapter 1. Then, the established research objectives are listed in Chapter 2. Chapter 3 provides the details of the research methodology. The results of this study are shown and discussed in Chapter 4.

CHAPTER 1

LITERATURE REVIEW

This chapter presents a literature review associated with the modeling of the occlusion effect (OE) of earplugs and the design of acoustic test fixtures (ATFs) for assessing the OE.

The OE of earplugs is related to the bone-conducted sound transmitted through the head into the earcanal (EC). Besides the earplug itself and the way it is inserted, the OE is also influenced by the bone-conducted stimulation and the ear anatomy. Section 1.1 provides an overview of the bone-conducted sound transmission and the OE. Section 1.2 briefly introduces the anatomies of human head and ear. Section 1.3 discusses the models of the open and occluded sound pressures in the EC and mainly focuses on those subjected to a bone-conducted stimulation, as this thesis is focused on the OE induced by a bone transducer. Section 1.4 covers the factors related to the earplug, the stimulation, and the ear anatomy influencing the OE. Section 1.5 introduces (i) the experimental assessment of the OE since in this thesis, experimental data are used as a reference to evaluate OE models and (ii) puts light on ATFs as they could be useful for assessing the OE as well as for validating and calibrating a model. Finally, Section 1.6 provides a synthesis of the research problems of this thesis.

1.1 Bone-conducted sound transmission and occlusion effect

Bone-conducted sound sources can be (i) physiological noises, like one's own voice, breathing, chewing, blood circulation, and (ii) a direct or indirect mechanical stimulation of the body, like a bone-transducer applied to the head (direct) or acoustically induced body vibrations (indirect). These sources can contribute to (i) the sound radiated into the EC; (ii) inertial motion of the middle ear ossicles; (iii) inertial motion of the cochlear fluids; (iv) elastic compression of the cochlear walls; and (v) pressure transmission from the cerebrospinal fluid (Stenfelt & Goode, 2005a; Stenfelt, 2011), causing a hearing sensation. Specifically, the bone-conducted sound radiated into the open EC is around 10 dB below other contributors at frequencies below 2 kHz

(Surendran & Stenfelt, 2022) but becomes more noticeable when the EC is occluded (Stenfelt, Wild, Hato & Goode, 2003). This change in hearing sensation between the occluded and open ECs is the OE.

The experienced OE is mostly assessed through questionnaires and interviews (Hansen, 1997; Kiessling, Brenner, Jespersen, Groth & Jensen, 2005; Kuk, Keenan & Lau, 2005; Mueller, 2003; Terroir *et al.*, 2021; Vasil-Dilaj & Cienkowski, 2011). The OE can also be quantified (i) subjectively from the auditory threshold alteration (Stenfelt & Reinfeldt, 2007; Reinfeldt *et al.*, 2013; Saint-Gaudens, Nélisse, Sgard & Doutres, 2022) and (ii) objectively, with the help of miniature microphones, from the EC sound pressure level (SPL) change between the occluded and open EC conditions when a subject is stimulated by bone-conducted sounds (Stenfelt & Reinfeldt, 2007; Reinfeldt *et al.*, 2013; Brummund *et al.*, 2014; Saint-Gaudens *et al.*, 2022; Surendran & Stenfelt, 2022). This thesis focuses on the objective OE.

1.2 Brief overview of the human head and ear anatomies

The human head (see Figure 1.1(a)) consists of the bony skull, which encloses the brain and is surrounded by soft tissues (ST). It rests on the neck with the support of seven cervical vertebrae. The brain includes an outer portion called gray matter and an inner section underneath called white matter. Sixty percent of the brain is fat with the remaining of it composed of water, protein, carbohydrates, and salts. The brain inside the skull is protected mechanically by a clear, colorless body fluid called the cerebrospinal fluid which acts as a shock absorber. The human skull consists of (i) the neurocranium forming the cranial cavity that houses the brain, (ii) the sutures, which are rigid joints between bones of the neurocranium, and (iii) the facial skeleton, formed by the bones supporting the face. Generally, the human skull is considered to contain 22 bones, including the occipital, parietal, frontal, nasal, lacrimal, and vomer which are flat bones and the others. The flat bones have a sandwich structure, composed of two thin layers of compact bone with cancellous bone between them. Surrounding the skull there are the skin and ST including the muscle, tendons, ligaments, fat, fibrous tissue, etc.

The human ears (see Figure 1.1(b)) are located on the sides of the head. The ear includes three parts: the outer ear, the middle ear, and the inner ear. The outer ear comprises the pinna, the EC and ends at the eardrum (also called tympanic membrane). The pinna consists of the helix, the antihelix, and opens into the EC. The EC has a length (along a straight axis) of about 23 mm (Zwislocki & Goodman, 1980; Salvinelli *et al.*, 1991). Its outer part is surrounded by cartilage and its inner part near the eardrum by bone. The objective OE is quantified using sound pressures in the outer ear with and without a hearing protection device. The eardrum connects the outer ear to the middle ear, which sits inside the temporal bone and includes the tympanic cavity and the three ossicles (i.e., malleus, incus, and stapes). The inner ear sits in the bony labyrinth, and contains the semicircular canals, the utricle, the saccule, and the cochlea. The middle and inner ear components are known to have an influence on the subjective and perceptive OEs which involve all the bone-conduction pathways (Huizing, 1960; Stenfelt & Reinfeldt, 2007; Schroeter & Poesselt, 1986).

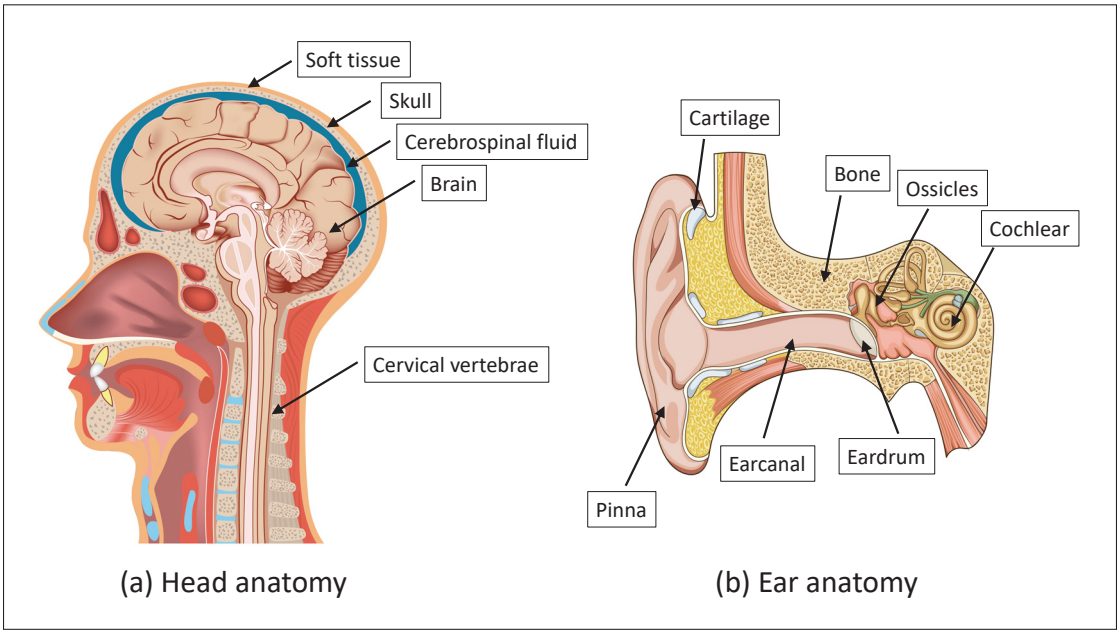

Figure 1.1 Human head and ear anatomy
Image courtesy of Adobe Stock

1.3 Models of the open and occluded sound pressures in the earcanal

The objective OE is quantified by the difference between the SPLs in the occluded and open ECs subjected to the same bone-conducted stimulation. Therefore, the modeling of the objective OE requires the modeling of the sound pressures in both the open and occluded ECs.

Many lumped-element models in the literature were dedicated to investigating the objective OE (Schroeter & Poesselt, 1986; Stenfelt & Reinfeldt, 2007; Tonndorf, 1966; Hansen, 1998; Zurbrügg *et al.*, 2014; Carillo *et al.*, 2020, 2021a). In these models, the open EC entrance is modeled as an acoustic impedance equal to the acoustic radiation impedance of a baffled circular piston of the same surface. The air within the EC cavity is accounted for as acoustic masses, compliances, and resistances. The EC cavity is simplified to stepped cylindrical ducts with cross-sections which are either uniform (Schroeter & Poesselt, 1986; Stenfelt & Reinfeldt, 2007; Tonndorf, 1966; Hansen, 1998; Zurbrügg *et al.*, 2014) or derived from the radii of the curvilinear axis of an anatomically correct EC (Carillo *et al.*, 2020). The spatial distribution of the EC wall vibration is idealized as volume velocity sources, with amplitudes and positions assumed or adjusted based on (i) measured sound pressures in the open and occluded ECs (Schroeter & Poesselt, 1986; Stenfelt & Reinfeldt, 2007; Tonndorf, 1966; Hansen, 1998; Zurbrügg *et al.*, 2014) or (ii) the EC wall normal velocity centroid computed using the finite element (FE) models of an external ear developed for investigating the objective OE (Carillo *et al.*, 2020, 2021a).

Regarding the modeling of the objective OE based on the FE method, there has been an increase of interest in this aspect during the last decade. The FE modeling has the advantage of considering precise geometries, material properties, boundary conditions, and stimulations. The existing FE models for investigating the objective OE, i.e., a 3D model and a 2D axisymmetric model, were firstly developed by Brummund *et al.* (2014; 2015). The 3D geometry of the FE model of Brummund *et al.* (2014) is constructed from cryosectional images of a female cadaver head; while the 2D geometry of the FE model of Brummund *et al.* (2015) is based on the averaged geometrical data of the external ear available in the literature. These models were later improved by Carillo *et al.* (2020; 2021a). More precisely, (i) the air within the EC cavity is

considered as a Navier-Stokes-Fourier compressible fluid instead of a perfect compressible fluid to account for the visco-thermal dissipation for better estimating the acoustic power balance in the open and occluded ECs; (ii) more realistic loading and boundary conditions are chosen to reproduce a "plausible" vibration pattern of the EC walls; (iii) the entrance plane of the EC is set at the EC opening normal to its curvilinear axis instead of a straight axis. However, several limitations still arise regarding these models.

- First and the most important, they only consider a portion of the external ear, which is a truncated part of the entire head. It is thus challenging to choose proper boundary and loading conditions in order to describe the real vibration response of the bone-conducted sound in the EC (Carillo *et al.*, 2020, 2021a). For now, the boundary conditions in these models are chosen so that the corresponding simulation results match the experimental ones at the best. According to Carillo *et al.* (2020), the EC wall vibration distribution is important to the OE, and a more realistic EC vibration pattern could be provided by a FE model of an entire human head.
- Second, their truncated geometries built from cryosectional images and averaged geometrical data do not represent any existing head or ear. As a result, they were validated against experimental data obtained on groups of participants rather than the corresponding head or ear. However, a rigorous method to evaluate the FE model would be to compare the simulation result with the experimental data obtained on the corresponding head or ear, as a model is established to be an accurate representation of the latter, at least to some extent. A possible solution for rigorous validation tests could be to fabricate a corresponding artificial head or ear (see details in Section 1.5).
- Third, similarly as in the aforementioned lumped-element models, the external air domain is accounted for by applying a radiation impedance corresponding to that of a baffled flat circular piston over the open EC entrance. As a result, the sound radiation from the external ST into the open EC is neglected in these models while it could contribute to the SPL computed at the eardrum. One may also wonder how the truncation of the outer ear from the entire head would affect the consideration of the acoustic radiation of the ST into the open EC, and thus the simulated objective OE.

To the author's knowledge, few models in the literature have focused solely on investigating the sound field in the open or occluded EC under bone-conducted stimulation. Taschke & Hudde (2006) developed a 3D FE head model that considers the skull, the ST, and the hearing organ for studying the pressure distribution in the open outer ear when the head is excited by forces applied to the ipsilateral temporal bone. Specifically, it is found that below 1.5 kHz, the bone-conducted sound transmission path from the outer ear, the eardrum, and the middle ear cavities (excluding the ossicles) to the inner ear is dominated by vibrations of the ST of the EC. Details concerning the FE modeling of this system are unavailable and no validation of the model is reported. One main drawback of this model is that it excludes several pathways of the bone-conducted sound due to a lack of structures of a human head in the model.

Besides, it is also worth mentioning that there are several numerical studies based on the FE method simulating and investigating different aspects related to the bone-conducted sound transmission through the human head under bone-conducted stimulation during the last decade (Kim, Chang & Stenfelt, 2014; Chang *et al.*, 2016; Chang, Kim & Stenfelt, 2018; Chang & Stenfelt, 2019; Prodanovic & Stenfelt, 2020; Lim, Dobrev, Röösli, Stenfelt & Kim, 2022; Stenfelt & Prodanovic, 2022). More precisely, Kim *et al.* (2014) developed a FE model of a human dry skull from cryosectional images of a cadaver head. Based on the same images, Chang *et al.* (2016) developed a whole head FE model, called LiU-Head. Using the LiU-Head, Chang *et al.* (2018) found the bone-conducted sound power is transmitted mostly by the skull bone, and secondly by the ST; Chang & Stenfelt (2019) studied the characteristics of different types of bone-conduction devices; Stenfelt & Prodanovic (2022) found that the soft tissue conduction is part of the classical bone-conducted hearing instead of an alternative hearing mechanism. The LiU-Head was also improved to include detailed middle and inner ear structures by Lim *et al.* (2022). However, these studies do not focus on the sound field in the EC.

1.4 Parameters influencing the occlusion effect induced by earplugs

The OE of earplugs observed on different human subjects exhibits a large variability (Stenfelt & Reinfeldt, 2007; Reinfeldt *et al.*, 2013; Brummund *et al.*, 2015; Saint-Gaudens *et al.*, 2022;

Surendran & Stenfelt, 2022). This can be explained by various factors related to the earplug, the stimulation, and the ear anatomy (Watson & Gales, 1943; Schroeter & Poesselt, 1986; Hansen, 1998; Stenfelt *et al.*, 2003; Stenfelt & Reinfeldt, 2007; Lee, 2011; Reinfeldt *et al.*, 2013; Zurbrügg *et al.*, 2014; Brummund *et al.*, 2015; Carillo *et al.*, 2021a; Carillo, Doutres & Sgard, 2021b; Saint-Gaudens *et al.*, 2022).

First, the OE of earplugs depends on the earplug itself (e.g., geometry, material properties, insertion depth, fit) (Watson & Gales, 1943; Schroeter & Poesselt, 1986; Hansen, 1998; Stenfelt & Reinfeldt, 2007; Lee, 2011; Brummund *et al.*, 2015; Sgard, Carillo & Doutres, 2019; Carillo *et al.*, 2021a). Several common observations regarding how the earplug affects the OE can be found in the literature.

- The OE is found to decrease with the insertion depth of the earplug (Mueller, 1994; Staab, 1996; Nielsen & Darkner, 2011; Branda, 2012). Through a model based on the electro-acoustic analogy, Tonndorf (1972) explained this by the reduction of the radiating surface of the EC walls or a gradual immobilization of the tympanic membrane. Berger & Kerivan (1983) gave possible explanations to this observation in their experimental measurements: the stiffer bony tissue might radiate less energy as compared with the ST or a gradual stiffening of the unoccluded EC walls is less likely to be vibrationally excited. Using a 2D FE model of an outer ear in conjunction with an associated lumped-element model, Carillo *et al.* (2021a) explained this observation by the decrease of the EC wall normal vibration through the investigation of the volume velocity imposed by the portion of the EC walls that is not covered by the earplug.
- The OE is found to be influenced by the fit of the earplug. In fact, in the field of hearing aids, the vent (Kuk, 1991; Carle, Laugesen & Nielsen, 2002; Kiessling *et al.*, 2005; Keidser, Carter, Chalupper & Dillon, 2007), which means creating an incomplete seal, is usually used to reduce the OE, although having feedback issues (Chung, 2004; Borges, Costa, Naylor & Ferreira, 2014; Winkler, Latzel & Holube, 2016). The experimental study of Kiessling *et al.* (2005) related this to the acoustic mass of the air column in the vent. The recent study of Carillo *et al.* (2021b) using a 3D FE model of an outer ear in conjunction

with an associated lumped-element model explained this by both the acoustic mass and the acoustic resistance of the incomplete seal, which influence the acoustic impedance seen by the EC walls.

- Acrylic or silicone earplugs are found to induce higher OEs than foam earplugs (Hansen, 1998; Lee, 2011; Brummund *et al.*, 2014, 2015). Through experiments, Hansen (1998) proposed that the higher OE induced by an acrylic earplug compared with a foam earplug is related to the mass of the earplug. Through the acoustic power balance approach using the FE models of the OE, Brummund *et al.* (2014; 2015) found that the medial surface of a silicone earplug injects more acoustic power into the EC cavity than that of a foam earplug. Through a design of experiment performed on the material properties of earplugs using a 2D axisymmetric FE model of an outer ear, Carillo *et al.* (2021a) attributed the higher OE induced by a silicone earplug compared with that of a foam earplug to the higher Poisson's ratio of silicone.

It can be seen that recent studies of Carillo *et al.* (2021a; 2021b) have contributed significantly to better understanding the contribution of the earplug to the OE. However, their studies based on the 3D and 2D FE models of truncated outer ears suffer from the limitations listed in Section 1.3, some of which could be alleviated by a FE model of an entire human head. To the author's knowledge, there seems to be no whole head model for investigating the OE presently.

Second, the OE depends on the stimulation. In real life, the OE is induced by one's own physiological noises. There are studies on the OE induced by one's own voice (Hansen, 1997, 1998; Vasil-Dilaj & Cienkowski, 2011; Sgard *et al.*, 2016), or other physiological noises, like mastication, heart beats, blood flow, swallowing, and footsteps (Hansen, 1997, 1998; Stone, Paul, Axon & Moore, 2014). In laboratory conditions, the bone transducer is the commonly used bone conduction stimulation for measuring the OE (Stenfelt & Reinfeldt, 2007; Reinfeldt *et al.*, 2013; Brummund *et al.*, 2014; Surendran & Stenfelt, 2022). In this case, the bone transducer is usually placed on the ipsilateral mastoid, the contralateral mastoid, or the forehead center of participants. According to (Reinfeldt *et al.*, 2013), the magnitude and repeatability of their measured OEs are influenced by the bone transducer position, which is speculated to affect the excitation on

the ST surrounding the EC. To the author's knowledge, no model has been used to investigate how the stimulation position affects the OE. Since the existing FE models of truncated ears for the OE cannot be used to investigate this, a whole head model is necessary. It is worth mentioning that the FE head model of Chang *et al.* (2016) was used to compare the vibratory responses under bone-conducted stimulations placed at various positions with the corresponding experimental data. However, the authors did not discuss the effect of the stimulation position on the bone-conducted sound transmission or acoustic pressure in the EC. Besides, one may also question how the OE is sensitive to the stimulation positions on a specific zone of the head, for example, the ipsilateral mastoid. This may help quantify the contribution of this factor to the large variability of the experimental results in the literature (Stenfelt & Reinfeldt, 2007; Reinfeldt *et al.*, 2013; Brummund *et al.*, 2015).

Third, the OE depends on the ear anatomy. Stenfelt *et al.* (2003) measured the OEs for the case of a glass cover occluding the EC entrance in (i) intact ECs, (ii) ECs with the cartilage and soft tissue parts removed, and (iii) bony ECs with the eardrum removed. Results show that the OE is the highest for the intact EC, and the SPL in the occluded bony EC is similar to that in the open intact EC. It is found that the vibration of the cartilage and ST in the EC is the main contributor to the sound pressure in the EC under bone conduction stimulation. Then, in 2007, Stenfelt & Reinfeldt developed a lumped-element model of the OE and investigated the sensitivity of the OE to the EC size using the maximum, average, and minimum EC geometrical data presented by Stinson & Lawton (1989). The maximum difference is found between the cases of an earplug deeply inserted into a small EC and an average EC (3 dB at 0.6 kHz). Later, Zurbrügg *et al.* (2014) used a lumped-element model to study the influences of the EC diameter and length on the OE. The EC diameter is found to have an effect on the OE at frequencies higher than 0.5 kHz. Both Stenfelt & Reinfeldt (2007) and Zurbrügg *et al.* (2014) concluded that the EC size has a minor influence on the OE. However, the real human ear anatomy is much more complex: the EC surrounding tissues (i.e., distribution and material properties) vary greatly between individuals. Recently, Carillo *et al.* (2021a) used 2D axisymmetric models to study the effect on the OE of different transitions between cartilaginous and bony tissues

along the EC. Straight transition at the EC half-length as well as slanted and curved transitions determined from the 3D outer ear anatomical model of Brummund *et al.* (2014) are considered. Results have shown that the EC wall vibration distribution depends on the transition between the two tissues, in other words, the ear anatomy. As mentioned in previous paragraphs, the vibration pattern of the EC walls significantly affects the contribution of the earplug to the OE. However, there seems to be no study that could better reproduce the EC wall vibration and thus the OE by considering a realistic ear anatomy (including the surrounding tissues) as well as the entire head. Another aspect of the ear anatomy influencing the OE is the material properties of the biological tissues. Some of them have been reported to vary largely between individuals (Peterson & Dechow, 2003; Grellmann *et al.*, 2006; Auperrin *et al.*, 2014) but there seems to be no study dedicated to assessing the effects of these parameters on the OE. Besides, specifically for the ST, the limited information concerning their material properties found in the literature shows contradictions with each other. More details are provided in Appendix I. However, further investigations on determining the ST material properties are beyond the scope of this thesis. In this thesis, the focus is rather put on studying the influence of the ST Poisson's ratio on the OE using different values adopted in the literature. In fact, the ST are commonly considered to be quasi-incompressible. According to the analytical study of Sarvazyan (1975), the ST Poisson's ratio is close to the theoretical limiting value of incompressible materials, namely 0.5, in the frequency range below 10^3 – 10^4 Hz. However, in the existing FE models of the OE (Brummund *et al.*, 2014, 2015; Carillo *et al.*, 2020, 2021a), the ST Poisson's ratio is assumed to be 0.4. In the FE model of a whole human head of Chang *et al.* (2016) for simulating the bone-conducted sound transmission, the ST Poisson's ratio is set at 0.45.

1.5 Experimental assessment of the objective occlusion effect

The objective OE can be assessed on human subjects in the laboratory (e.g., Stenfelt & Reinfeldt, 2007; Nélisse, Le Cocq, Boutin, Voix & Laville, 2013; Brummund *et al.*, 2015; Saint-Gaudens *et al.*, 2022) or in the field (e.g., Nélisse *et al.*, 2013). As field measurements are beyond the scope of this study, they are not discussed in the thesis. On the other hand, laboratory measurements are

conducted in controlled environments, and thus can provide a high measurement repeatability for better studying a targeted phenomenon. In laboratory conditions, the subject is usually submitted to a bone-conducted stimulation on his/her forehead or mastoid generated by a bone transducer (Stenfelt & Reinfeldt, 2007; Reinfeldt *et al.*, 2013; Brummund *et al.*, 2015; Saint-Gaudens *et al.*, 2022). This can also be realized using one's own voice (e.g., list of words, numbers or using vowels) or by chewing (e.g., different types of food) (Nélisse *et al.*, 2013; Saint-Gaudens *et al.*, 2022). As introduced in Section 1.1, the assessment of the objective OE of earplugs is normally achieved by using miniature microphones to measure the SPLs in a subject's EC open and occluded by an earplug. In practice, the sound pressure in the EC is usually measured at a secure distance from the eardrum surface (Stenfelt & Reinfeldt, 2007; Reinfeldt *et al.*, 2013; Nélisse *et al.*, 2013; Saint-Gaudens *et al.*, 2022) for reasons of comfort and security (Bonnet, 2019). More precisely, Stenfelt & Reinfeldt (2007) placed the probe tube opening of a microphone at a distance of 3 mm from the eardrum; Reinfeldt *et al.* (2013) inserted a microphone probe tube 25 mm into the EC relative to the tip of the tragus; Nélisse *et al.* (2013) positioned a miniature microphone halfway between the entrance and the eardrum in the open ear and a few millimeters from the earplug in the occluded ear; Saint-Gaudens *et al.* (2022) used earpieces equipped with miniature microphones connected to probe tubes 15 mm into the EC relative to the tragus. It can be seen that different experimental studies set up the measurement position in the EC differently. However, in numerical studies (Brummund *et al.*, 2014, 2015; Carillo *et al.*, 2020, 2021a), the objective OE is usually derived from the sound pressures in the open and occluded ECs computed at the eardrum surface. One may wonder how the OE is affected by the position in the EC where it is evaluated (Surendran & Stenfelt, 2022). This question can also be asked differently: when the head is excited under bone-conducted stimulation, if the transfer function that relates the SPL evaluated at a distance from the eardrum in the EC to the SPL at the eardrum equal or not for the open EC case and the case occluded by an earplug. In fact, when the EC is exposed to an external sound field, the following relation can be established for the same evaluation position in the occluded and open ECs (Chan & Geisler, 1990; Gilman & Dirks,

1986; Sgard, Viallet & Nélisse, 2015):

$$TF_{\text{open}} = TF_{\text{occluded}}, \tag{1.1}$$

where

$$TF_{\text{open}} = L_{\text{p}_\text{E}} - L_{\text{p}_\text{M}}, \tag{1.2}$$

and

$$TF_{\text{occluded}} = L'_{\text{p}_\text{E}} - L'_{\text{p}_\text{M}}, \tag{1.3}$$

with L_{p_E} (respectively L'_{p_E}) the SPL at the eardrum and L_{p_M} (respectively L'_{p_M}) the SPL measured in the open EC (respectively the occluded EC) (see Figure 1.2).

It remains to be investigated for the case of a bone-conducted stimulation. For now, to the author's knowledge, the acoustic pressure distribution in the EC under bone-conducted stimulation has only been studied using a FE model of a truncated outer ear (Carillo *et al.*, 2020). These authors found an acoustic pressure gradient close to the EC opening in the open EC while a homogeneous acoustic pressure distribution at low frequencies in the EC with an acoustically rigid occlusion at the entrance.

Instead of direct measurements on human subjects, ATFs can accommodate a large variety of experimental setups, reduce the measurement time, and provide repeatable results (Berger, 1986; Schroeter & Poesselt, 1986). An appropriate ATF could serve as a useful tool for (i) measuring the objective OE of earplugs at exactly the eardrum position and as a precursor to human subject tests, and (ii) validating and calibrating OE prediction models mentioned in Section 1.3.

In the field of hearing protection, commercial ATFs are manikins with built-in heating system, circumaural and interaural skin simulations, pinnae, artificial ECs, instrumented occluded ear simulator inside each EC, etc. (ANSI, 2020). Their geometric dimensions and physical characteristics (e.g., acoustic impedance at the eardrum) are designed to be representative of a real human head (Schroeter & Poesselt, 1986). Their self-insertion losses are supposed to be sufficiently high in order to eliminate the potential contribution of the bone-conducted sound

(Berger, 1986; Berger & Voix, 2019). As mentioned in Section 1.1, the OE is induced by the bone-conducted sound transmission through the human head. As a result, commercial ATFs are commonly used to assess the attenuation of hearing protection devices, but not to assess the OE.

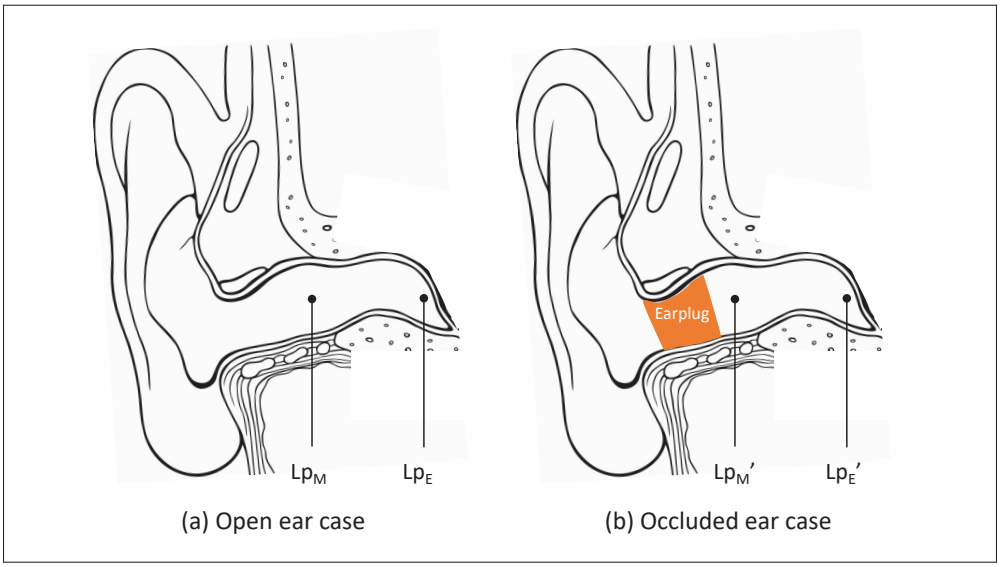

Figure 1.2 SPLs measured at the eardrum L_{p_E} (respectively L'_{p_E}) and in the EC L_{p_M} (respectively L'_{p_M}) for the open ear and occluded ear cases

However, an ATF could incorporate the bone-conducted sound transmission through the head. There are a few custom-made artificial heads incorporating the bone conduction in the literature in the field of hearing protection. Clavier, Wismer, Wilbur, Dietz & O'Brien (2010) designed and fabricated an artificial head from the skull geometry of a living human subject retrieved from computed tomography (CT) data using material with a sound speed similar to the bone. The skull is also filled inside and covered outside by silicone gel. These authors measured (i) the attenuation of a helmet using the artificial head and (ii) the sound propagation around and inside the artificial head equipped with the helmet in order to validate a corresponding computational model. Norris, Chambers, Kattamis, Davis & Bieszczad (2011) fabricated another full artificial head from detailed CT data. Compared with the artificial head of Clavier *et al.*, this one seems to be improved in terms of the ear anatomy, having realistic pinnae, ECs, and variation in the "ST" thickness along the EC length. Norris *et al.* concentrated on the earplug attenuation and design parameters (e.g., girth, insertion depth). Unfortunately, not much information concerning these

two studies is provided since they were conducted under the framework of military research. Besides, the two artificial heads could be but were not used to assess the OE of earplugs.

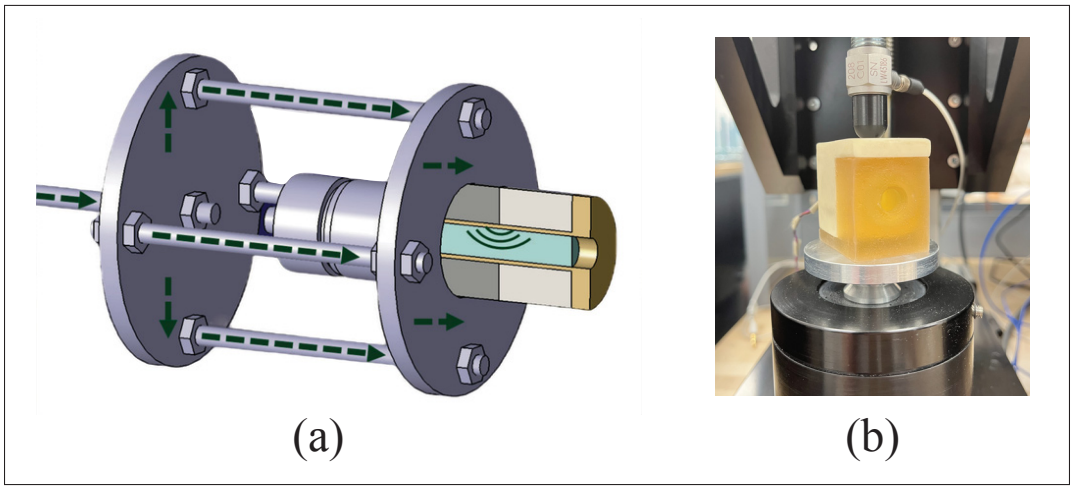

Figure 1.3 Experimental setups for the cylindrical artificial ear and parallelepiped-shaped artificial ear
Adapted from Brummund (2014, p. 146) and Luan *et al.* (2022, p. 3)

To the author's knowledge, Brummund, Sgard, Petit, Laville & Boutin (2013) are the first to design and fabricate an ATF dedicated to evaluating the OE. This ATF consists in a cylindrical artificial human outer ear approximately corresponding to the shape of the simplified axis-symmetric FE model of the OE in (Brummund *et al.*, 2015). The EC is surrounded by bony, soft, and cartilaginous tissues which are made up of rigid polyurethane foam and two different types of silicone rubber (see Figure 1.3(a)). Such an ATF is designed for measuring the tympanic sound pressure with an IEC 60318-4 ear simulator (IEC, 2010), which can mimic an average human eardrum impedance. Brummund *et al.* (2013) concluded that it is feasible to use an ATF built from a simplified outer ear geometry for evaluating the OE. Cyr-Desroches (2021) designed and built another simplified artificial ear for the OE that can facilitate the experimental manipulation in practice with boundary and loading conditions easy to reproduce in the model. The artificial ear is made of materials with sound speeds similar to real human tissues, and has a parallelepiped shape with a cylindrical EC (see Figure 1.3(b)) and proportions of the volumes of the bone, cartilage, and ST surrounding the EC same as the artificial ear proposed

by Benacchio *et al.* (2018). The latter was built based on the ear geometry of a living human subject. It thus has an anatomically correct geometry although still having some simplifications . It also uses materials with sound speeds similar to real human tissues. The artificial ears of Benacchio *et al.* (2018) and Cyr-Desroches (2021) also do not take into account the middle and inner ears. The eardrum is replaced with an acoustically rigid material thus representing an "infinite" impedance. A microphone is inserted at the eardrum position and allows for measuring the sound pressure. These artificial ears both have corresponding FE models which make it possible to compare simulated and measured OEs. They are found to be able to reproduce several common behaviors of the OE, including (i) the decreasing tendency with frequency and (ii) different magnitudes for different earplug types. It can be seen that the existing ATFs dedicated to evaluating the OE consider truncated outer ears of various complexities. It is challenging for them to reproduce accurately the bone-conducted sound transmission through the head, and thus the real vibro-acoustic response of the EC. To the author, there is still a need for an ATF which can account for the bone conduction through the entire head. Like a whole head model, such an ATF could lead to more realistic EC vibration patterns in the EC and would allow for evaluating the OEs for different stimulation positions.

1.6 Summary

The objective OE originates from the bone-conducted sound transmitted through the head into the EC. The large variability of the OE measured on participants has been related to the occlusion device (e.g., earplug), the stimulation, and the ear anatomy.

To investigate the objective OE of earplugs, numerical models, also referred to as virtual testers, based on the FE method considering the outer ear, a truncated part of the head, have been established. These models do not provide a sensitivity analysis on the biological tissue material properties. They could be but were not used to investigate the sound fields in the ECs (open and occluded by an earplug), which would help better justify the choice of the microphone position in the EC for measuring the sound pressures under bone-conducted stimulation. More importantly, the geometries considered in these models make it (i) challenging to choose proper

boundary and loading conditions for obtaining the real vibration response of the bone-conducted sound in the EC, (ii) only possible to be evaluated by experimental data obtained on groups of participants, and (iii) impossible to investigate the OEs for different stimulation positions. Besides, by applying an equivalent acoustic radiation impedance at the EC entrance, these models neglect the possible sound radiation from the external ST into the open EC and require to choose the position of the EC entrance.

Several artificial ears, also referred to as experimental testers, have also been designed and fabricated to estimate the OE of earplugs. Their capabilities for reproducing realistic EC vibration patterns in the EC are also limited due to the consideration of only a part of the outer ear. They also do not allow for placing the bone transducer at different positions.

The present literature review indicates the need to further study the OE by developing improved virtual and experimental testers which would fill some gaps pointed out in the previous studies of the OE.

CHAPTER 2

RESEARCH OBJECTIVES

This research aims at solving several issues in the studies of the occlusion effect (OE) mentioned in Chapter 1. Prospectively, the outcome of this work could provide useful virtual and experimental testers for assessing the objective OE induced by earplugs under bone-conducted stimulation.

Three specific objectives are identified.

- The first is to develop a finite element (FE) model of an entire human head wearing or not the earplug that can simulate the OE, in the continuation of the most recent numerical studies on the OE. The FE model should be based on the real geometry and structure of the head of a living participant in order to be validated and calibrated using the OE measured on the corresponding head.
- The second is to fabricate and evaluate an augmented acoustic test fixture that can be used for assessing the OE and for validating and calibrating the associated FE head model.
- The third is to investigate several factors influencing the OE which remain to be further studied according to the literature, including (i) the acoustic radiation of the external soft tissues into the open earcanal (EC), (ii) the material properties of the EC surrounding tissues, (iii) the position of the microphone in the EC where the OE is evaluated, and (iv) the stimulation positions of the bone transducer using the FE head model. Specifically, the last three factors could help explain the variability of the experimental OEs obtained on a group of participants. It is important to note that the model should make it possible to assess the effects on the OE of the various factors related to the earplug, the stimulation, and the ear anatomy.

CHAPTER 3

METHODOLOGY

This chapter presents the research methodology for realising the three specific objectives identified in Chapter 2. More precisely, a finite element (FE) model of an entire human head wearing or not earplugs is developed from *in-vivo* medical images of a participant's head for simulating the occlusion effect (OE) of earplugs (see Section 3.1). Based on the same geometrical model as the FE head model, an augmented acoustic test fixture (ATF) is fabricated using tissue mimicking materials (section 3.2). Then, as a preliminary step for the purpose of ultimately validating and calibrating the FE head model, experiments are carried out on both the ATF and the participant for evaluating the FE head model as well as the ATF itself (see Section 3.3). Finally, the FE head model is used to investigate several factors that may influence the simulated OEs (see Section 3.4).

3.1 Development of the finite element model of a human head

This section presents the geometries (see Section 3.1.1), material properties (see Section 3.1.2), boundary, coupling and loading conditions (see Section 3.1.3), meshing (see Section 3.1.4), and FE problem solving (see Section 3.1.5) of the developed FE head model. The FE head model is able to quantify not only the OE of earplugs which is an acoustic indicator, but also the input mechanical impedance at the stimulation position which is a vibratory indicator (see Section 3.1.6).

3.1.1 Geometries

3.1.1.1 Head including the ear

The head geometrical data of a mid-aged male participant having normal auditory function were obtained from high resolution magnetic resonance imaging (MRI) and cone-beam computed

tomography (CT) scans. The medical imaging acquisition protocol was approved by Research Ethics Boards of CHUM and ÉTS jointly (CHUM-CE18.064 and ÉTS-H20180205). Three hundred and twenty sagittal MRI images covering the participant's head from its top to base (see Figures 3.1(a) and 3.1(b)) with a 0.63 mm isotropic resolution were obtained with a Siemens 3T Skyra scanner. In addition, the lower part of the skull bone (field of view: 18 cm × 16 cm) was imaged with a Cone-Beam CT NewTom 5G scanner (QR, Verona, Italy). Five hundred and thirty-nine axial images with a 0.3 mm isotropic resolution were acquired (see Figures 3.1(c) and 3.1(d)). Most of the head geometry is reconstructed from the MRI images. The cone-beam CT images help distinguish the structures that are difficult to identify from the MRI images, like the temporal bone, the cervical spine and other bony parts. Compared with the conventional CT scanner using an equivalent protocol, the cone-beam CT imaging technique induces a less effective radiation dose (Nardi *et al.*, 2017), which makes it possible to scan a healthy subject.

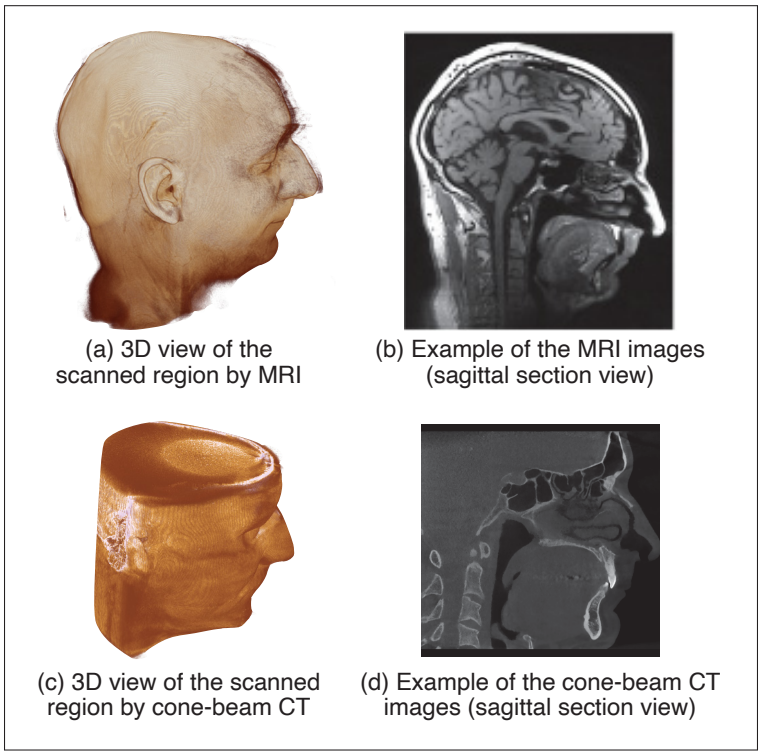

Figure 3.1 MRI and cone-beam CT images of the participant's head, and 3D views of the scanned region in the open source software platform 3D slicer

The types of commercial software Materialise Mimics and 3-Matics (Leuven, Belgium) were used to semi-automatically segment the images and to reconstruct the head in 3D. The reconstructed head comprises the brain, the cerebrospinal fluid, the skull bone, the auricular cartilages and the soft tissues (ST) (see Figure 3.2(a)). The brain part includes the cerebrum, the cerebellum, the brainstem, the spinal cord and the ventricles. The bony part includes the various bones of the skull (e.g., the temporal, parietal, frontal bones), the teeth and the upper cervical spine (C1 – C3). As the cortical and the spongy bones could not be differentiated completely from the images, the bony part is rather considered as a homogeneous equivalent solid domain. The cerebrospinal fluid fills the region between the brain and the bone. The skin, the fat, the muscle, the eyeballs and the nasal cartilage are all considered as ST. The entire head structure involves no air-filled spaces except the external earcanal (EC) cavities (left and right): the air cavities other than the ECs are filled either with ST (e.g., oral and nasal cavities) or with bone (e.g., temporal bone inner cavities). Geometry adaptations are applied based on *a priori* knowledge (Bicak, 2012; Chang *et al.*, 2016) since some structures and details could not be precisely differentiated mainly due to their low contrast and to the artifacts in the images.

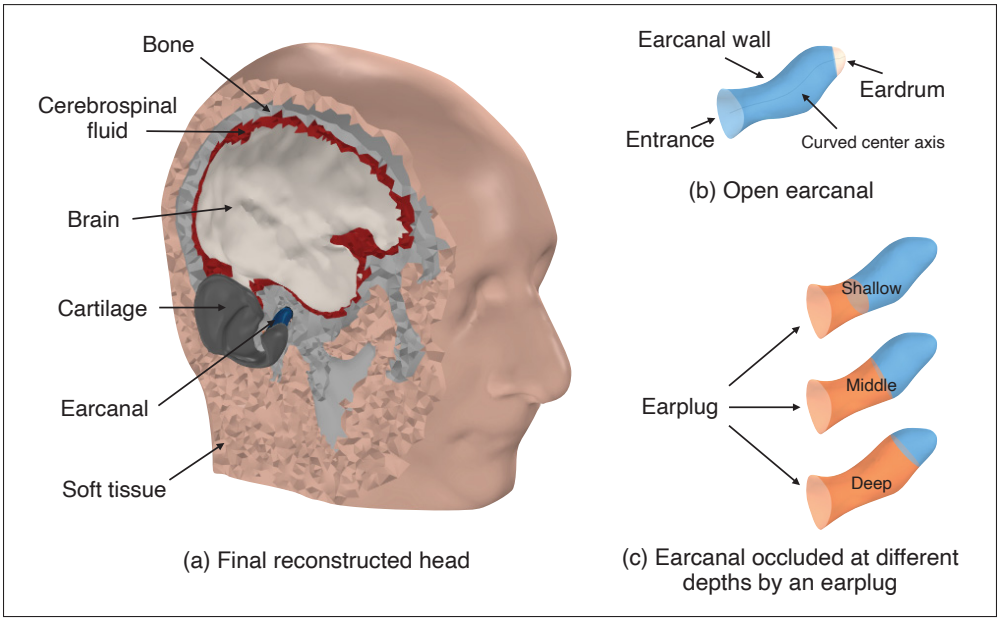

Figure 3.2 Final reconstructed head with interior structures indicated

The external ECs are reconstructed from the medical images. The EC curvilinear axes are estimated using an iterative method inspired by Stinson & Lawton (1989). The entrance plane of each EC is set at the EC opening normal to its curvilinear axis. The ECs are closed by the bony tissue at the location of the eardrum. Due to the image resolution, the position of the eardrum can only be approximately determined. Human ear anatomy (Standring, 2015) is considered to reconstruct the curved surface at the eardrum position. The middle and inner ears are not modeled also due to the image resolution. Since the present study only focuses on the objective OE, these structures which contribute to the subjective OE are deemed to be less important. They are filled with the bony tissue during the segmentation process. The middle ear cavity is then recreated using a small quasi-semi-spherical void. The right ear is believed to be more precisely reconstructed since there are less image artifacts for this ear than for the left one. Besides, the transcranial transmission is beyond the scope of the present study, thus all the computations are carried out at the right ear (see Figure 3.2(b)). The right EC has a volume of 1294.6 mm^3 and a curvilinear length of 27.7 mm. Its entrance area is about 62.3 mm^2. The eardrum area is about 43.5 mm^2.

The reconstructed anatomical structures including the ear are imported as STL (Standard Triangle Language) files from Materialise 3-Matics (Leuven, Belgium) into COMSOL Multiphysics® v.5.5 (COMSOL AB, Stockholm, Sweden) to create the final CAD geometry of the open ear case (see Figure 3.2(a)).

3.1.1.2 Earplug

The geometry of the occluded ear is created from the open ear by occluding the EC using an earplug. The circumferential boundary of the earplug is supposed to fit perfectly the shape of the EC walls. There is no deformation of the EC walls induced by the earplug and the seal between them is complete. Two types of earplugs are examined in this work, namely foam and silicone. In order to investigate how the earplug material affects the OE for a given insertion depth while controlling for its geometry, these two earplug types have an identical geometry. In addition, a simplified geometry is considered for the earplug. More specifically, the face

of the earplug in contact with the external environment coincides with the EC entrance and is supposed to be planar. The protruding part of the earplug in the concha bowl is neglected. The earplug face in contact with the occluded EC cavity is also modeled as planar and normal to the curvilinear axis of the EC.

Given that the earplug outer face is flush with the EC entrance, a specific insertion depth in the EC corresponds to a specific earplug length. In this work, three insertion depths are examined: shallow, middle, and deep. This is achieved by inserting fully into the EC a short, medium and long earplug respectively (see Figure 3.2(c)). The short earplug occluding the EC at a shallow depth (about 8.4 mm along the curvilinear axis of the EC) is located within the outer first third part of the EC where the surrounding tissues are composed of ST and cartilage. The medium earplug occluding the EC up to its middle part (about 14.3 mm along the curvilinear axis of the EC) reaches the bony portion. The long earplug deeply occludes the EC (about 20.7 mm along the curvilinear axis of the EC) and its medial face is located within the bony portion of the EC. These insertion depths are chosen based on the EC geometry and the ranges of the shallow, middle, and deep insertions found in the literature (Berger & Kerivan, 1983; Stenfelt & Reinfeldt, 2007; Berger, 2013; Brummund *et al.*, 2014). The volumes of the short, medium and long earplugs are correspondingly 426.8, 766.7 and 1116.9 mm^3. Note that the earplug does not have the same length for the three insertion depths. This is not as if an earplug of a given length were inserted at various depths in the EC. The chosen earplugs could correspond to roll-down foam earplugs which would have been more or less shortened or custom molded earplugs without protuberance in the concha bowl which would reach the bony part of the EC and would be successively shortened (Tufts, Chen & Marshall, 2013).

3.1.2 Material properties

3.1.2.1 Biological tissues

The brain, the bone, the ST and the auricular cartilages are hypothesized to behave as linear isotropic elastic solids while the cerebrospinal fluid is considered as an acoustic fluid domain.

Table 3.1 summarizes the material properties of the biological tissues used in this study (called the reference tissue material property set in the following).

Table 3.1 Material properties for the components in the model

	E^* [MPa]	ρ [kg/m^3]	ν	η	c [m/s^2]
Cartilage	7.2	1 080	0.32	0.3	–
	(Grellmann *et al.*, 2006)	(Maroudas, Muir & Wingham, 1969; Chang *et al.*, 2016)	(Grellmann *et al.*, 2006)	(Chang *et al.*, 2016)	–
ST	0.5	1 030	0.45	$3\times10^{-5}\times f$	–
	(Sarvazyan *et al.*, 1995)	(Taschke & Hudde, 2006)	(Chang *et al.*, 2016)	(Chang *et al.*, 2016)	–
Bone	8 000	1 700	0.335	0.1	–
	(Auperrin *et al.*, 2014; Chang *et al.*, 2016; Brummund *et al.*, 2014)	(Auperrin *et al.*, 2014; Chang *et al.*, 2016)	(Peterson & Dechow, 2003)	(Chang *et al.*, 2016)	–
Brain	0.035	1 000	0.45	$3\times10^{-4}\times f$	–
	(Chang *et al.*, 2016)				
Cerebrospinal fluid	–	1 000	–	–	1 500
	(Chang *et al.*, 2016)				
Foam earplug	0.45	220	0.1	0.1	–
	(James, 2006)	(James, 2006)	(James, 2006)	(Brummund *et al.*, 2014)	–
Silicone earplug	0.85	1 050	0.48	0.1	–
	(Sgard *et al.*, 2010)				
Air (20 ℃)	–	1.2	–	–	343
Screw	200 000	7 850	0.33	–	–

* E: Young's modulus, ρ: density, ν: Poisson's ratio, η: loss factor, c: speed of sound, f: frequency [Hz]

3.1.2.2 Earplugs

The earplugs are modeled as linear isotropic elastic solids under the assumption of small deformation. The properties of the silicone earplug are derived from the literature (Sgard *et al.*, 2010). Given the EC geometry, the material properties (i.e., Young's modulus, density and

Poisson's ratio) for a foam earplug compressed at a 30% radial strain are adopted from the study of James (2006). The loss factor of the foam earplug is taken from the study of Brummund *et al.* (2014). Material properties of both earplugs are specified in Table 3.1.

3.1.2.3 Air-filled earcanal cavity and external air

The head is assumed to be immersed in an infinite acoustic domain (i.e., air). Air also fills the ECs. The visco-thermal dissipation within the EC is not considered in this study since it does not significantly affect the sound pressure level (SPL) in the EC in the interested frequency range (Carillo *et al.*, 2020). The properties of air are also indicated in Table 3.1.

3.1.3 Boundary, coupling and loading conditions

The infinite external air domain is accounted for using a spherical air-filled volume surrounding the head, coupled to a perfectly matched layer (PML, see Figure 3.3 (a)) (Sgard *et al.*, 2019). The PML simulates the Sommerfeld condition and makes it possible for the sound waves scattered by the EC and the head to propagate outward as in a free field (Berenger, 1994; Hu, 1996). Note that according to preliminary studies, for the PML implementation in COMSOL Multiphysics®, the polynomial stretching option and default values for the PML scaling factor and curvature parameter are adopted.

Due to the truncation at the head base, the ST and bone have artificial boundaries (see Figure 3.3(a)) that are considered to be both free.. "Free" here means that the boundary is actually coupled to the external air. The effect of the boundary condition on the simulated OE is also studied (see Section 3.4.1). At the interfaces between solid domains, the continuity of stress vectors and displacements is assumed. At the interface between a solid domain and a fluid domain, the fluid-structure coupling condition applies, namely the continuity of the normal displacement and normal stress vector. The eardrum surface is defined as a locally reacting specific acoustic impedance boundary condition based on Shaw & Stinson's lumped middle ear model (Shaw & Stinson, 1981, 1983; Schroeter & Poesselt, 1986). This is a reasonable

simplification for the physical structures of the middle ear since the present study concentrates on the frequency range below 1.0 kHz while the sound pressure originating from the inertia of the middle ear ossicles is expected to have an effect in the 1 – 3 kHz frequency range (Stenfelt, Hato & Goode, 2002; Stenfelt *et al.*, 2003; Stenfelt & Goode, 2005a). Note that this prevents any acoustic energy from being radiated into the EC by the eardrum. The rest of the middle ear cavity boundaries are set to be free.

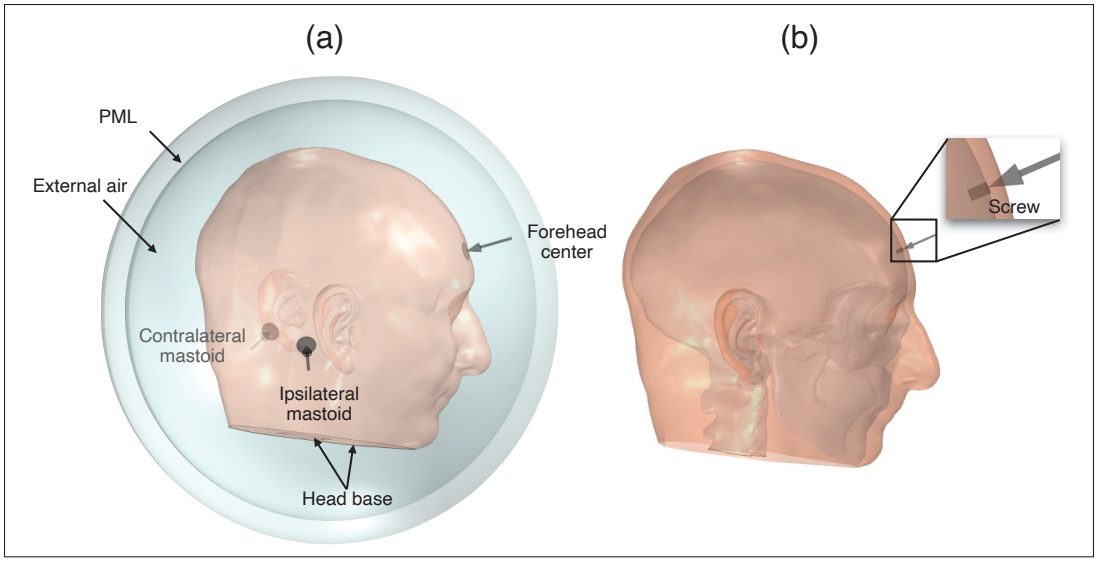

Figure 3.3 Final reconstructed head with boundary, coupling, and loading conditions

The head is stimulated mechanically in two different ways (see Figure 3.3). First, for simulating the OE (see Section 3.1.6.1), a 1 Pa harmonic pressure is applied on the ST at different positions (e.g., the ipsilateral mastoid, the contralateral mastoid, the forehead center) over an area of about 175 mm^2, corresponding to the contact area of the frequently clinically used bone transducer RadioEar B-71 (see Section 3.3.1). The ST surface of the reconstructed head is curved at the stimulation position. If a B-71 bone transducer is used, the contact stimulation surface is flat. Two choices are then possible: (i) a portion of the ST is cut out to flatten them at the stimulation position; (ii) the ST surface to which the bone transducer is attached is kept curved and a harmonic pressure equivalent to a force applied on the same surface is used as loading condition. Due to the technical difficulty in cutting out the ST, the second choice has been made in this

work. Figure 3.3 shows the directions of the resultant forces applied on three different positions situated on different parts of the head (i.e., the ipsilateral (right) mastoid, contralateral (left) mastoid and forehead center). Second, for simulating a vibratory indicator (i.e., input mechanical impedance, see Section 3.1.6.2), a steel screw (see Table 3.1 for its material properties) inserted into the skull bone is used to excite directly the latter around the forehead center. The screw is simulated as a cylinder of 3 mm diameter and 5 mm length, which has approximately the same size as the screws used in the experiments (Stenfelt & Goode, 2005b). A 1 N force is exerted on the screw cross-section along its longitudinal axis.

3.1.4 Meshing

All the domains are meshed using quadratic tetrahedral elements except for the PML domain which is meshed using quadratic triangular prisms. To save the computational time, the frequency range of interest (0.1 – 1.12 kHz) is split into different frequency bands. For a given frequency band, the whole system (except the brain domain and the PML) is re-meshed with a criterion of six elements per wavelength ($\lambda = c/f$ with f the frequency and c the speed of sound in the domain of interest) at the maximum frequency (f_{max}) of the band. More specifically, a maximum mesh size is defined for the physics to investigate. Hence, in a solid domain, the initial number of mesh elements is chosen with c either the compression wave speed $c_c = \sqrt{\frac{E(1-\nu)}{\rho(1+\nu)(1-2\nu)}}$, or the shear wave speed $c_s = \sqrt{\frac{G}{\rho}}$, with E, ρ, ν and G the Young's modulus, density, Poisson's ratio and shear modulus, respectively. Preliminary simulation results show that the criterion based on the compression wave speed compared with the stricter criterion based on the shear wave speed is sufficient to achieve the convergence of the simulation results. Preliminary studies also indicate that the brain can be meshed coarsely by the predefined "extra coarse" mesh size calibrated for "general physics" in COMSOL Multiphysics®. In addition, a minimum mesh size is chosen to capture the geometry of each domain with a sufficient precision in each frequency band. The number of mesh elements depends greatly on the tissue material property set (see Section 3.4.3.1). As an indication of the number of mesh elements, the open ear case has 541 449 elements at 0.2 kHz and 594 832 elements at 1.12 kHz when adopting the reference material

property set, which takes about 20 hours for calculation (using the PC workstation specified in Section 3.1.5). For the occluded case, the number of mesh elements depends also on the earplug type and insertion depth.

3.1.5 Finite element problem solving

The fluid-structure coupled problem is solved in the frequency domain using COMSOL Multiphysics® v.5.5. All the calculations are carried out using a PC workstation (Intel Xeon Gold 6136 CPU, 2 processors, 1.00 TB RAM) with 64-bit Windows 10 Pro operating system. The simulations are performed in the frequency range from 0.1 to 1.1 kHz with a 5 Hz step up to 0.7 kHz and a 20 Hz step for the rest. Since the OE is the most significant for frequencies below 1.0 kHz (Stenfelt *et al.*, 2003), computations at higher frequencies are not carried out. Third octave band responses (0.125 – 1.0 kHz) are then determined from narrow band responses using an in-house MATLAB routine (MATLAB 2019b, The MathWorks, Inc., Natick, Massachusetts, United States) based on the ANSI S1.11 standard (ANSI, 1986). The choice of the narrow band frequency resolution is a compromise between the accuracy of the third octave band responses of the simulations and the computational cost based on preliminary studies.

3.1.6 Vibratory and acoustic indicators

The FE head model is developed to predict the OE which is an acoustical transfer function. As the OE is intimately linked to the vibratory response of the head under bone-conducted stimulation, the input mechanical impedance is also examined as a complementary indicator to gain confidence in the model for predicting a vibratory transfer function at the location of the stimulation. This section describes how these two quantities are calculated.

3.1.6.1 Occlusion effect

The computation of the OE requires to evaluate both the SPLs at the eardrum surface for the open ear case (Lp_{open}) and the occluded ear case (Lp_{occluded}). The sound pressure is computed

and surface averaged on the eardrum boundary before calculating the SPL. The OE is then derived from the difference between the two cases:

$$OE = Lp_{\text{occluded}} - Lp_{\text{open}}. \tag{3.1}$$

In this study, the OEs corresponding to different configurations of the earplug insertion depth and type, stimulation position on the ST as well as tissue material property set (see Section 3.4.3.1) are computed. The default configuration is the reference material property set, free head base, stimulation placed on the ipsilateral mastoid, and EC occluded by the mediumly inserted foam earplug.

3.1.6.2 Input mechanical impedance

To evaluate the input mechanical impedance, the velocity at the same position and in the same direction as the excitation on the screw which is inserted into the skull bone around the forehead center is computed (Chang *et al.*, 2016). The mechanical point impedance (Z) is then derived from the ratio of the force (F) and the velocity (v),

$$Z = \frac{F}{v}. \tag{3.2}$$

3.2 Fabrication of the acoustic test fixture

This section presents the design and fabrication of an augmented ATF for assessing the OE of earplugs (see Figure 3.4) as well as for the purpose of ultimately validating and calibrating the FE head model of the OE presented in Section 3.1. The ATF is made from the same geometrical model of the participant's head as the FE head model. It thus incorporates the physical characteristics of the participant's head taken from the medical images and allows for considering the bone-conducted sound transmission through the head.

Precisely, the STL files of the anatomical structures (i.e., the brain, the cerebrospinal fluid, the bone, the auricular cartilage and the ST) reconstructed from the medical images of the participant (see Section 3.1.1.1) were sent to the company True Phantom Solutions (Windsor, Canada) for the fabrication of the ATF. The materials used in the ATF mimic the biological tissues of human beings. It is important to note that the eardrum and the small void behind it in the FE head model (see Section 3.1.1.1) are replaced by material mimicking the bone in the ATF due to manufacturing challenges. Unlike commercial ATFs, no heating system or instrumentation is included. Urethane-based soft resins of different hardnesses are used for the ST, the cartilage and the brain; ceramic-reinforced epoxy-based composite material for the bone; and distilled water for the cerebrospinal fluid.

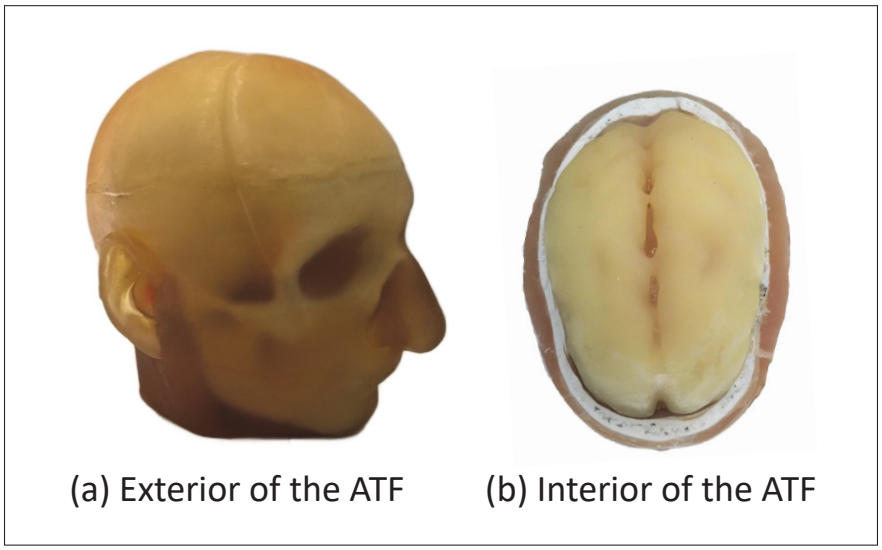

Figure 3.4 Augmented ATF fabricated based on the same geometrical model as the FE head model

Solid materials are assumed to be linear elastic isotropic with a constant structural loss factor. The mechanical properties of each domain are listed in Table 3.2. They are obtained from the manufacturer, as well as from tensile tests using dumbbell material specimens and quasi-static mechanical analyses using cylindrical material specimens (see also Benacchio, Doutres, Wagnac & Sgard, 2020), except for those of the cerebrospinal fluid (i.e., water).

Table 3.2 Mechanical properties of the materials used in the ATF

	E^* [MPa]	ρ [kg/m^3]	ν	η	c [m/s^2]
Cartilage	1.65	1 075	0.26	0.05	–
ST	0.17	1 007	0.49	0.045	–
Bone	13 600	2 267	0.31	0.1	–
Brain	0.094	990	0.31	0.05	–
Cerebrospinal fluid	–	1 000	–	–	1 498

* E: Young's modulus, ρ: density, ν: Poisson's ratio, η: loss factor, c: speed of sound

3.3 Evaluations of the finite element head model and the acoustic test fixture

Measurements are carried out on both the ATF and the participant in order to evaluate the FE head model. The experimental data obtained on the participant are also used to evaluate the ATF itself. It is important to recall that the ultimate goal is to use the experimental results obtained on the ATF and the participant to validate and calibrate the FE head model. However, due to the time limitation, only preliminary evaluations of the FE head model and the ATF have been done during this thesis. The following of this section presents the experimental setups and procedures (see Section 3.3.1) as well as the corresponding simulations carried out using the FE head model (see Section 3.3.2).

3.3.1 Experiments

The experiments are conducted in an audiometric cabin at normal room temperature (20 ℃). For the experiments on the ATF, the latter is placed on a chair with a soft cushion (see Figure 3.5(a)). It allows us to approximate a free boundary condition at the ATF bottom, which is convenient to reproduce in simulations. This setup is similar to that in the study of Stenfelt & Goode (2005a), in which cadaver heads were placed on a soft pillow for decoupling the head from the support.

3.3.1.1 Stimulation

For the measurements on both the ATF and participant, the bone conduction stimulation is achieved with a RadioEar B-71 transducer (RadioEar, New Eagle, USA). Since the fabricated

ATF does not include an artificial mouth (ITU-T, 1996), one's own voice is not chosen for providing the stimulation as in some published studies in the literature (Nélisse *et al.*, 2013; Saint-Gaudens *et al.*, 2022). The B-71 transducer is attached to the mastoid portion of the temporal bone with a headband (see Figure 3.5(b)) and comprises a circular interface of 175 mm^2. White noise filtered in third octave bands (bands 0.25 – 1.0 kHz) is used to drive the B-71 transducer through an in-house MATLAB routine (MATLAB 2019b, The MathWorks, Inc., Natick, Massachusetts, United States) and National Instruments analog output device (National Instruments Corp., Austin, TX, USA). The signal to noise ratio for the B-71 transducer is bad for frequencies lower than 0.2 kHz which are thus not considered in the experiments. The stimulation level is chosen to ensure that the SPL in the open EC is at least about 10 dB higher than the background noise.

Figure 3.5 Experimental setup for the measurements on the ATF

The influence of the airborne sound transmitted from the transducer housing into the EC in the frequency range from 0.25 kHz to 1.0 kHz is verified using the method of Stenfelt & Goode (2005a), which is recalled in the following. The B-71 transducer is first placed on the right mastoid. Then, by putting a piece of fibrous material between the ATF and the transducer's

headband, the transducer is hanged just in front of the right mastoid without touching the ATF or any other structures. The two transducer positions could be considered the same in terms of airborne sound radiation. For each transducer position, the SPL inside the open EC (using the open earpiece, see Section 3.3.1.2) and the SPL at 5 cm in front of the B-71 transducer are measured simultaneously. For the first position, the SPL measured in front of the transducer is due to the airborne component of the bone-conducted stimulation, whereas for the second position, it is solely from the sound radiation of the transducer. In a third step, in order to verify the contribution of the airborne sound, the EC sound pressures for the two positions are compared after both being normalized by the corresponding pressures assessed in front of the transducer (i.e., airborne radiation). Results show that the EC sound pressure (after normalization) for the first transducer position is much higher than that for the second position in the interested frequency range (see Section 4.1.2), indicating that such a system is promising for OE measurements with a negligible influence of the airborne sound.

3.3.1.2 Devices for earcanal sound pressure measurements

The experimental OE requires measuring the SPLs in the open and occluded ECs. For the open case, the open earpiece of Bonnet and his colleagues (2020) is used (see Figure 3.6(a)). It was designed to be almost acoustically transparent to acoustic excitation and is validated for the present project to maintain its acoustic transparency to bone conduction stimulation. The latter is done by using a probe tube instrumented with a miniature microphone (FG-23329-D65, Knowles®, USA) (see Figure 3.6(b)) to measure the SPL at approximately the same position in the EC of the ATF as the open earpiece. The position of the probe tube in the EC is controlled with the help of a plastic-coated wire. Compared with the open earpiece, this in-house device is contactless with the EC walls.

For the occluded case, a probed classic foam earplug (a “surrogate” classic foam earplug) is used. Its probe tube instrumented with a miniature microphone (FG-23329-D65, Knowles®, USA) (see Figure 3.6(c)) allows for measuring the SPL at the medial surface of the earplug that is in contact with the EC cavity. This facilitates the measurement in the occluded EC without

causing any possible incomplete seal. In addition, the geometry and material properties of a classic foam earplug are better known compared with most commercial earplugs. This kind of earplug is also considered in the FE head model (see Section 3.1.1.2).

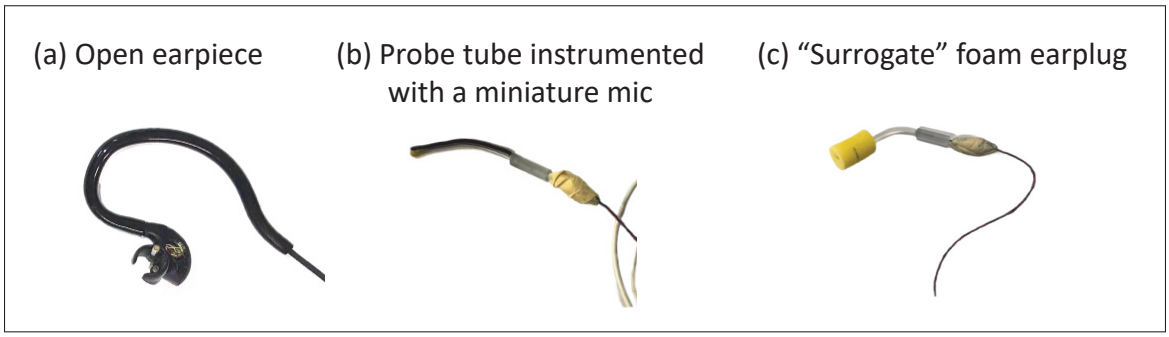

Figure 3.6 Devices for EC sound pressure measurements

3.3.1.3 Measurements on the acoustic test fixture

Measurements are only carried out in the right EC of the ATF, which is believed to be more precisely reconstructed due to fewer image artifacts than the left side (see also Section 3.1.1.1). The transducer is placed on the ipsilateral (i.e., right) side.

After positioning the B-71 transducer, measurements begin with the open case. Then, while maintaining the position of the transducer, the open earpiece is removed and the SPL in the EC occluded by the probed foam earplug is measured. The probe tube of the open earpiece has an insertion depth of approximately 8 mm into the EC. Therefore, the probed foam earplug is inserted at a similar depth into the EC during the measurements with the help of a marker on the earplug (see Figure 3.6(c)). The insertion depth of the probed foam earplug is also checked immediately after its removal from the EC (before it expands to restore its original form). This insertion depth corresponds to the shallow insertion (i.e., 8.4 mm) in the FE head model (see Section 3.1.1.2). It is worth mentioning that at room temperature, about 15 minutes have to be waited after the insertion of the earplug before carrying out the measurements in order to have the earplug sufficiently expanded in the EC and thus to have a good seal. Measurements are

repeated three times by removing and repositioning the B-71 transducer and the in-ear devices to account for the associated variability.

3.3.1.4 Measurements on the participant

The protocol for the acoustic measurements on the participant was approved by Research Ethics Boards of CHUM and ÉTS jointly. In the audiometric cabin, the participant sits on a chair with a soft cushion. Measurements on the participant (see Figure 3.7) follow a similar procedure as on the ATF, including the insertion depth of the open and occluded devices, and the three repeated measurements of the SPLs in the open and occluded ECs. To correspond to the measurements on the ATF, only the SPLs in the right EC are measured. For each repetition, the B-71 transducer is placed on the participant's right mastoid by the experimenter. Then, the participant is in charge of inserting the open and occluded devices into his right EC, while the experimenter is responsible for verifying the positions of these devices and taking photos for record. Due to the human body temperature, when the participant claims that the earplug is sufficiently expanded in the EC, the waiting time is much shorter (about 1 – 2 min) than that for the ATF (about 15 min).

(a) Open EC case (b) Occluded EC case

Figure 3.7 Measurements on the participant

3.3.2 Simulations

3.3.2.1 Case of the acoustic test fixture

For comparing with the experimental OE obtained on the ATF, simulations are carried out (i) using the material properties of the ATF (see Table 3.2) and (ii) with the bone replacing the eardrum and the small void behind it in the original model (see Section 3.1.1.1) to mimic the ATF geometry. To reproduce the experiments, the model considers a stimulation at the ipsilateral (i.e., right) side, a free boundary condition at the head base and a foam earplug (i.e., the default configuration). The earplug is inserted at the shallow insertion depth (i.e., 8.4 mm).

3.3.2.2 Case of the participant

For comparing with the experimental OE obtained on the participant, the simulations are carried out using the default configuration except that the earplug is inserted at the shallow insertion depth. It should be kept in mind that the geometry of the FE head model comprises several simplifications compared with the participant's head as mentioned in Section 3.1.1.1. Besides, it is worth recalling that an acoustic impedance boundary condition representing that of the eardrum (based on Shaw & Stinson's model) is applied on the eardrum surface (see Section 3.1.3), unlike the ATF case.

3.3.2.3 Calculation of the occlusion effect

To correspond to the experiments, the open and occluded EC sound pressures which are required to derive the OE, are computed and averaged over the cross-section of the EC that coincides with the earplug medial surface instead of the eardrum surface.

3.4 Investigations of the factors affecting the simulated occlusion effect of earplugs

This section presents the simulations carried out using the FE head model to investigate several factors that may affect the simulated OE of earplugs, including the boundary condition at the

head base (see Section 3.4.1), the modeling of the external air (see Section 3.4.2), the material properties of the EC surrounding tissues (see Section 3.4.3), the position in the EC where the OE is evaluated (see Section 3.4.4), and the stimulation position (see Section 3.4.5). It is important to note that unless otherwise specified, the default configuration (i.e., the reference material property set, free head base, stimulation placed on the ipsilateral mastoid, and EC occluded by the mediumly inserted foam earplug) is adopted.

3.4.1 Boundary condition at the head base

The FE models of truncated outer ears in the literature are sensitive to the boundary and loading conditions (see Section 1.3). The present FE head model considers free boundaries at the head base. The effect of the boundary condition on the artificial boundaries at the head base due to the truncation is therefore studied. The simulated OEs for a free head base are compared with those for a fixed head base. The cases of the EC occluded respectively by the shallowly, mediumly and deeply inserted foam earplugs and of the stimulation placed respectively at the ipsilateral mastoid, contralateral mastoid and forehead center are considered.

3.4.2 Modeling of the external air

By applying a radiation impedance over the open EC entrance, the FE models of truncated outer ears in the literature neglect the possible contribution of the sound radiation from the external ST into the open EC (see Section 1.3). Instead, the present FE head model considers the external air domain by a spherical air-filled volume surrounding the head coupled to a PML. The difference in the simulated OEs between these two methods is investigated using the present FE head. For the case where the radiation impedance is used, besides the EC entrance position (E1) indicated in Figure 3.2, two more positions (E2 and E3) at a plane 1 – 2 mm deeper into the EC are also considered in order to study the associated effect on the simulated sound pressure in the open EC. For the occluded ear cases, the EC is kept occluded by the mediumly inserted foam earplug.

3.4.3 Material properties of the earcanal surrounding tissues

The material properties of the biological tissues exhibit large inter-individual variability (see Section 1.4). Since the tissue material properties are difficult to assess in-vivo on the participant and the FE head model is initially built with given material properties (see Section 3.1.2.1), Section 3.4.3.1 analyzes the potential variability of the simulated OE which could be induced by different tissue material properties, using the published values in the literature. It is also mentioned in Section 1.4 that the value of ST Poisson's ratio adopted by the numerical studies in the literature dealing with the OE, namely 0.4, seems to be in contradiction with the value (i.e., the theoretical limiting value of incompressible materials 0.5) mentioned by Sarvazyan (1975) in the frequency range below 1.0 kHz. It is unclear how the value of ST Poisson's ratio may affect the OE. The independent effect of ST Poisson's ratio is thus specifically studied in Section 3.4.3.2.

3.4.3.1 Statistical analysis on the tissue material properties

The variability of the simulated OEs associated with that of the material properties of the EC surrounding tissues (i.e., cartilage abbreviated to "carti", bone and ST) is studied. Eight parameters are concerned, which are E_{carti}, ρ_{carti}, ν_{carti}, E_{ST}, ρ_{ST}, E_{bone}, ρ_{bone} and ν_{bone}, where E, ρ and ν denote respectively Young's modulus, density and Poisson's ratio, and the subscript refers to each material. According to the experimental data (i.e., maximum, average and minimum values) of these parameters available in the literature, different tissue material property sets are considered (see Table 3.3) which are proposed based on two methods: "one factor at a time" (No. 1 – No. 16) and definitive screening design (Jones & Nachtsheim, 2011), more specifically a three-level fractional factorial design (No. 17 – No. 32). Odd property numbers between 1 and 15 correspond to the minimum values of the eight parameters, while even property numbers between 2 and 16 to their maximum values. Different tissue material property sets can be considered to correspond to different participants. The default values given in Table 3.1 are used for the other tissue material properties which are not included in the statistical analysis.

Table 3.3 Tissue material property sets

No.	E_{carti} *	ρ_{carti}	ν_{carti}	E_{ST}	ρ_{ST}	E_{bone}	ρ_{bone}	ν_{bone}
Reference	7.2	1080	0.32	0.5	1030	8000	1700	0.335
1	3.8	1080	0.32	0.5	1030	8000	1700	0.335
2	10.6	1080	0.32	0.5	1030	8000	1700	0.335
3	7.2	1000	0.32	0.5	1030	8000	1700	0.335
4	7.2	1160	0.32	0.5	1030	8000	1700	0.335
5	7.2	1080	0.26	0.5	1030	8000	1700	0.335
6	7.2	1080	0.38	0.5	1030	8000	1700	0.335
7	7.2	1080	0.32	0.3	1030	8000	1700	0.335
8	7.2	1080	0.32	0.7	1030	8000	1700	0.335
9	7.2	1080	0.32	0.5	890	8000	1700	0.335
10	7.2	1080	0.32	0.5	1170	8000	1700	0.335
11	7.2	1080	0.32	0.5	1030	4000	1700	0.335
12	7.2	1080	0.32	0.5	1030	12000	1700	0.335
13	7.2	1080	0.32	0.5	1030	8000	1500	0.335
14	7.2	1080	0.32	0.5	1030	8000	1900	0.335
15	7.2	1080	0.32	0.5	1030	8000	1700	0.19
16	7.2	1080	0.32	0.5	1030	8000	1700	0.48
17	7.2	1160	0.38	0.7	1170	12000	1900	0.48
18	7.2	1000	0.26	0.3	890	4000	1500	0.19
19	10.6	1080	0.38	0.3	1170	4000	1500	0.48
20	3.8	1080	0.26	0.7	890	12000	1900	0.19
21	10.6	1000	0.32	0.3	1170	12000	1900	0.19
22	3.8	1160	0.32	0.7	890	4000	1500	0.48
23	10.6	1160	0.38	0.5	890	12000	1500	0.19
24	3.8	1000	0.26	0.5	1170	4000	1900	0.48
25	10.6	1000	0.26	0.7	1030	12000	1500	0.48
26	3.8	1160	0.38	0.3	1030	4000	1900	0.19
27	10.6	1160	0.26	0.3	890	8000	1900	0.48
28	3.8	1000	0.38	0.7	1170	8000	1500	0.19
29	10.6	1160	0.26	0.7	1170	4000	1700	0.19
30	3.8	1000	0.38	0.3	890	12000	1700	0.48
31	10.6	1000	0.38	0.7	890	4000	1900	0.335
32	3.8	1160	0.26	0.3	1170	12000	1500	0.335

* E: Young's modulus [MPa], ρ: density [kg/m^3], ν: Poisson's ratio

3.4.3.2 Study on the effect of soft tissue Poisson's ratio

In the present study, for studying independently the effect of ST Poisson's ratio on the OE, the following values of ST Poisson's ratio are considered:

- 0.48 and 0.49, the values close to the theoretical limiting value of incompressible materials (i.e., 0.5);
- 0.45, the value adopted by the reference material property set (see Table 3.1) according to the study of Chang *et al.* (2016);
- 0.4, the value adopted by the OE numerical studies in the literature (Brummund *et al.*, 2014, 2015; Carillo *et al.*, 2020, 2021a).

3.4.4 Influence of the position in the earcanal where the occlusion effect is evaluated

In the present study, the FE head model is used to investigate the transfer function in the open EC and the EC occluded by an earplug under a bone-conducted stimulation (see Section 1.5). To better visualize the variation of the sound field in the EC, all the three insertion depths of the earplug mentioned in Section 3.1.1.2 are considered (i.e., shallow insertion: 8.4 mm, middle insertion: 14.3 mm, and deep insertion: 20.7 mm).

3.4.5 Stimulation position

Investigating the sensitivity of the OE to the stimulation position on the ipsilateral mastoid part of the head may help quantify the contribution of this factor to the variability of the experimental results (see Section 1.4). In Section 3.1.3, the stimulation is originally applied at one position of the ipsilateral mastoid part of the head as indicated in Figure 3.3, which is shown in Figure 3.8 as P1. Two supplementary stimulation positions around the ipsilateral mastoid are now considered and are indicated respectively as P2 and P3 in Figure 3.8. The vertical distance between P1 and P2 is about 15 mm and the horizontal distance between P2 and P3 is about 15 mm. These three positions cover approximately the entire region of the mastoid and are thus chosen in order to study the sensitivity of the OE to the stimulation position placed on the ipsilateral mastoid part of the head. The stimulation position in the experiments should be included in the region covered by P1, P2 and P3.

Similarly to what is described in Section 3.1.3, at each of the stimulation positions, the head is stimulated mechanically by a 1 Pa harmonic pressure applied on the ST over an area of about 175 mm^2. The simulations in this section are performed with the shallowly inserted foam earplug. The shallow insertion depth is chosen since it corresponds to the insertion depth adopted in the experiments, and the simulated OEs for the three stimulation positions can thus be compared with the experimental OE obtained on the participant (see Section 3.3).

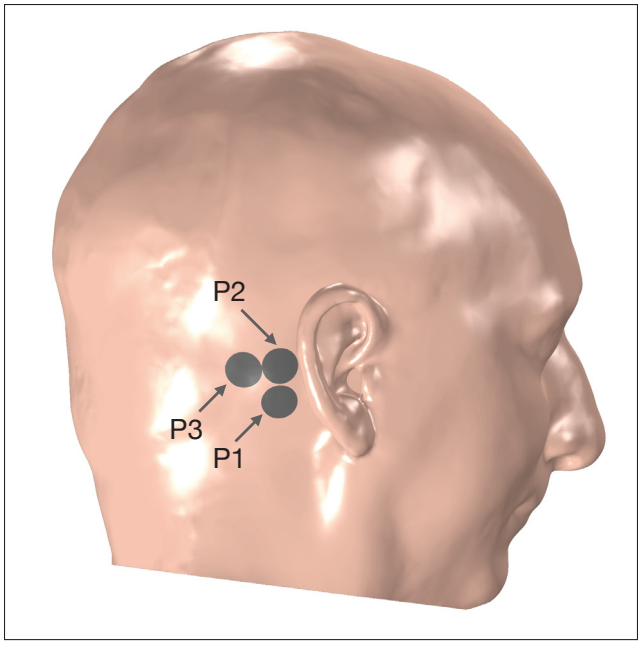

Figure 3.8 Head stimulated at three positions on the ipsilateral mastoid part of the ST

3.5 Summary

For evaluating the FE head model and investigating the factors influencing the OE using the FE head model, various configurations of the biological tissue material properties, boundary conditions, stimulation positions, insertion depths and types of the earplug have been adopted. The justifications of the choices are mentioned previously in the corresponding sections. Figure 3.9 summarises these configurations for the convenience of the readers.

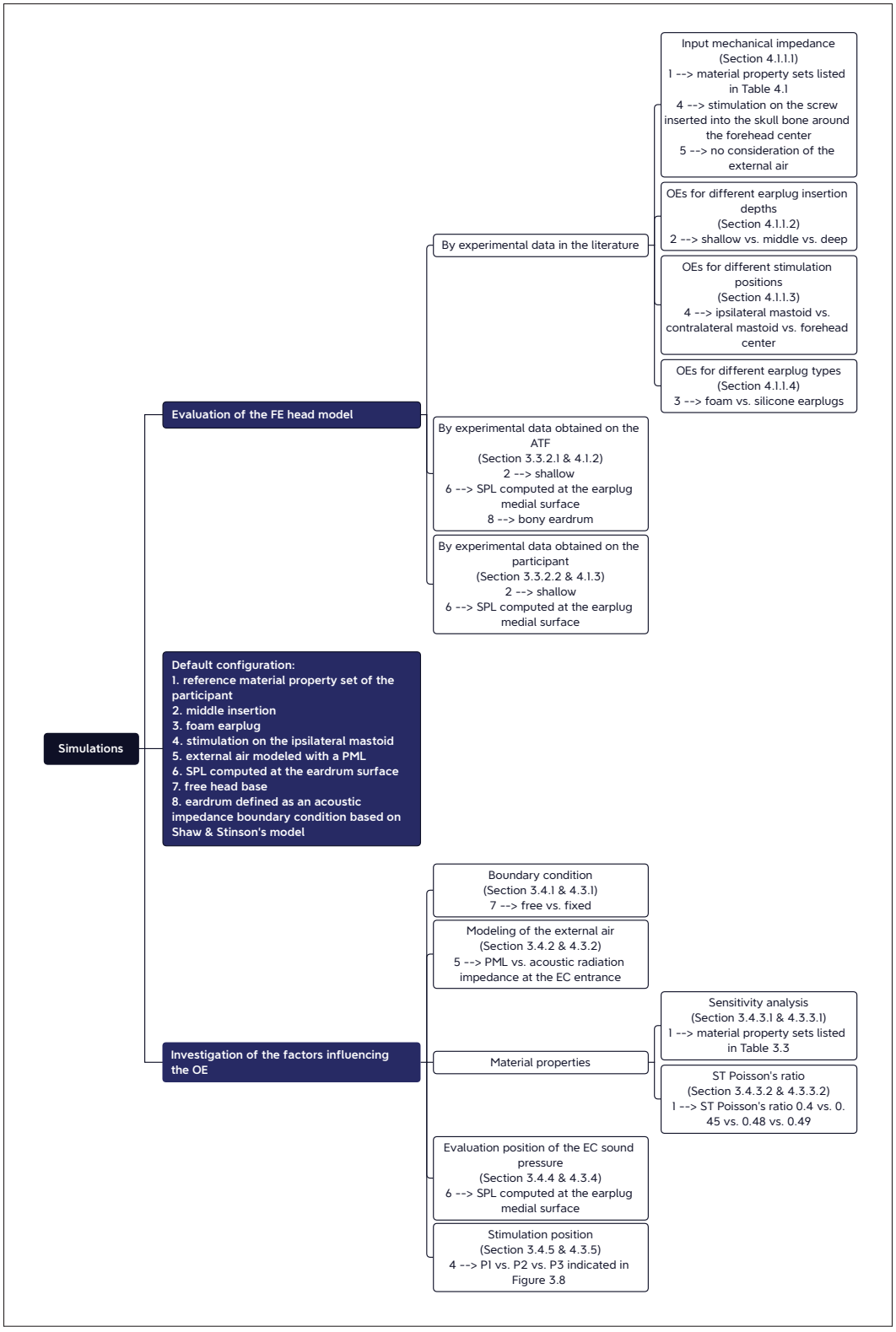

Figure 3.9 Simulation configurations

CHAPTER 4

RESULTS AND DISCUSSION

At first, this chapter presents the evaluation of the finite element (FE) model of the human head (see Section 4.1) and the evaluation of the acoustic test fixture (ATF, see Section 4.2). Then, the factors affecting the simulated occlusion effect (OE) are discussed (see Section 4.3). It should be recalled that unless otherwise specified, the simulations are carried out with the default configuration (i.e., the reference material property set, middle insertion of the foam earplug and stimulation on the ipsilateral mastoid).

4.1 Evaluation of the finite element model of the human head

The simulation results of the FE head model (including the input mechanical impedance and the OE) are first compared with the data in the literature (see Section 4.1.1). Specifically, the simulated OEs are compared with the experimental data in the literature obtained on groups of participants. It is important to recall that the comparison with the experimental OEs measured on a group of participants was adopted for the purpose of "validating" or evaluating the FE models of the OE by the previous numerical studies in the literature (Brummund *et al.*, 2014, 2015; Carillo *et al.*, 2021a). In the present study, the FE head model is also evaluated by the experimental data obtained on the ATF (see Section 4.1.2) and the participant (see Section 4.1.3), which is an advantage of this FE head model as a result of its development from the medical images of the participant.

4.1.1 Comparison with the experimental data in the literature

In the following, the simulation results of the input mechanical impedance (see Section 4.1.1.1) and the OE (see Sections 4.1.1.2 – 4.1.1.4) are compared with the data in the literature. More precisely, in accordance with the available experimental data in the literature, the OEs of different earplug insertion depths (see Section 4.1.1.2), stimulation positions (see Section 4.1.1.3) and earplug types (see Section 4.1.1.4) are considered.

4.1.1.1 Input mechanical impedance of the skull

The input mechanical impedance is computed with the present model. Results are compared with (i) the experimental data of Stenfelt & Goode (2005b) obtained from six cadavers' heads and (ii) the simulation result of Chang *et al.* (2016) obtained from a FE model of a cadaver's head. As Chang *et al.* (2016) have used their FE head model to simulate this indicator, this provides a valuable opportunity to compare the mechanical point impedance responses during a vibratory stimulation for the two different FE head models. Especially, adopting the same material properties, boundary conditions and excitation allows for having an idea of the effect of the head geometry on the input mechanical impedance. In accordance with the FE head model of Chang *et al.*, the head base is free, the fluid-structure coupling with the external air domain is not considered, and the simulated screw has a similar size as in their study. However, note that in the two FE head models, no skin removal at the stimulation position is considered unlike in the experiments of Stenfelt & Goode.

Table 4.1 Tissue material property sets adopted for simulating the input mechanical impedance

No.	E_{carti} *	ρ_{carti}	ν_{carti}	E_{ST}	ρ_{ST}	E_{bone}	ρ_{bone}	ν_{bone}
sim.1	7.2	1080	0.32	0.5	1030	8000	1700	0.335
sim.2	7.2	1080	0.32	0.5	1030	4000	1700	0.335
sim.3	7.2	1080	0.32	0.5	1030	12000	1700	0.335
sim.4	7.5	1000	0.45	0.7	900	4000	2200	0.3

* E: Young's modulus [MPa], ρ: density [kg/m^3], ν: Poisson's ratio

Figure 4.1 compares the simulated input mechanical impedances as magnitude (a) and phase (b). Four tissue material property sets (see Table 4.1) are adopted in the simulations: (i) the reference tissue material property set (sim.1), (ii) the material property set No. 11 listed in Table 3.3 (sim.2), (iii) the material property set No. 12 listed in Table 3.3 (sim.3), and (iv) the tissue material property set of Chang *et al.* (sim.4). The simulation results of the present model are compared with the simulation result of Chang *et al.* (2016) and the experimental data of Stenfelt & Goode (2005b). Sim.2 and sim.3 differ from sim.1 only by the Young's modulus of the skull bone. The two tissue material property sets are chosen to confirm the important

effect on the input mechanical impedance of the Young's modulus of the skull bone in the stiffness-controlled frequency range 0.5 – 1.0 kHz as pointed out by the sensitivity analysis of Chang *et al.* on the tissue material properties. Note that for the material property set of Chang *et al.*, the properties for the cortical bone are adopted for the skull bone.

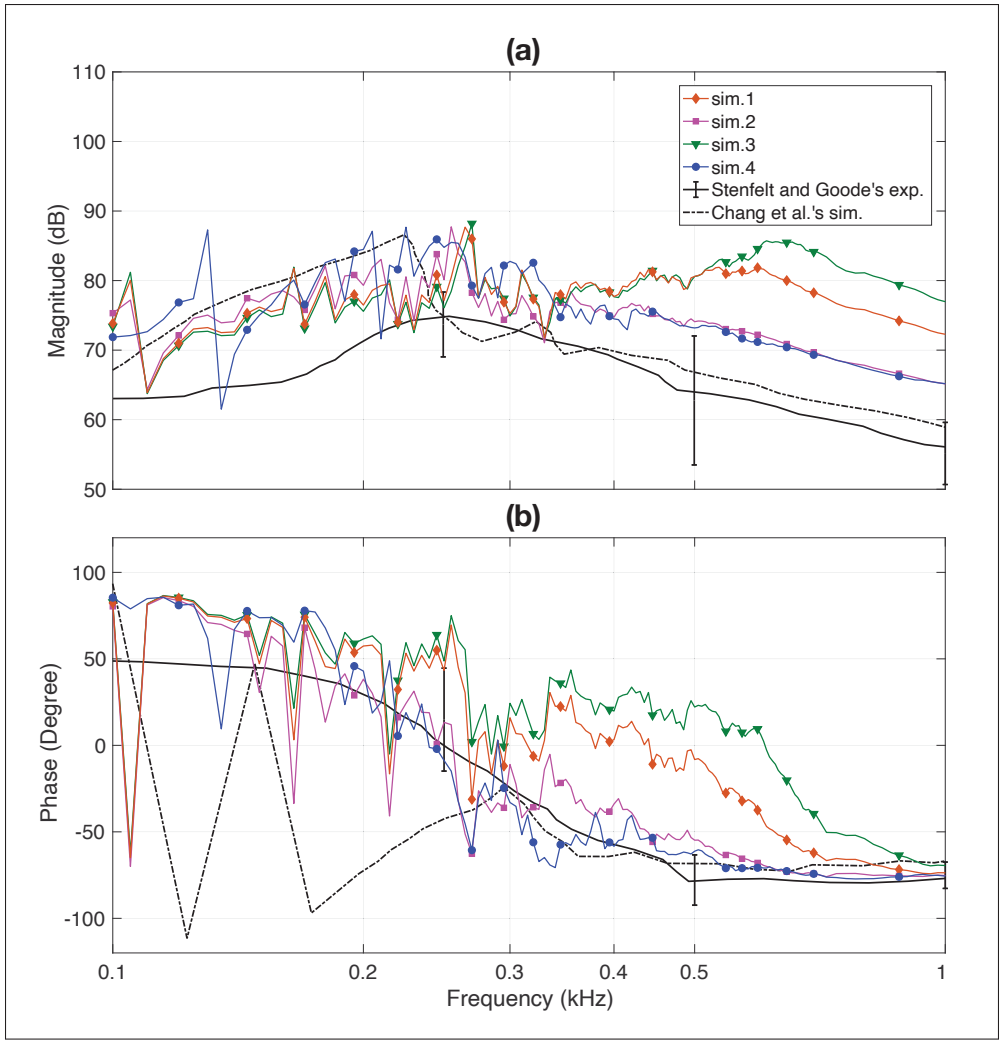

Figure 4.1 Magnitude (dB, factor 20, ref. 1 Ns/m) and phase of the input mechanical impedance simulated by the head model using different tissue material properties, compared with that simulated by Chang *et al.* (2016) and that measured by Stenfelt & Goode (2005b)

As can be seen from the figure, compared with the simulation result of Chang *et al.*, those of the present model have more oscillations at frequencies below 0.5 kHz. This may be due to the

finer resolutions adopted in the frequency range of interest. In their study, the simulation was performed with a 25 Hz resolution between 0.1 and 0.5 kHz and with a 50 Hz resolution between 0.5 and 1.0 kHz. In the present study, the resolution is 5 Hz in the 0.1 – 0.7 kHz frequency range and 20 Hz in the 0.7 – 1.0 kHz frequency range. The simulation results of the present model highlight its intricate modal behavior at low frequencies. At frequencies above 0.5 kHz, the result of sim.4 has a difference of about 5 dB with the simulation result of Chang *et al.*, which is likely due to the stiffer bone (only cortical) in the current study compared with the sandwich structure in the study of Chang *et al.*

The results of sim.1 – sim.4 all present a similar tendency with frequency as the average experimental data. The differences between the different simulation results reveal the sensitivity of the response to the material properties. At frequencies below around 0.2 kHz, the impedance magnitudes increase with frequency indicating a mass-dominated system while at frequencies above around 0.5 kHz, the impedance magnitudes decrease with frequency indicating a stiffness-dominated system. Between 0.2 kHz and 0.5 kHz, the magnitudes show several resonances and the phases have drastic changes, which is consistent with the individual experimental data shown in the study of Stenfelt & Goode (2005b).

The differences between the results of sim.1 – sim.3 display the effect of the Young's modulus of the skull bone on the input mechanical impedance. This effect could also be an important contributor to the differences between the current simulation results and the results in the literature at frequencies above 0.5 kHz. However, the impedance magnitudes of sim.2 and sim.4 both obtained with the same Young's modulus of the skull bone as in the study of Chang *et al.* are still relatively high in the stiffness-dominated frequency zone compared with those in the study of Stenfelt & Goode as well as the study of Chang *et al.* This may result from a difference in the skull bone modeling as well as a thicker skull bone and/or a smaller curvature radius at the stimulation position (Stenfelt & Goode, 2005b). Besides, the two simulated and the experimentally used screws are not exactly the same.

Finally, it can be concluded that the present FE head model is promising for reproducing the vibratory response of the head under bone-conducted stimulation.

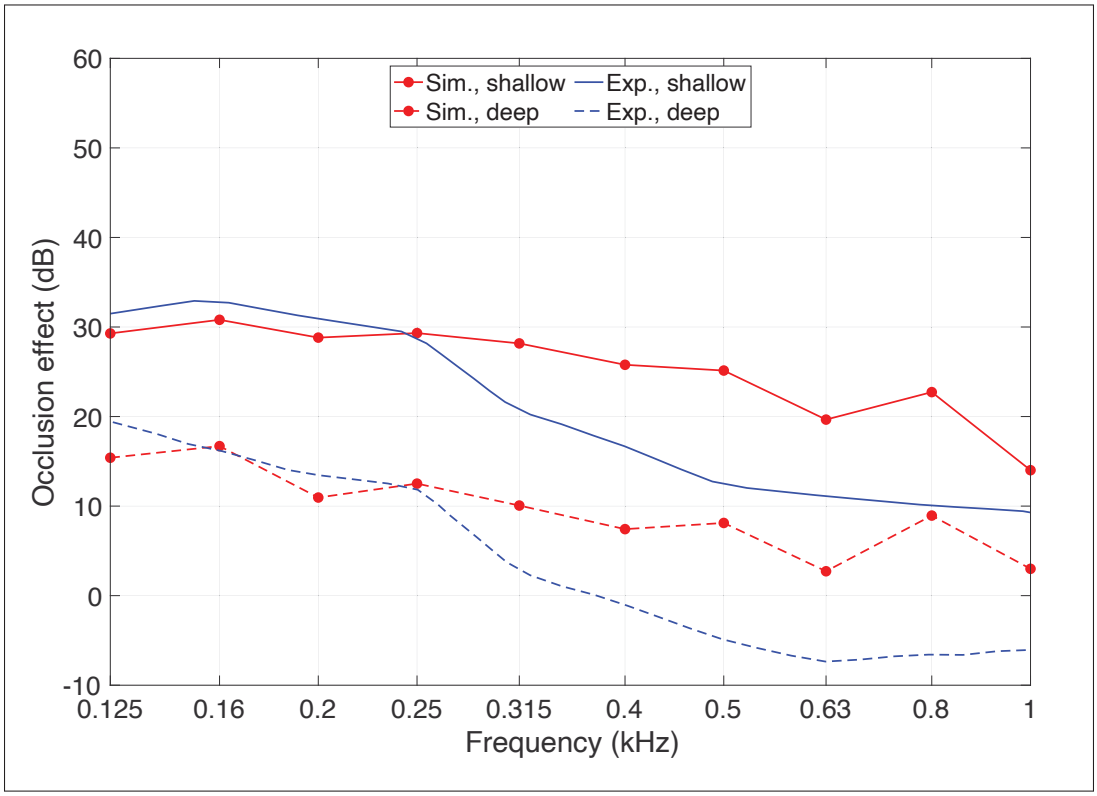

Figure 4.2 Simulated OEs of the foam earplug at different insertion depths for the forehead stimulation versus the experimental data of Stenfelt & Reinfeldt (2007)

4.1.1.2 Occlusion effects for different earplug insertion depths

Figure 4.2 compares the simulated OEs with the median experimental OEs of Stenfelt & Reinfeldt (2007) for the shallowly (7 mm in the experiments) and deeply (22 mm in the experiments) inserted foam earplugs. Both data sets are obtained with the stimulation placed on the forehead center. It is necessary to recall that for the simulations in the present study, the excitation is always applied on the soft tissues (ST), except for the simulations of the mechanical impedance where the excitation is put directly on the skull bone (see Section 3.1.3). In Figure 4.2, a deviation of about 1 dB on average is found between the simulated and experimental results for

each of the two insertions in the 0.125 – 0.25 kHz frequency range whereas a deviation of about 10 dB is found in the 0.25 – 1.0 kHz frequency range. These discrepancies are acceptable as Stenfelt & Reinfeldt mentioned that the spread of the sound pressure level (SPL) was typically between 5 and 10 dB from the median values except for frequencies below 0.2 kHz although the mean and standard deviation of the experimental data were not given. More importantly, it is found that the difference in the OEs between the shallow and deep insertions of the foam earplug is about the same for the experiments and the simulations (15 dB). The model is able to reproduce the decrease in the OE amplitude with the earplug insertion depth, which is a common behavior of the OE found in the previous experimental and numerical studies. This decrease was explained by the decrease of the earcanal (EC) wall normal vibration in the recent study of Carillo *et al.* (2021a).

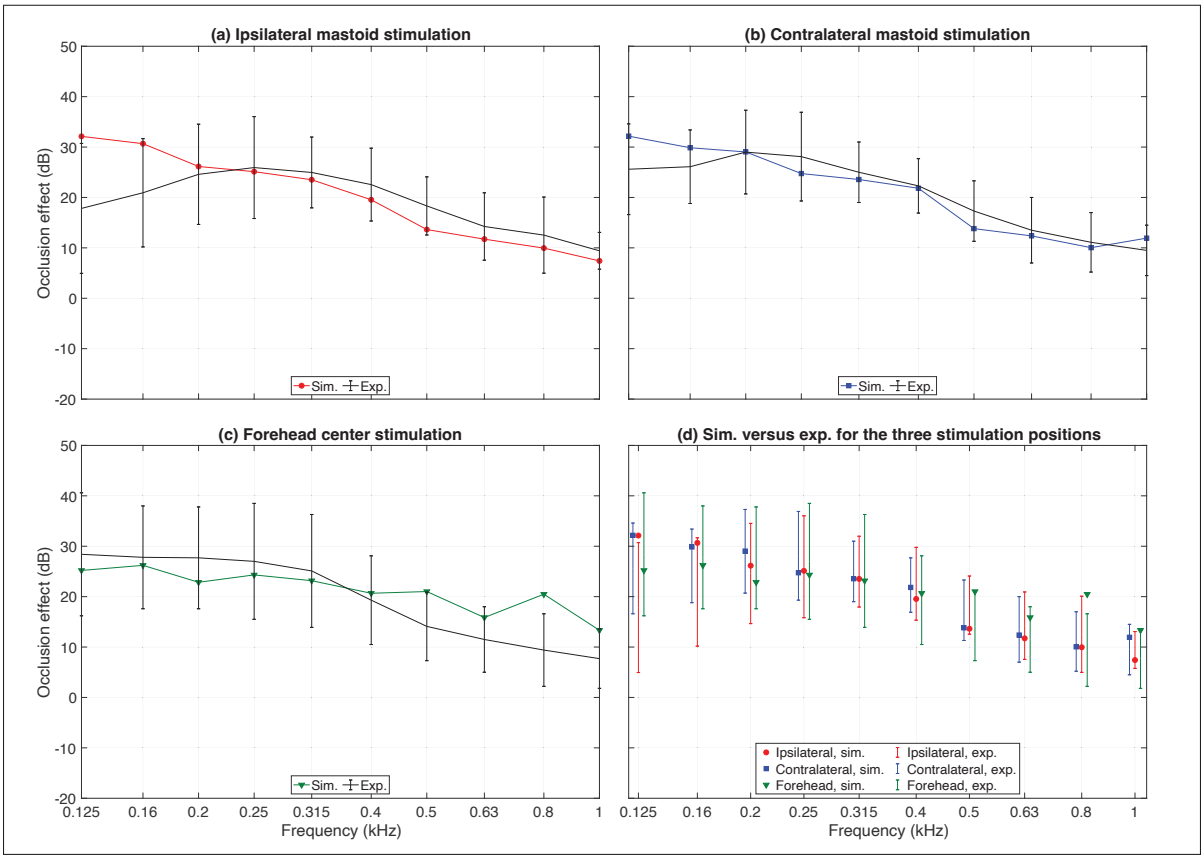

Figure 4.3 Simulated OEs of the mediumly inserted foam earplug for three different stimulation positions versus the corresponding experimental data of Reinfeldt *et al.* (2013)

4.1.1.3 Occlusion effects for different stimulation positions

Figure 4.3 compares the simulated OEs and the experimental OEs (mean ± S.D.) of Reinfeldt *et al.* (2013) for the ipsilateral mastoid (a), contralateral mastoid (b) and forehead center (c) stimulations, respectively. The simulation results (markers) and experimental data (error bars) for the three positions are all presented in Figure 4.3(d). Note that in the experiments, the inserted part of the foam earplug is about 10 mm long , whereas in the simulations, the middle insertion depth of the foam earplug is about 14.3 mm. As can be seen from the figure, the simulated OEs for the three stimulation positions are generally within one standard deviation of the corresponding experimental data in the whole frequency range (0.125 – 1.0 kHz). For the forehead stimulation, the simulated OE fluctuates in the 0.5 – 0.8 kHz frequency range, which can also be noticed in the individual OE measurements of Stenfelt & Reinfeldt (2007). Although there seems to be a local maximum at 0.8 kHz, looking at the narrow band simulated SPLs in the open and occluded ECs for explaining this OE behavior do not point out any obvious resonance or antiresonance phenomenon.

Figure 4.3(d) shows that the three stimulation positions generate similar simulated OEs in the 0.25 – 0.4 kHz frequency range. In the entire frequency range of interest (0.125 – 1.0 kHz), the difference between the OEs for the two mastoid stimulations is about 1.2 dB on average, whereas the difference between the OEs for the ipsilateral mastoid and forehead stimulations is about 4.5 dB on average. Different vibration directions excite the structures differently and affect the energy exchanges between the various domains. As the two mastoid stimulations are placed at approximately symmetric positions across the midsagittal plane of the head which itself is quasi-symmetric, they excite the head in approximately opposite directions. It is therefore reasonable to have rather similar acoustic responses in the EC for the two mastoid stimulations. On the other hand, the forehead stimulate excites the head in a different direction from the mastoid stimulations, thus leading to a relatively different acoustic response in the EC. Besides, in the experimental study of Reinfeldt *et al.*, a statistically significant difference was found at 0.125 kHz between the OEs for the ipsilateral mastoid stimulation and the other two stimulation positions, which was attributed by these authors to the ST that were more excited for this position

compared with the others at low frequencies. However, this difference is not observed in the present simulation results. This may be due to the specific head considered in the study and this needs further investigations. The above-mentioned similarities and differences between the OEs of the three stimulation positions are also observed for the cases of shallowly and deeply inserted foam and silicone earplugs but the associated results are not presented here for the sake of conciseness.

4.1.1.4 Occlusion effects for different earplug types

Figure 4.4 shows the simulated OEs for the foam and silicone earplugs in four third octave bands (0.125, 0.25, 0.5, and 1.0 kHz) in comparison with the experimental OEs of Brummund *et al.* (2015). During the measurements, the insertion depths of the foam earplug were between 8.5 mm and 13.7 mm and those of the silicone earplug were between 10.4 mm and 13.0 mm. Simulation results for the shallowly (8.4 mm), mediumly (14.3 mm), and deeply (20.7 mm) inserted earplugs are all presented in the figure. The simulated OEs for the shallow and middle insertions of the two earplug types lie all within one standard deviation of the corresponding experimental results since the two insertion depths in the simulations are close to those chosen in the experiments. However, since the deep insertion in the simulations is deeper than those in the experiments, the simulated OEs for this insertion may fall outside one standard deviation of the corresponding experimental results, such as at 0.5 kHz and 1.0 kHz for the foam earplug and at 0.5 kHz for the silicone earplug.

At 1.0 kHz, there is an increase in the simulated OE generated by the silicone earplug for the three insertions, which is not observed for the foam earplug. A similar phenomenon in the 1.1 – 1.8 kHz frequency range was observed in the study of Brummund *et al.* (2014). Through a study of power balance, Brummund *et al.* attributed this phenomenon to the increase in the power radiated by the medial surface of the silicone earplug into the EC cavity.

Figure 4.4 indicates that the simulated OE generated by the silicone earplug is larger than that by the foam earplug for a given insertion depth, which is in accordance with the experimental

results. The differences between the simulated OEs of the two earplugs get more significant with the insertion depth, which is in accordance with the observation in Lee's experimental study using a foam earplug and a medical balloon type earplug made of silicone (Lee, 2011). Lee found that the statistically insignificant difference in the OEs between the two earplugs at a 2 mm insertion became significant at a 11 mm insertion.

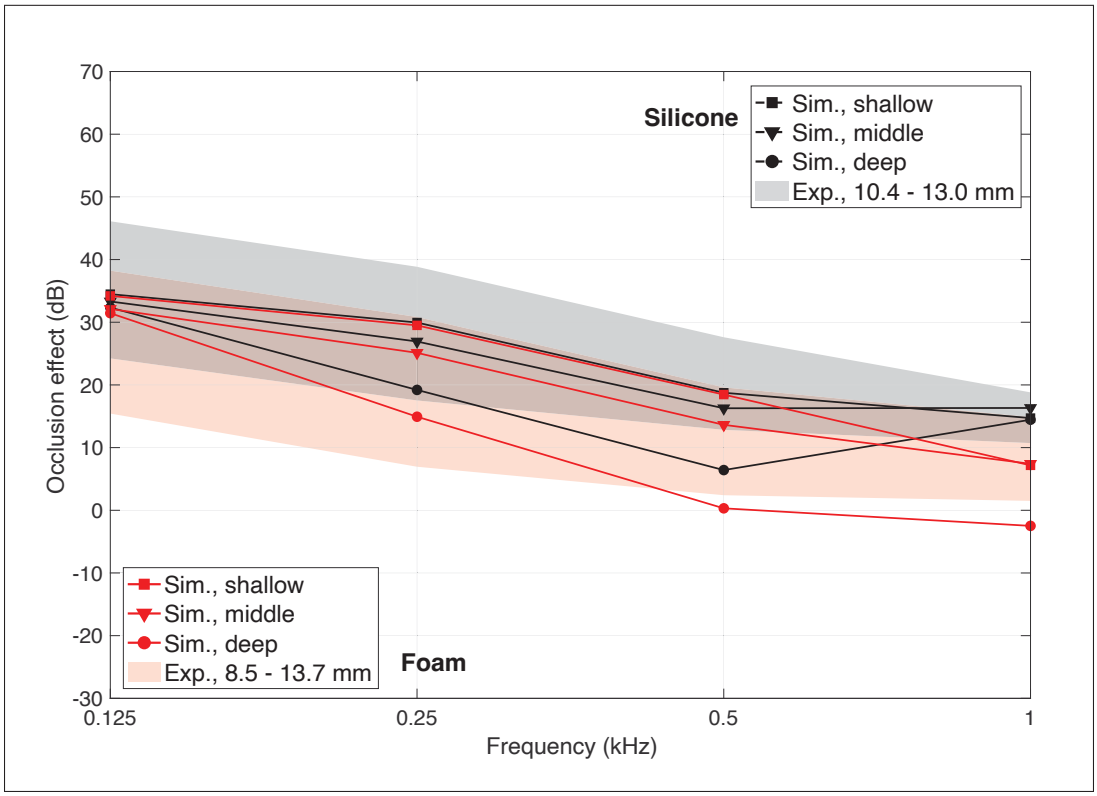

Figure 4.4 Simulated OEs of the foam and silicone earplugs at various insertion depths for the ipsilateral mastoid stimulation versus the experimental data of Brummund *et al.* (2015) (mean ± S.D.) in four selected third octave bands

4.1.2 Comparison with the experimental data obtained on the acoustic test fixture

The FE head model is then evaluated using the experimental data obtained on the augmented ATF with the foam earplug inserted shallowly into the EC. It is worth mentioning that the evaluation of the ATF itself is presented in Section 4.2. Figure 4.5 compares the simulated and experimental OEs for the case of the ATF. The simulated and mean experimental OEs are found

to agree with each other quite well, both having a relatively steady tendency with frequency, which is discussed in Section 4.2. The largest difference between them is about 3 dB at 0.63 kHz, while for the rest frequencies, their differences are less than 3 dB. However, it can also be observed that in the frequency range from 0.5 kHz to 1.0 kHz, the simulated OE is outside the boundaries of the experimental standard deviations.

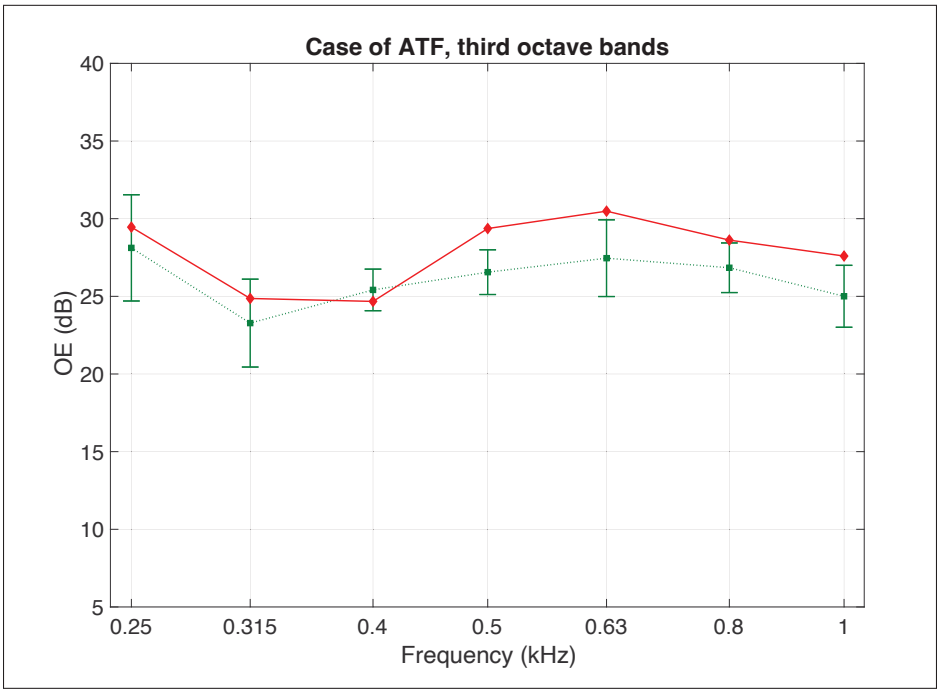

Figure 4.5 Comparison between the simulated OE and the experimental OE (mean ± S.D.) for the case of the ATF

In the following, for explaining the difference between the simulated and experimental OEs, several factors related to the FE modelings of the earplug and the ATF as well as the experimental setup are discussed. It is probable that the difference between the simulated and experimental OEs results from a combination of several factors rather than a single factor.

- FE modeling of the earplug: The modeled foam earplug is different from the probed foam earplug used in the experiments.
  - In terms of the material properties, the data used in the simulations are adopted from the literature due to the difficulty of direct measurements. In addition, the material properties

of the earplug depend also on its compression rate when it is inserted into the EC, which is in reality spatially inhomogeneous. To have an idea of the extent to which the material properties of the earplug affect the OE, a supplementary study is carried out. The effects of the Young's modulus, density and Poisson's ratio of the foam earplug are studied by a 2^3 full factorial design of experiment using the FE model of the ATF. The lower and upper levels of each parameter correspond to the original value of the parameter and a variation of +50% departing from this value, respectively (see Table 4.2). Results (not presented here) show that these properties have an influence of about 1 – 5 dB on the OE in the concerned frequency range (both the main effects and interactions are concerned). As a result, the material properties of the earplug may be an important factor for explaining the differences between the simulated and experimental OEs observed in Figure 4.5.

  - In terms of the geometry, the modeled earplug ignores the probe tube passing through the real earplug and the protruding part in the concha bowl in practice. Its geometry is also simpler compared with the part of the real earplug that is inserted into the EC, since it is challenging to reproduce the latter. Due to the technical difficulty in replicating the realistic geometry of the earplug, including both the inserted and non-inserted parts, its effect on the simulated OE is thus not investigated here.

- FE modeling of the ATF
  - Stimulation position: The stimulation position in the model may differ slightly from the position of the transducer in the experiments and could lead to a difference of about 0 – 3 dB in the simulated OEs (more details are given in Section 4.3.5).
  - Boundary conditions: The free head base in the model may not correspond exactly to the experiments. The ATF is placed on a soft cushion during the experiments. From an acoustical viewpoint, there is hardly sound radiation from the ATF bottom. However, in the model, the head base can still radiate sound into the external air domain and may somewhat contribute to the simulated OE. Mechanically speaking, the ATF bottom is not totally freely movable. A supplementary numerical study (results not presented here) is carried out to investigate the effect on the simulated OE of various boundary conditions at the head base in the FE model of the ATF. The tested boundary conditions include free,

fixed and elastic ones. For the latter, total spring constants between 10^5 N/m and 10^{18} N/m are considered. These two values are chosen since their corresponding simulation results are almost the same as the results for the free and fixed boundary conditions, respectively. Slight differences between the various cases are found around 0.63 kHz. At this frequency, compared with the free case, the OE magnitude for the fixed case is 0.3 dB higher, while the OE magnitude for the elastic boundary with a total spring constant of 10^9 N/m is 0.6 dB lower. In addition, the differences in the OE between the various cases are also found to be related to the SPL in the open EC rather than the occluded EC.

- ATF materials: In the model, the materials of the ATF are assumed to be linear elastic isotropic with constant structural loss factors, while they may exhibit more complex behaviors in reality (e.g., nonlinear, visco-elastic, and anisotropic with loss factors varying with frequency). Besides, the parameter study presented in Section 4.3.3.1 may give an idea of how the material properties of the EC surrounding tissues would affect the OE, for example, the Young's moduli of the EC surrounding tissues could have an effect on the OE of as much as 6 dB in the frequency range of 0.25 – 1.0 kHz.
- EC model: In the FE model of the ATF, the insertion of the earplug is assumed not to deform the EC due to the lack of knowledge about how the EC geometry is modified and about the mechanical properties of the EC surrounding tissues under prestress which could lead to a stiffer system and thus a lower OE (Carillo *et al.*, 2021a). The effect of neglecting the prestress is not investigated quantitatively in this thesis.
- Manufacturing defects: Due to manufacturing defects, the ATF does not completely correspond to the head model in terms of geometry. Through a computed tomography scan, tiny air bubbles are found inside the ATF, especially inside the bone mimicking material. Although a FE model could be used to evaluate the effect on the OE of the manufacturing defects by taking them into account in the head geometrical model, this is time-consuming (and even challenging) and could not be completed in this thesis.

• Experimental setup

- Position in the EC where the OE is evaluated: Although the experimental and simulated OEs are both evaluated at the position of the medial surface of the shallowly inserted

earplug, the exact positions in the EC may not be the same in the experiments and simulations, due to the difficulty of reproducing the geometry of the inserted part of the earplug in the model. This may introduce a difference of around 1 dB in the resulting OEs (more details are given in Section 4.3.4).

- Device for measuring the SPL in the open EC: In the frequency range of interest, the open earpiece in contact with the EC walls may affect the measured SPL by up to 2.5 dB compared with the probe tube contactless with the EC walls (see Section 3.3.1.2).
- Besides, the assessment of the airborne sound transmitted from the transducer housing into the EC (see Section 3.3.1.1) shows that the combination of the bone conducted sound and airborne radiation is more than 13.9 dB for most frequencies (7.6 dB for 1.0 kHz) above the airborne radiated sound. It is therefore unlikely to contribute to the experimental results.

Table 4.2 Upper and lower limits of each property regarding the foam earplug adopted in the 2^3 full factorial design of experiment

	Young's modulus [MPa]	**Density [kg/m^3]**	**Poisson's ratio**
Upper limit	0.1	220	0.1
Lower limit	0.15	330	0.15

4.1.3 Comparison with the experimental data obtained on the participant

Finally, the FE head model is evaluated by the experimental data obtained on the participant. Figure 4.6 compares the simulated and experimental OEs for the case of the participant. Note that the experimental data for the participant is also used to evaluate the ATF, which is presented in Section 4.2. In Figure 4.6, the simulated and experimental OEs for the participant generally agree with each other in the frequency range of interest. Their difference is about 5 dB at 0.4 kHz and 0.5 kHz, and about 3 dB or less at the other frequencies. These differences could be attributed to most of the factors discussed in Section 4.1.2 as well as the locally reacting acoustic impedance defined at the eardrum surface. The latter is based on Shaw & Stinson's model (see Section 3.1.3), which probably differs from the actual eardrum impedance of the participant. The

substitution of the real eardrum impedance of the participant by Shaw & Stinson's impedance model can generate a maximum difference of 3 dB in the simulated OEs (see Section 4.2).

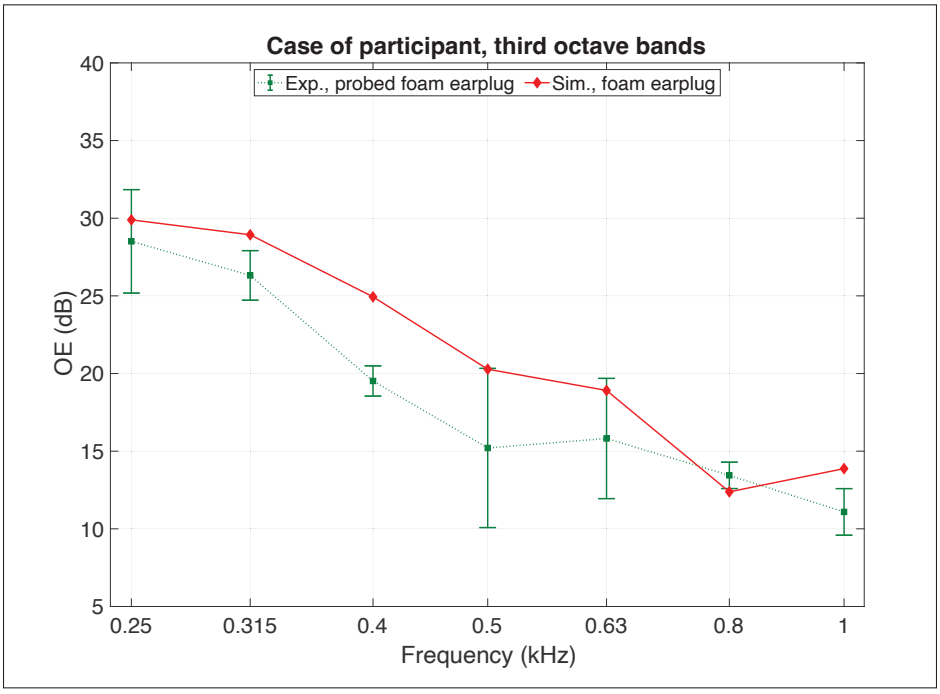

Figure 4.6 Comparison between the simulated OE and the experimental OE (mean ± S.D.) for the case of the participant

Besides, a few remarks should be made regarding some of the factors discussed in Section 4.1.2 for the case of the participant.

- Regarding the boundary condition, the simulated OE for the free head base is chosen to compare with the experimental OE, but an elastic head base would *a priori* correspond better to the reality. However, according to the results shown in Section 4.3.1, the simulated OEs for the shallowly inserted foam earplug are almost the same for the free and fixed head bases in the frequency range from 0.25 kHz to 1.0 kHz. The boundary condition is thus unlikely to contribute to the differences between the simulated and experimental OEs here.
- Concerning the geometry of the head model, it differs from the participant's head due to (i) the simplifications and (ii) the artifacts in the medical images for reconstructing the head geometry (see also Section 3.1.1.1). The associated effects are challenging to evaluate and could not be investigated in this thesis.

- Concerning the material properties of the biological tissues as well as of the foam earplug adopted in the model, they were obtained at different temperatures (e.g., ambient or other temperatures), whereas the OE measurements on the participant are carried out at body temperature. In addition, the material properties of the biological tissues are not obtained on the participant due to the measurement difficulty and ethical issues but rather from the literature. However, in the frequency range 0.315 – 0.5 kHz, the parameter study on the material properties of the EC surrounding tissues presented in Section 4.3.3.1 shows that no single parameter significantly affects the OE. In this frequency range, the difference between the simulated and experimental OEs for the participant may result from a combined influence of the material parameters.

4.1.4 Summary

To conclude, the evaluation of the FE head model with respect to the experimental data available in the literature as well as those obtained on the ATF and the participant is quite satisfactory, keeping in mind that no attempt has been made to calibrate the parameters in the FE head model for getting closer results to the experimental data.

4.2 Evaluation of the acoustic test fixture

Figure 4.7 compares the experimental OE for the ATF with that for the participant. It can be observed that the OE for the participant decreases with frequency, from around 28 dB at 0.25 kHz to around 11 dB at 1.0 kHz. This agrees with the experimental and numerical studies in the literature (e.g., Reinfeldt *et al.*, 2013; Brummund *et al.*, 2015). On the other hand, the OE for the ATF does not vary much with frequency (as already observed in Figure 4.5). According to the case of the participant as well as the studies in the literature (e.g., Reinfeldt *et al.*, 2013; Brummund *et al.*, 2014), the OE is expected to decrease with frequency by about 12 – 20 dB from 0.25 kHz to 1.0 kHz. The OE for the ATF is around 28 dB at 0.25 kHz, which agrees with the value for the participant at the same frequency. However, it does not decrease as expected at frequencies above 0.5 kHz, with a value of around 25 dB at 1.0 kHz.

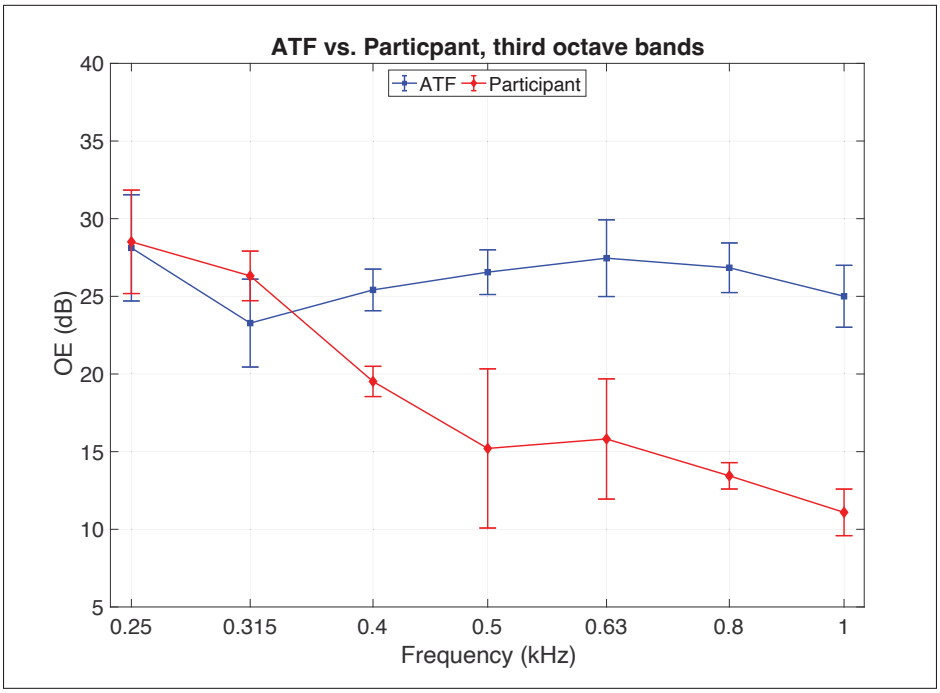

Figure 4.7 Comparison between the experimental OEs (mean ± S.D.) for the cases of the ATF and the participant

The primary reason is attributed to the materials used in the ATF. Comparing the material properties of the ATF with the reference material property set of the biological tissues adopted in the model for the participant (see Table 4.3), the most different parameters are the Young's moduli of the cartilage, the ST and the bone, as well as the density of the bone. At frequencies around 1.0 kHz, the parameter study in Section 4.3.3.1 shows that (i) the effect of the material properties of the bone is negligible, (ii) a lower Young's modulus of the ST reduces the OE, but (iii) a lower Young's modulus of the cartilage increases the OE. It thus seems reasonable to assume that the Young's modulus of the cartilage is the primary reason for the high OE magnitudes at high frequencies and should be increased inn future ATF. A supplementary study (results not presented here) using the ATF model is indeed carried out: the Young's modulus of the cartilage mimicking material is set to the same value as in the model for the participant (i.e., 7.2 MPa) rather than 1.65 MPa. As expected, the simulated OE at 1.0 kHz is decreased from 26.9 dB to 13.1 dB. However, although the OE is also decreased at frequencies between 0.5 kHz

and 0.8 kHz, it is still relatively high compared with the values in the case of the participant. There could be other material properties, together with the Young's modulus of the cartilage, that contribute to the relatively steady OE magnitudes as a function of frequency.

Table 4.3 Material properties of the ATF in comparison with the reference material property set of the participant

		E^* [MPa]	ρ [kg/m^3]	ν	η	c [m/s^2]
Cartilage	ATF	1.65	1 075	0.26	0.05	–
	Participant	7.2	1 080	0.32	0.3	–
ST	ATF	0.17	1 007	0.49	0.045	–
	Participant	0.5	1 030	0.45	$3 \times 10^{-5} \times f$	–
Bone	ATF	13 600	2 267	0.31	0.1	–
	Participant	8 000	1 700	0.335	0.1	–
Brain	ATF	0.094	990	0.31	0.05	–
	Participant	0.035	1 000	0.45	$3 \times 10^{-4} \times f$	–
Cerebrospinal fluid	ATF	–	1 000	–	–	1 498
	Participant	–	1 000	–	–	1 500

* E: Young's modulus, ρ: density, ν: Poisson's ratio, η: loss factor, c: speed of sound, f: frequency [Hz]

Additional remarks should be made here.

- Supplementary simulations are also performed to investigate the effect of replacing the eardrum and the small void behind it by the bone (see Section 3.3.2.1) using the model of the ATF. It is found that the simulated OE is about 3 dB lower than the simulation result displayed in Figure 4.5 in the entire frequency range of interest (i.e., 0.25 – 1.0 kHz). The OE at frequencies above 0.5 kHz is thus not much reduced and the behavior of the OE as a function of frequency remains unchanged. Therefore, the modification at the eardrum in the ATF model could not explain the behavior of the OE (high magnitudes) at high frequencies.
- The decrease with frequency of the OE induced by an acoustically rigid occlusion at the EC entrance was explained by the ratio between the acoustic impedances of the open and occluded EC cavities that decreases with frequency in the literature (Berger & Kerivan, 1983; Hansen, 1998; Stenfelt & Reinfeldt, 2007; Zurbrügg *et al.*, 2014; Carillo *et al.*, 2020). Recently, Carillo and his colleagues (2021a) showed that the OE induced by an earplug depends also on the ratio between the amplitudes of the volume velocities imposed on the

EC cavity by the EC walls and the earplug medial surface (for the occluded case). In this thesis, as shown in Figure 4.8, this ratio is found to increase with frequency for the case of using the material property set of the ATF, but to remain relatively steady with frequency for the case of using the reference material property set of the participant in the frequency range of interest (0.25 – 1.0 kHz). This should contribute to the different tendencies (steady vs. decreasing) of the OE with frequency for the two cases (ATF vs. participant).

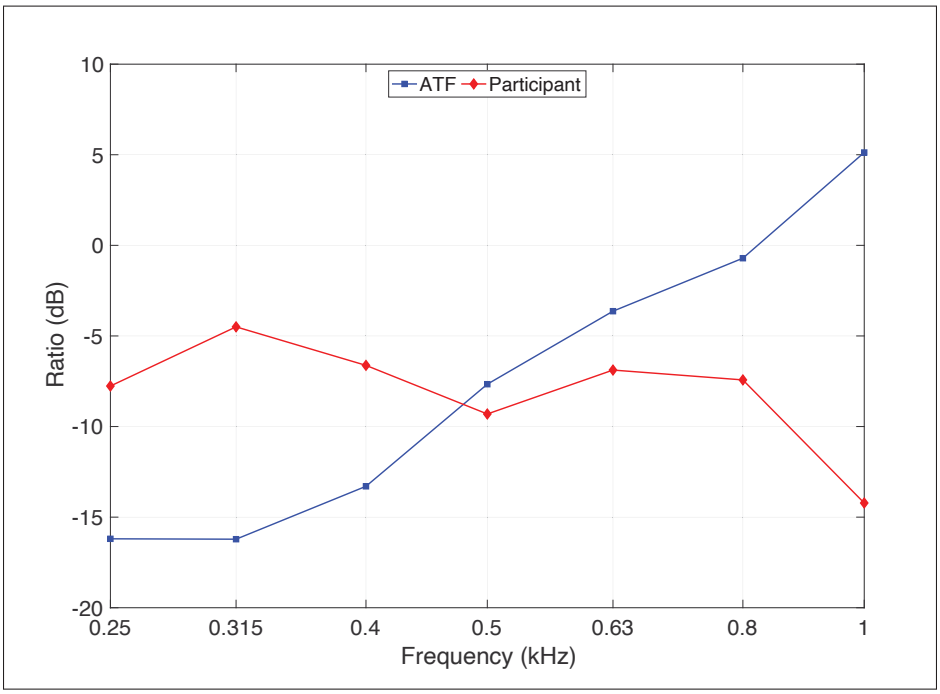

Figure 4.8 Ratios between the amplitudes of the volume velocities imposed on the occluded and open EC cavities ($20\log_{10}\left(|\hat{q}^{\mathrm{occl}}/\hat{q}^{\mathrm{open}}|\right)$) computed using the FE head model for the cases of the ATF and the participant

To conclude, the comparison between the experimental OEs obtained on the ATF and the participant shows that the present ATF cannot reproduce the OE measured on the participant that decreases with frequency. According to Section 4.1.3, the simplifications in geometry adopted by the ATF (also by the FE head model) are not responsible for the relatively steady OE tendency measured on the ATF. Therefore, the different OE tendencies observed in Figure 4.7 probably result from the differences in the mechanical properties between the materials used for

fabricating the ATF and the biological tissues. Future work could concentrate on the materials used for the ATF in order to have an improved ATF for assessing the OE. This could begin with mechanical tests on urethane-based soft resins of different hardnesses (Benacchio *et al.*, 2020). Another possible reason is that the temperature of the participant is higher than that of the ATF which is not heated during the experiments. This could also lead to different material mechanical properties of the earplug.

4.3 Factors affecting the simulated occlusion effect of the earplug

This section presents and discusses the effects on the simulated OE of several factors. First, the effect of the boundary condition at the head base is investigated to see if the present head model is improved compared with the FE models of truncated outer ears in terms of artificial boundaries (see Section 4.3.1). Second, different approaches for modeling the external air are compared to investigate how the sound radiation from the external ST affects the sound pressure in the open EC (see Section 4.3.2). Third, the effects of the material properties of the EC surrounding tissues are analyzed in order to verify the sensitivity of the OE to the tissue properties (see Section 4.3.3). Then, the influence of the position in the EC where the OE is evaluated (see Section 4.3.4) and the stimulation position (see Section 4.3.5) are explored for better understanding the variability of the experimental OE obtained on groups of participants in the literature. It is necessary to note that the conclusions in this section may be different if the simulations are configured differently, for example using other tissue material property sets and types of earplugs.

4.3.1 Boundary condition at the head base

Figure 4.9 compares the simulated OEs for the free and fixed head bases in the cases of shallowly, mediumly and deeply inserted foam earplugs and three different stimulation positions: (a) ipsilateral mastoid, (b) contralateral mastoid and (c) forehead center. For all the cases considered, the simulated OEs for both boundary conditions are close to each other at frequencies above 0.25 kHz. Unlike the FE models of truncated outer ears dealing with the OE which are sensitive to the

boundary and loading conditions applied on their artificial boundaries in the whole frequency range of interest (0.1 – 1.0 kHz) (Carillo *et al.*, 2020), the effect of the boundary condition at the head base is mainly found at very low frequencies (< 0.25 kHz). In this frequency range, the skull bone moves as a rigid body (Stenfelt & Goode, 2005b). Different boundary conditions cause different amounts of sound energy radiated into the EC cavity by the EC walls and the earplug medial surface (for the occluded ear case). No attempt is made to adjust the artificial boundary conditions to obtain the simulation results which better mimic the experimental data. It seems therefore reasonable to use the free boundary condition at the head base in the present study.

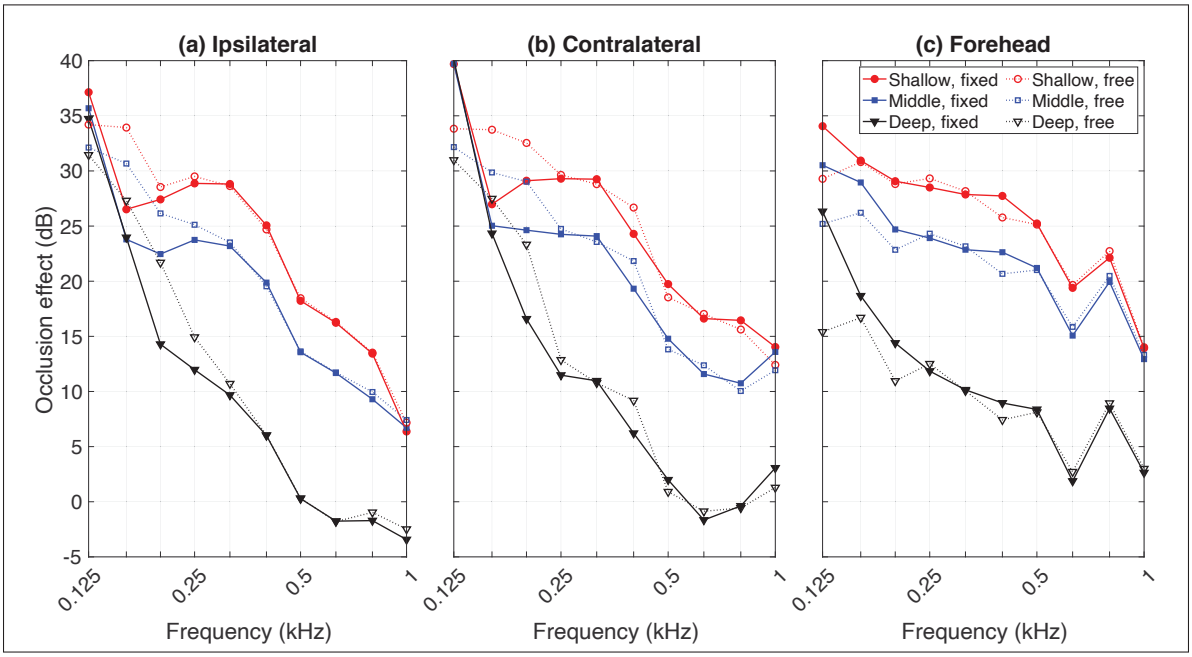

Figure 4.9 Simulated OEs of the foam earplug at various insertion depths, for the free and fixed head bases, and three stimulation positions

4.3.2 Modeling of the external air

Figure 4.10(a) displays the simulated OEs for the two approaches of modeling the external air, namely the perfectly matched layer (PML) approach and the radiation impedance approach, in comparison with the experimental OEs of Reinfeldt *et al.* (2013) and Brummund *et al.* (2015) in

third octave bands. Figure 4.10(b) presents only the corresponding SPLs in the open EC as the SPLs in the occluded EC are not affected by the external air.

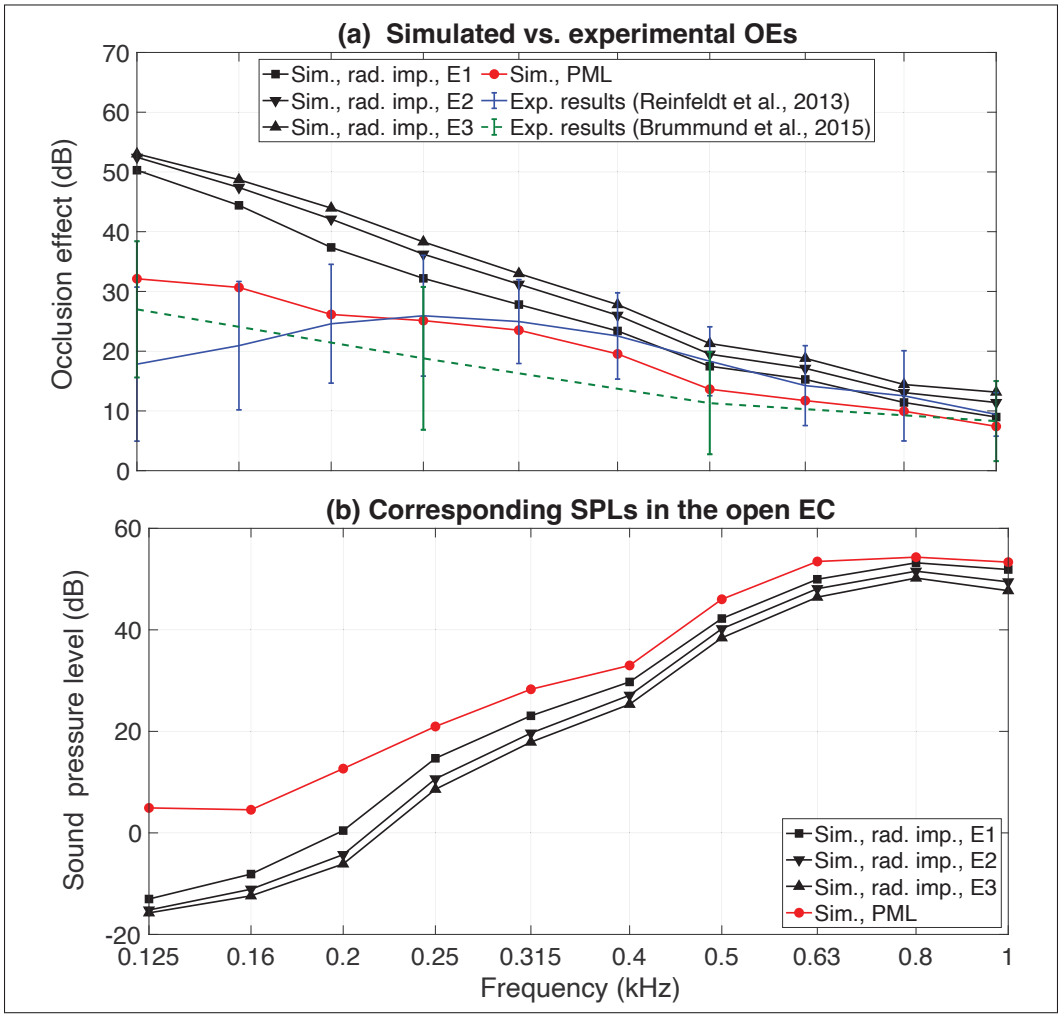

Figure 4.10 Simulated OEs with the fully coupled PML and radiation impedance (rad. imp.) at three different EC entrances (E1 – E3) (versus experimental data in the literature), and the corresponding SPLs at the eardrum surface in the open EC

By applying a radiation impedance over the EC entrance, the simulated OE is found to decrease with frequency with a slope of –40 dB/decade regardless of the position of the EC entrance. This behavior can be observed in the electro-acoustic models (Stenfelt & Reinfeldt, 2007; Hansen, 1998) and the FE models of truncated outer ears using either the radiation impedance approach (Brummund *et al.*, 2015; Carillo *et al.*, 2020) or using the PML approach (Sgard *et al.*, 2019)

in the literature. The OEs computed using these models were usually much larger than the experimental OEs at very low frequencies. This was attributed to the incomplete seal in the experiments which reduced the measured OEs. However, Figure 4.10 shows that the simulated OE using the present FE head model with the PML approach is comparable with the experimental data.

The difference between the simulated OEs with the PML and radiation impedance approaches can be attributed to two factors. First, by applying a radiation impedance, it is found that a 1 – 2 mm deeper EC entrance induces a 2 – 4 dB lower SPL in the open EC, thus a 2 – 4 dB higher OE amplitude. This is related to the EC impedance seen by its walls which depends on the chosen entrance position (Carillo *et al.*, 2020). The latter affects the acoustic mass of the open EC seen by its walls and the volume velocity imposed to the open EC (Carillo *et al.*, 2020). However, the entrance position does not fully explain the difference between the two approaches at frequencies below 0.3 kHz where the simulated OE with the radiation impedance approach can be up to 20 dB higher than with the PML approach. This could be explained by the second factor, i.e., the radiation from the head vibrations into the surrounding air that subsequently enters the open EC. It is with the entire head that this radiation can be accounted for adequately. However, note that the present discussion is limited to the cases where a bone conduction device is used to excite the external tissues. For the cases of using the physiological noises as excitation, such as chewing, where these tissues are excited differently, no reduction of the OE at low frequencies was observed in the experimental results (Saint-Gaudens, Nélisse, Sgard, Laville & Doutres, 2019). Consequently, the consideration of the entire head in the model in conjunction with the PML for considering the external air provides simulated OEs that better agree with the experimental data.

4.3.3 Material properties of the earcanal surrounding tissues

4.3.3.1 Statistical analysis on the tissue material properties

Figure 4.11 displays the simulated OEs for the various tissue material property sets listed in Table 3.3 (grey lines) which are compared with the experimental data of Reinfeldt *et al.* (2013) and Brummund *et al.* (2015). The inserted part of the earplug is about 10 mm long in the measurement of Reinfeldt *et al.* and 8.5 – 13.7 mm in the measurement of Brummund *et al.* It is found that the individual simulated OEs for different tissue material property sets fall almost all within one standard deviation of the experimental data.

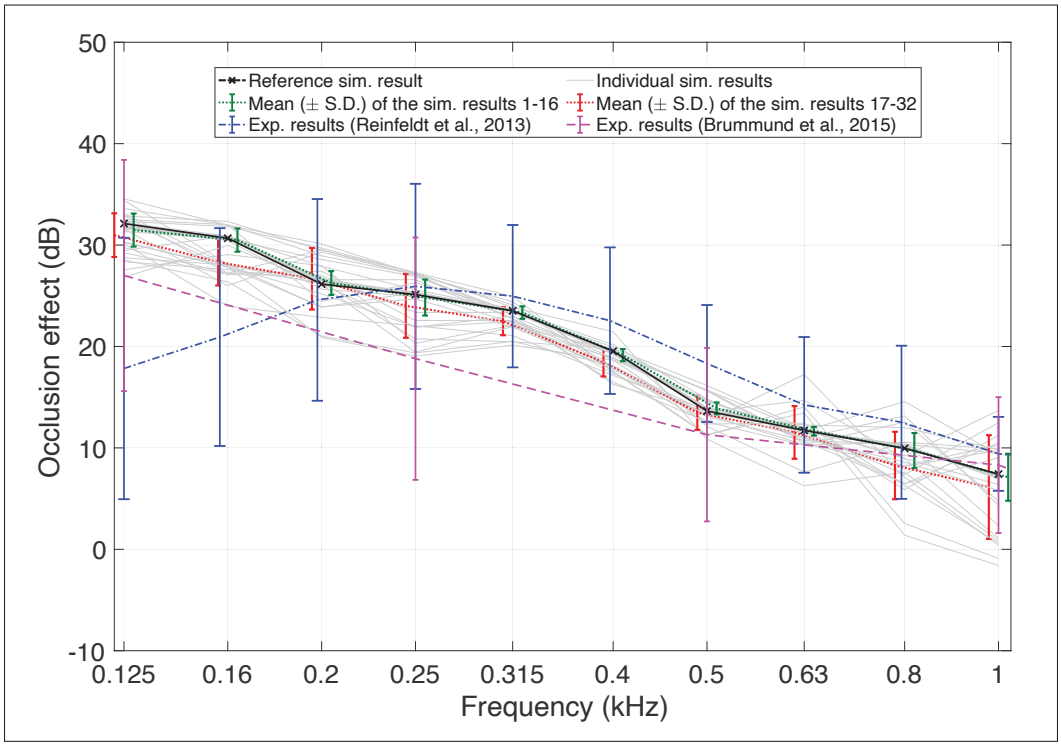

Figure 4.11 Simulated OEs for various tissue material property sets compared with experimental data in the literature. The mediumly inserted foam earplug, ipsilateral mastoid stimulation and free head base are used

The simulation results also highlight the variability of the OE induced by the changes in the material properties of the EC surrounding tissues. As the computed standard deviations for

both the “one factor at a time” method and the definitive screening design (i.e., the three-level fractional factorial design) are much lower than the measured standard deviation of a group of participants, there may be other factors which are controlled for in the simulations contributing to the widespread measured OEs between individuals, such as the head (ear) geometry and the positions of microphones. With the geometry of the head model controlled for, the variation of the tissue material properties can be regarded as an intra-individual difference due to the fact that an individual’s tissue material properties vary with age. It is also found that the standard deviation obtained by the “one factor at a time” (sims. 1 – 16, green dotted curve with error bars) method is lower than that by the definitive screening design (sims. 17 – 32, red dotted curve with error bars). This suggests that the interactions between the parameters play important roles in the variation of the OE.

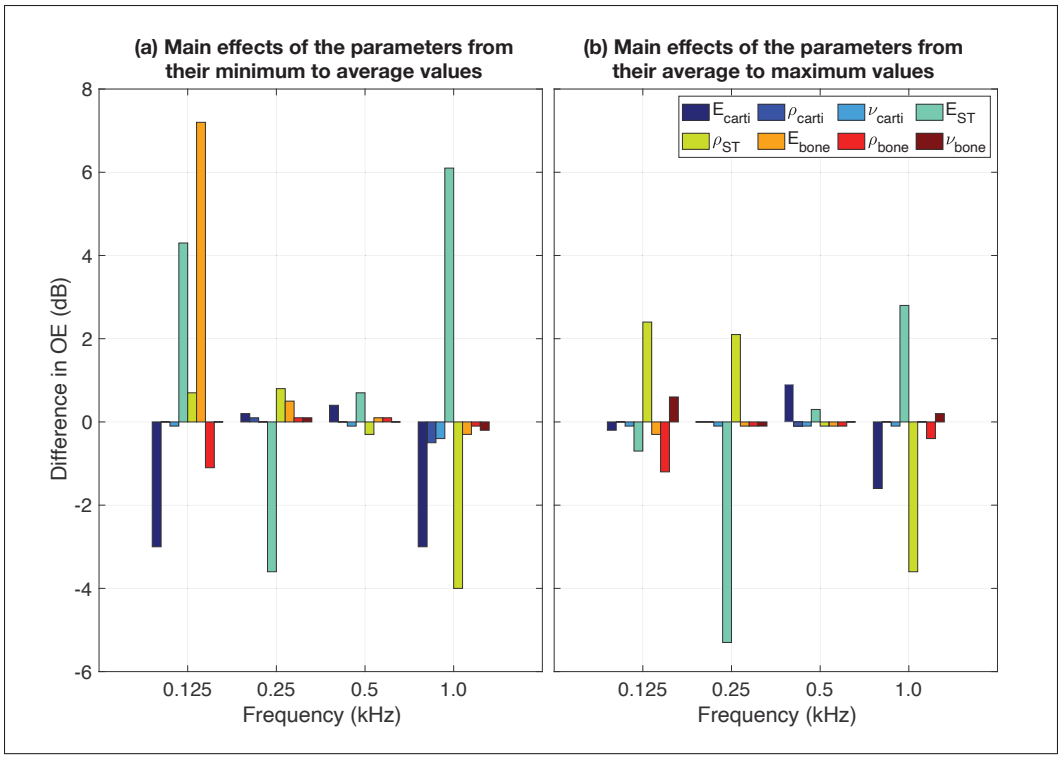

Figure 4.12 Effects on the OE of the material properties of the EC surrounding tissues in four selected third octave bands

Figure 4.12 shows the effect on the OE (dB, in four third octave bands) of each parameter by varying it from its minimum value to its average value, then from its average value to its maximum value. An effect less than 1 dB is considered to be negligible. It can be observed that the material properties of the ST and the cartilage affect the OE the most. Their effects depend largely on the frequency band of interest, the OE being more affected by a change in the ST material properties than those of the cartilage. Another interesting finding is that the OE at low frequencies is sensitive to the Young's modulus of the skull bone. A lower Young's modulus of the skull bone can reduce the OE amplitude in the 0.125 kHz frequency range by up to 7 dB.

The findings of the statistical analysis may be difficult to validate experimentally, but they can still give some insights into how different biological tissue material properties and the interactions between them affect the OE. In addition, they provide clues for calibrating the model through experimental measurements on the participant.

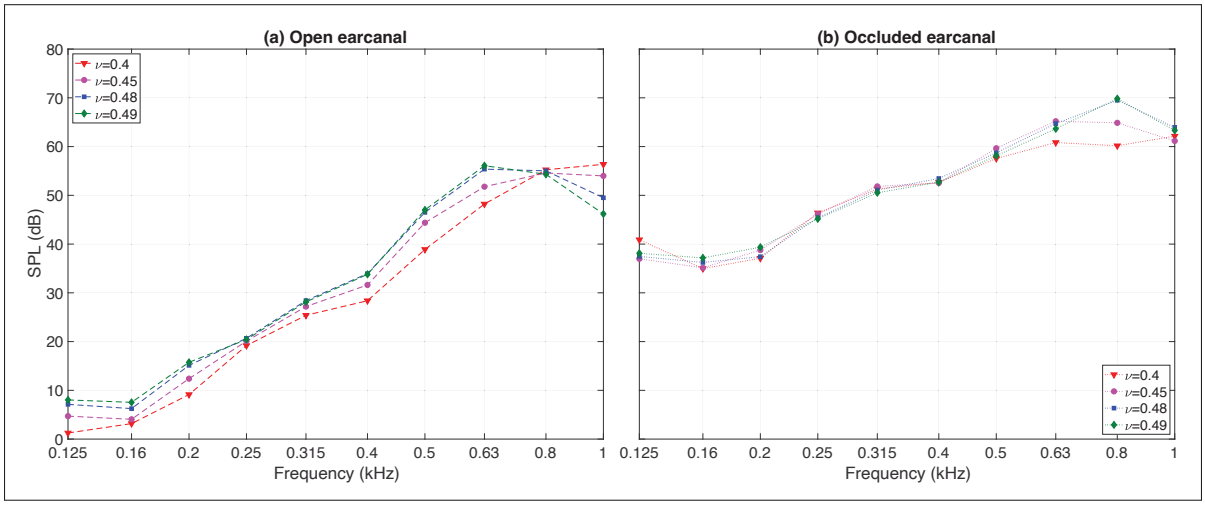

Figure 4.13 SPLs in the ECs open and occluded by the mediumly inserted foam earplug for different ST Poisson's ratios

4.3.3.2 Study on the effect of the soft tissue Poisson's ratio

Figures 4.13(a) and (b) show the simulated SPLs in the open and occluded ECs, respectively, for different values of ST Poisson's ratio (i.e., 0.4, 0.45, 0.48, and 0.49) (see dashed red curve

with downward triangles, dashed purple curve with circles, dashed blue curve with squares, and dashed green curve with diamonds).

In Figure 4.13(a), a common phenomenon can be observed in the open case at frequencies up to 0.8 kHz that the SPL becomes higher as the Poisson's ratio increases. Supplementary simulation results of the volume velocity computed on the EC lateral walls show that the increase in the Poisson's ratio intensifies the vibration of the EC walls, and thus increases the sound radiation into the EC cavity. In particular, the blue and green curves are almost overlapping in most of the frequency bands studied due to very close values of ST Poisson's ratio. However, the phenomenon that the SPL increases with the Poisson's ratio cannot be clearly observed in Figure 4.13(b), since the SPL in the occluded EC is not only attributed to the radiation of the EC walls (i.e., ST), but also involves the earplug/EC walls interaction and the radiation of the earplug medial surface (Carillo *et al.*, 2021a). The volume velocities calculated on (a) the non-occluded part of the EC walls and (b) the earplug medial surface in the occluded case are provided in Figure 4.14 for further analyzing the influence of ST Poisson's ratio on the SPL in the occluded EC.

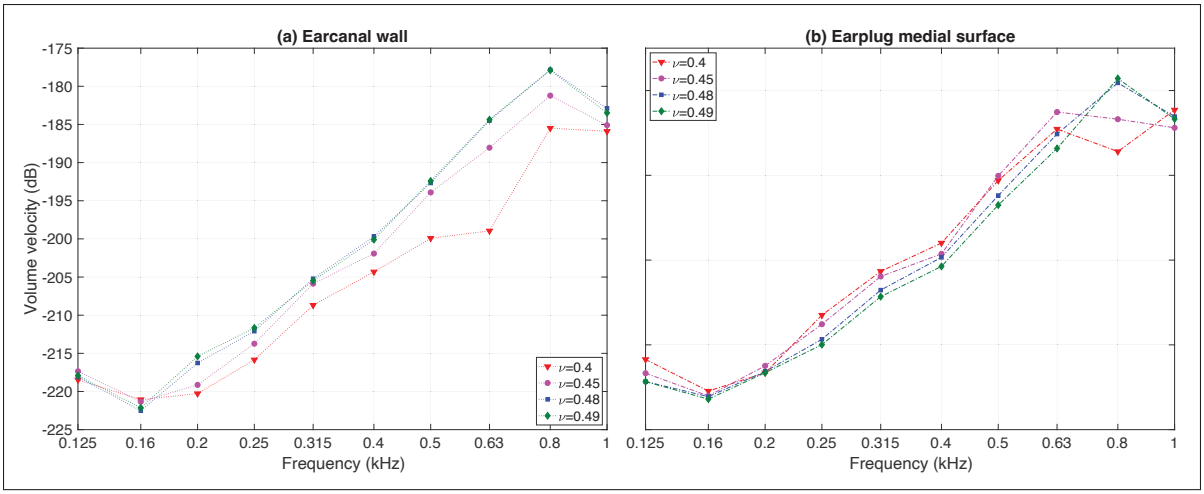

Figure 4.14 Volume velocity (dB, factor 20, ref. 1 m^3/s) imposed by the non-occluded part of the EC walls and the earplug medial surface for different ST Poisson's ratios

In Figure 4.14(a), a phenomenon similar to that observed in the open case is clearly found at frequencies above 0.2 kHz, i.e., the increase in the Poisson's ratio leads to an increase in the volume velocity on the EC walls, and thus intensifies the sound radiation from the latter into the EC cavity. However, a completely opposite tendency is observed between the volume velocity (on the earplug medial surface) and ST Poisson's ratio at frequencies from 0.2 to 0.5 kHz in Figure 4.14(b). It appears that in this case, the increase in the Poisson's ratio decreases the mechanical energy transferred from the ST into the earplug via the EC walls, and as a result decreases the sound radiation from the earplug medial surface into the EC cavity.

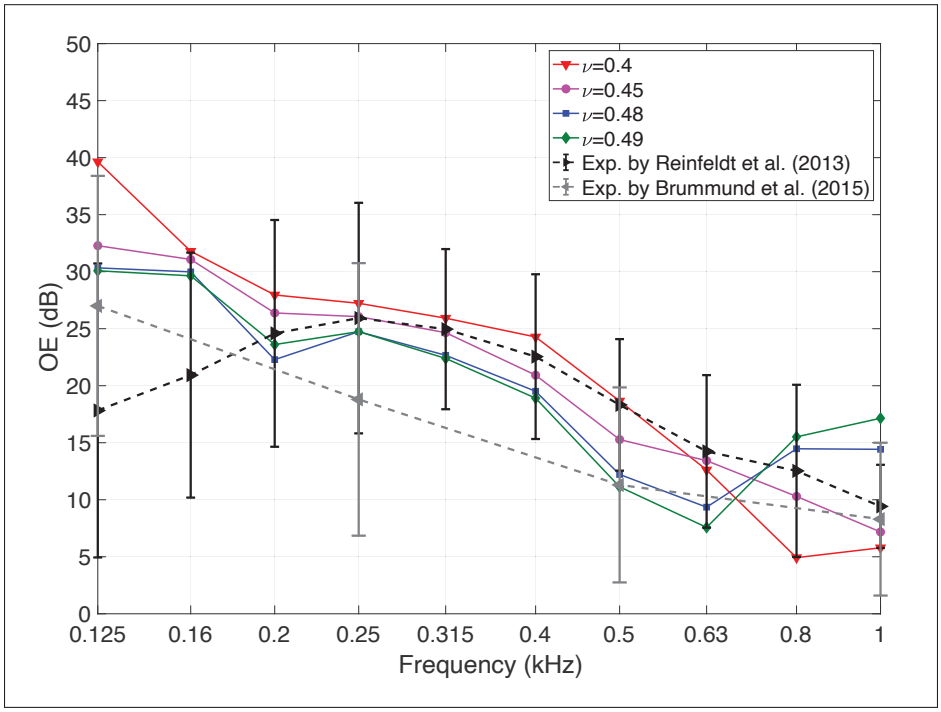

Figure 4.15 OEs of the mediumly inserted foam earplug for different ST Poisson's ratios

Figure 4.15 shows the corresponding OEs for different values of ST Poisson's ratio, together with experimental data[1] of Reinfeldt *et al.* (2013) and Brummund *et al.* (2015) displayed respectively using dashed black and dashed grey curves. It can be observed that the OE simulation results

[1] The simulation results in Sections 4.3.2 and 4.3.3 are not compared with the experimental data obtained on the participant of this project due to different earplug insertion depths used for the simulations and experiments.

either lie within the range of the experimental data or are quite close to them in the whole frequency range concerned. Overall, the OE is found to decrease at frequencies up to about 0.63 kHz as the Poisson's ratio increases. As explained above, this observation should be related to the increase of the SPL in the open EC when the ST Poisson's ratio increases. In higher frequency bands, the evolution of OE with the ST Poisson's ratio is less obvious possibly due to a more complicated behavior of the system. Moreover, the differences between the OEs obtained with various ST Poisson's ratios are not negligible, and rather pronounced at 0.5 kHz and above, especially around 1.0 kHz where a difference of up to 13 dB can be found. This indicates that the ST Poisson's ratio alone has an important influence on the OE in the associated frequency bands. Such a finding could also partially explain the inter-individual variability of the OE observed on human subjects.

4.3.4 Influence of the position in the earcanal where the occlusion effect is evaluated

Figure 4.16(a) shows the SPLs in the open EC computed at the positions of (i) the medial surface of the shallowly inserted earplug (black solid curve), (ii) the medial surface of the mediumly inserted earplug (red dash-dotted curve with plus signs), (iii) the medial surface of the deeply inserted earplug (blue dashed curve with circles) and (iv) the eardrum surface (green dotted curve with diamonds) respectively. It can be seen that the SPLs computed at the medial surfaces of the mediumly and deeply inserted earplugs are in almost perfect agreement with that computed at the eardrum surface. The SPL computed at the medial surface of the shallowly inserted earplug differs a bit more evidently from that computed at the eardrum surface, but with a mean difference of lower than 1 dB (i.e., 0.88 dB) in the interested frequency range. It appears that the difference between the SPL computed at a position in the open EC and that computed at the eardrum position is negligible.

Figure 4.16(b) shows the SPLs in the EC occluded by the shallowly, mediumly and deeply inserted earplugs computed at the earplug medial surface (red solid curves with squares, circles and diamonds respectively) and the eardrum surface (blue dashed curves with squares, circles and diamonds respectively). It can be seen that in the occluded EC, for a given insertion depth,

the SPLs computed at the earplug medial surface and the eardrum surface are quite similar to each other in the interested frequency range with the largest difference of only 0.6 dB found at 1.0 kHz for the shallow insertion case.

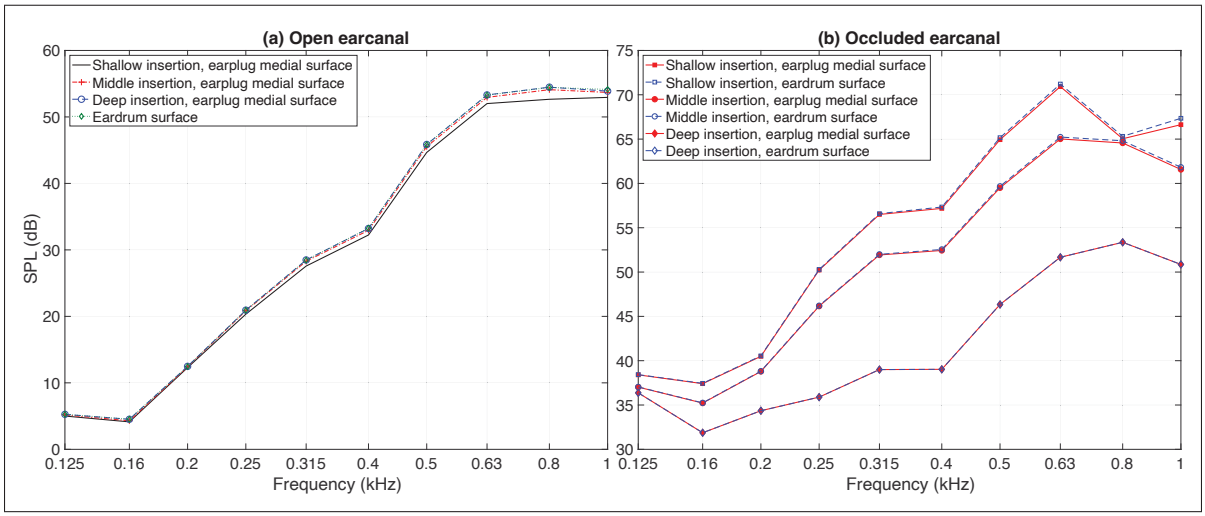

Figure 4.16 SPLs in the open and occluded ECs computed at the eardrum surface and at the earplug medial surface, respectively

As a result, as can be observed from Figure 4.17, the OEs evaluated at the earplug medial surface and the eardrum surface are in almost perfect agreement for the mediumly and deeply inserted earplug case. The OE evaluated at the earplug medial surface is about 1 dB higher than the OE evaluated at the eardrum surface for the shallowly inserted earplug cases. This suggests the similarity between the OEs computed at the earplug medial surface and the eardrum surface regardless of the insertion depth of the earplug.

For better understanding this observation, Figure 4.18 shows the sound fields in the open as well as the shallowly occluded ECs at three chosen frequencies (i.e., 0.125 kHz, 0.5 kHz and 1.0 kHz) as examples. In the open EC, at very low frequencies (e.g., 0.125 kHz), the sound field can approximately be considered to be uniformly distributed with the SPLs at different positions showing a difference of less than 2 dB (see Figure 4.18(a)). However, at higher frequencies, the uniformly distributed sound field can only be found in the inner portion but not the outer portion of the open EC (see Figures 4.18(b) and (c)). Close to the EC entrance, the variation of the SPL

is about 8 dB at 0.5 kHz and up to 12 dB at 1.0 kHz. This explains why in Figure 4.16(a), the black curve is more different from the other two at higher frequencies. According to (Carillo *et al.*, 2020), the SPL varies between the EC entrance and approximately the curvilinear position of the EC wall normal velocity centroid due to the acoustic mass of the EC outer portion, while it is almost homogeneous up to the eardrum position due to the acoustic compliance of the EC inner portion. In the EC occluded by the earplug, regardless of the frequency, the sound field is always approximately spatially uniform (see Figures 4.18(d) – (f)). This has been explained by the acoustic compliance of the EC in the study of Carillo *et al.* (2020) which uses an acoustically rigid occlusion at the EC entrance. As a result, for the shallow insertion case, the OEs obtained for the two positions are slightly different from each other since the sound field near the EC entrance is not uniformly distributed, whereas for the middle and deep insertion cases, the OEs computed at the earplug medial surface and the eardrum surface are nearly equal. It can also be deduced that the OEs obtained for the two positions could be more different if the insertion depth were shallower.

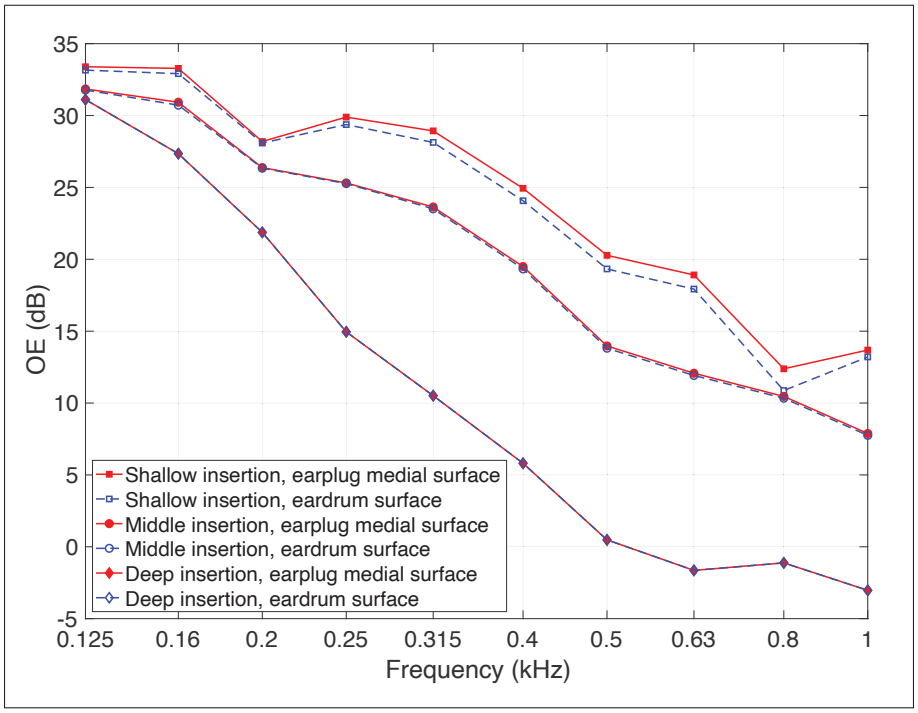

Figure 4.17 OEs computed at the eardrum surface versus OEs computed at the earplug medial surface

Finally, the above findings suggest that the position in the EC where the sound pressure is evaluated can explain partially the differences between the simulated and experimental OEs in Sections 4.1.2 and 4.1.3, given that these differences are less than 3 dB for most of the frequencies of interest. More precisely, due to the difficulty of reproducing the geometry of the earplug inserted into the EC, the earplug medial surface in the simulations and experiments could not be the same. To recall, the medial surface of the shallowly inserted earplug is the position adopted in the simulations and experiments mentioned in Sections 4.1.2 and 4.1.3 for evaluating the SPL in the EC. In other words, the simulated and experimental OEs may be evaluated at different positions, which could contribute partially to the differences between them. On the other hand, it appears that the measurement position of the SPL in the EC (not too close to the EC entrance) under a bone-conducted stimulation may not be a significant contributor to the large variability of the experimental OEs in the literature. It is therefore reasonable to place the microphone at a distance from the eardrum (e.g., at the position of the earplug medial surface) to measure the SPL in the EC. The advantage of this setup compared with those with a microphone or probe tube position close to the eardrum is that it is safer and more comfortable for the participant but can provide very similar results.

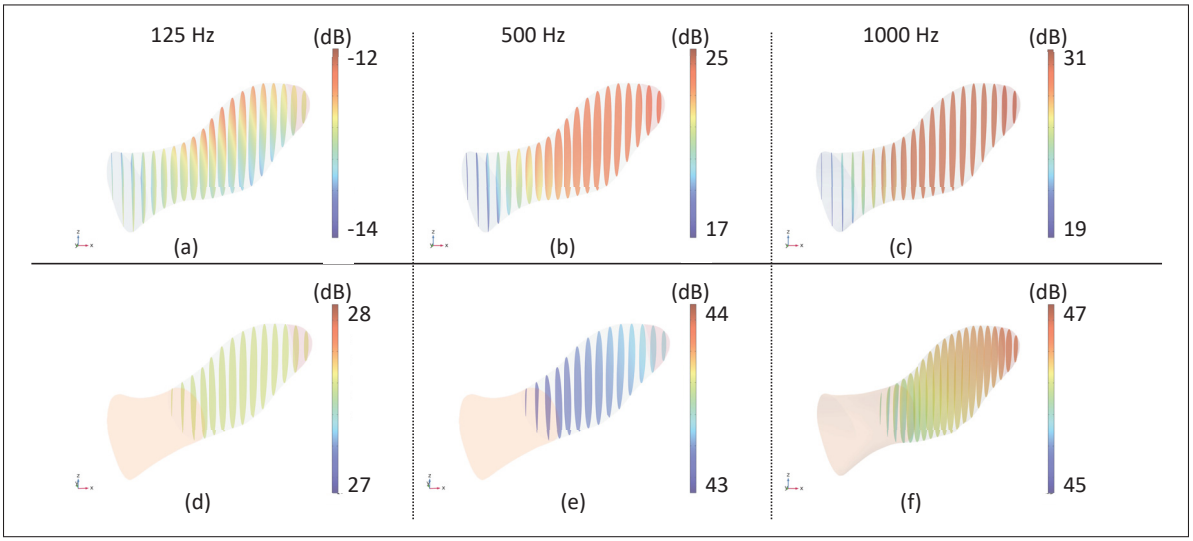

Figure 4.18 SPLs (dB, factor 20, ref. 2×10^{-5} Pa for the colorbar) in the ECs open (a–c) and occluded (d–f) by a shallowly inserted earplug at frequencies of 0.125 kHz, 0.5 kHz and 1.0 kHz, respectively

4.3.5 Stimulation position

Figure 4.19 shows the SPLs in the open and occluded ECs for the stimulation applied to the three positions on the ipsilateral part of the head indicated in Figure 3.8 (dash-dotted red, blue and green curves) as well as their mean and standard deviation (black solid curve). It is found that when the head is stimulated at position P3, the SPL (dash-dotted green curve) is higher in both the open and occluded ECs at frequencies up to 0.5 – 0.6 kHz. This could be explained by the fact that such a stimulation position which is relatively closer to the ST surrounding the EC, excites more the ST and cartilage (i.e., higher mechanical energy injected into the system) in the corresponding frequency ranges, and increases the sound radiation into the EC by its surrounding walls (Stenfelt *et al.*, 2003; Reinfeldt *et al.*, 2013).

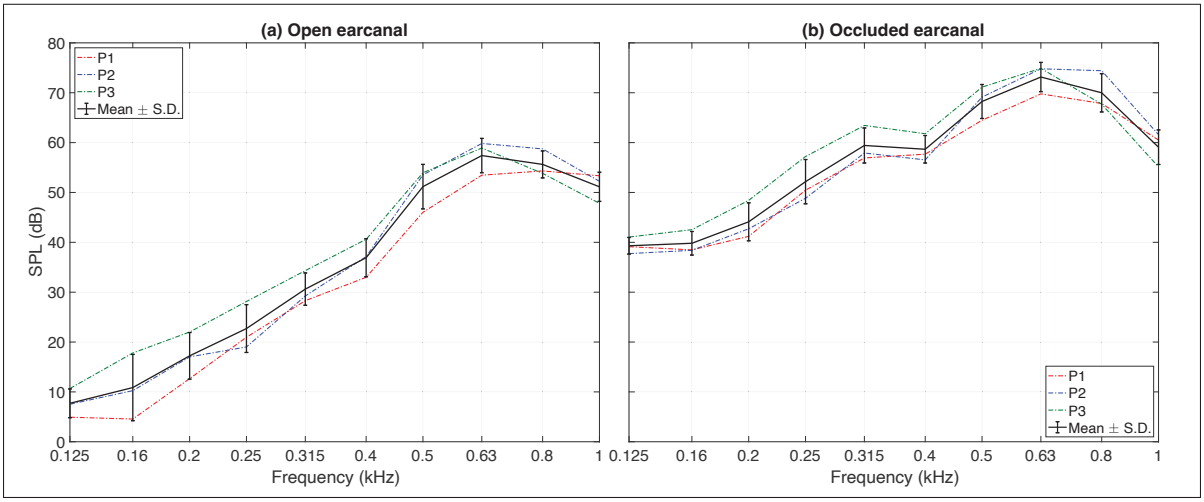

Figure 4.19 SPLs in the open and occluded ECs for the stimulation applied to three different positions of the ipsilateral mastoid. The mean (± S.D.) of the three simulation results are also presented

On the contrary, stimulation positions P1 and P2 are in general less important in terms of the SPL in the EC except at frequencies higher than about 0.7 kHz (dash-dotted red and blue curves). Additional simulation results of (a) the total mechanical energy (i.e., sum of the structural strain energy and kinetic energy) in the ST and (b) the volume velocity calculated on the EC walls for the open case are provided in Figure 4.20. These results confirm the explanation above and

show a similar hierarchization of the three stimulation positions in the corresponding frequency range. On the other hand, it is observed that the standard deviation of the SPLs in the open EC is lower than that in the occluded EC at 0.5 kHz and below. It could be explained by the fact that the SPL in the occluded EC is less sensitive to the change in the stimulation position due to the presence of the earplug which could reduce the contribution of the ST and cartilage (Reinfeldt *et al.*, 2013).

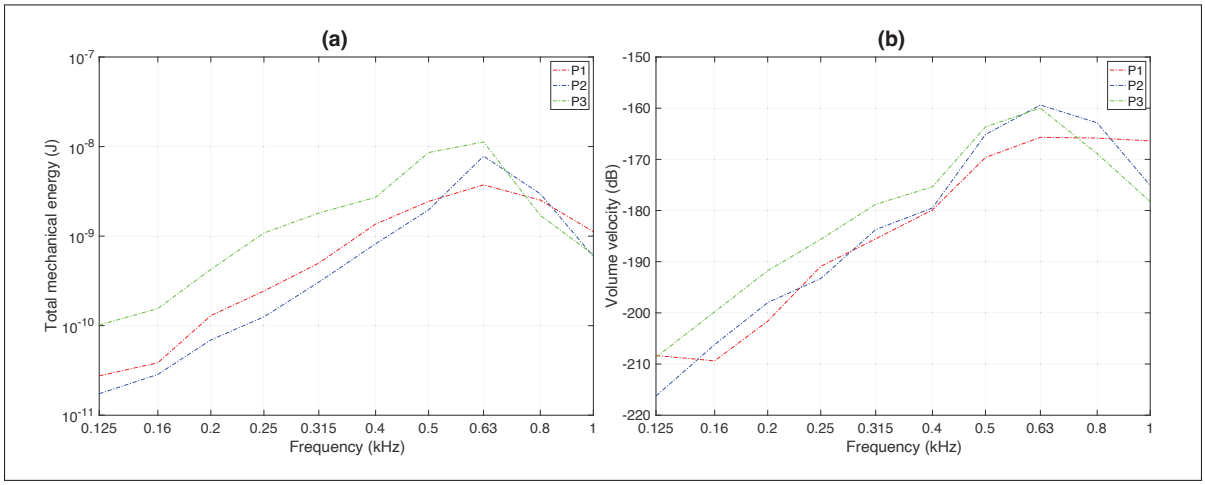

Figure 4.20 Total mechanical energy in the ST and acoustic volume velocity on the EC walls (dB, factor 20, ref. 1 m^3/s) in the open EC case for the stimulation applied to three different positions of the ipsilateral mastoid

Figure 4.21 shows the simulated OEs for the stimulation applied to the three positions (dash-dotted red, blue and green curves) as well as their mean and standard deviation (black curve). The simulation results are compared with the experimental data measured on the participant (purple curve, also shown in Figures 4.6 and 4.7).

The OE simulation results related to the three stimulation positions are in general not far from each other, except around 0.16 kHz where a difference of about 10 dB is observed between positions P1 and P3. This corresponds to the frequency range where the SPL in the open EC is found to be more sensitive to the change in the stimulation position (see Figure 4.19(a)). The standard deviation of the simulated OEs is generally between 0 and 5 dB. This phenomenon implies that subtle changes in the stimulation position during experiments can indeed contribute

to the variability of the measured OE. This should remain true for single measurements on a group of participants (e.g., measurements of Stenfelt & Reinfeldt, 2007; Reinfeldt *et al.*, 2013; Brummund *et al.*, 2015), and for repeated measurements on a single participant or an ATF with the bone transducer repositioned each time (as performed during the experiments described in Section 3.3). On the other hand, the simulation (black curve) is found to be close to the experimental data (purple curve) in the whole frequency range concerned. Moderate discrepancies are observed, which could be explained by the fact that the stimulation positions considered in the model do not correspond exactly to those used during the experiments. However, it should be noted that the difference in the stimulation positions in the experiments due to the repetitions may not be as large as the one between P1, P2 and P3 as depicted in Figure 3.8, but each stimulation position should be inside the region covered by the three positions.

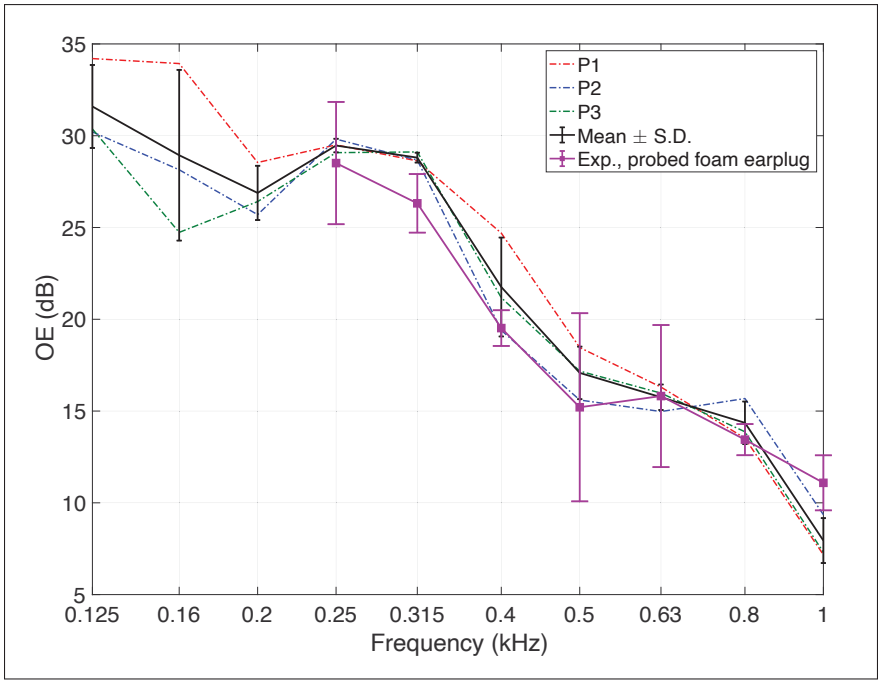

Figure 4.21 OEs for the stimulation applied to three different positions of the ipsilateral mastoid versus experimental data measured on the participant. The mean (± S.D.) of the three simulation results are also presented

Finally, it is appropriate to conclude that the OE is sensitive to the stimulation position for a given part of the head, like the ipsilateral mastoid. In other words, the stimulation position is indeed a factor contributing to the variability of the experimental data obtained on groups of participants shown in the literature. It can also explain the differences between the experimental and simulated OEs for the cases of the ATF and the participant in Sections 4.1.2 and 4.1.3, since it is probable that the stimulation is modeled at a slightly different position from the one in the experiments. Besides, the experiments are repeated three times, which involves the removal and repositioning of the bone transducer attached to the ipsilateral mastoid. It is difficult to retain exactly the same position of the bone transducer, especially for the measurements on the participant due to the presence of the hair, which may introduce a certain variability to the experimental data.

CONCLUSION AND RECOMMENDATIONS

In the continuation of the previous studies of the research group, this thesis aims at further studying the occlusion effect (OE) induced by earplugs by developing useful virtual and experimental testers. More precisely, a finite element (FE) model of an entire human head and a corresponding augmented acoustic test fixture (ATF, i.e., an artificial head) were developed based on the real head geometry of a living participant. The academic achievements (grants, scientific papers, and communications) during my doctorate are listed in Appendix II.

In the following, this chapter concludes this doctoral project by summarizing the main results in relation to the research problems and objectives as well as the contributions of this thesis. It also reviews the limitations of the work and proposes opportunities for future research. Section 5.1 focuses on the FE model of the human head, while Section 5.2 focuses on the augmented ATF.

5.1 Finite element model of the human head

In this work, a FE model of an entire human head for simulating the OE was developed and evaluated. It was built from the real head geometry of a living participant. The anatomy of the participant's head, including the brain, the cerebrospinal fluid, the skull bone, the soft tissues (ST), and the auricular cartilages, was obtained using medical imaging techniques (i.e., cone-beam computed tomography and magnetic resonance imaging). The material properties of the biological tissues were taken from the literature. The head is assumed to be immersed in an infinite air domain, which is accounted for using a spherical air-filled volume coupled to a perfectly matched layer (PML) in the model. A mechanical excitation, i.e., a harmonic pressure, is applied at various locations on the ST over an area of about 175 mm^2 which corresponds to the frequently clinically used bone transducer RadioEar B-71. The model was used to simulate the OEs of foam and silicone earplugs at shallow, middle and deep insertion depths as well as the OEs for different material property sets of the earcanal (EC) surrounding tissues. For

evaluating the FE head model, the simulated OEs were firstly compared with experimental data obtained on groups of participants in the literature, and secondly compared with experimental data measured on an ATF corresponding to the head model (see Section 5.2) and the participant whose head was scanned for reconstructing the geometrical head model.

5.1.1 Contribution

This work is a continuation of the previous studies of the research group which focused on FE models of truncated outer ears. Compared with the models of truncated outer ears, the FE model developed under the framework of this thesis for simulating the OE considers the entire head of a living participant. In general, it allows for further studying the OE of earplugs by reproducing more realistic vibro-acoustic responses of the open and occluded ECs. More precisely, it fills the gaps of previous studies in the following aspects.

- First, the head model only has artificial boundaries due to the truncation at the head base. It has been found to be insensitive to the boundary conditions at the head base in most of the studied frequency bands. As a result, unlike the truncated outer ear models, the boundary conditions at the head base were not adjusted to match the experimental results at the best.
- Second, the external air domain is modeled with the help of a PML instead of applying an acoustic impedance equal to the radiation impedance of a baffled circular piston of the same area over the open EC entrance. Thus, the simulation result has been found not to be affected by the choice of the EC entrance position which is related to the acoustic mass of the open EC seen by its walls and the volume velocity imposed to the open EC. More importantly, the consideration of the entire head immersed in an infinite air domain in the model has allowed for adequately considering the radiation from the head vibrations into the surrounding air that subsequently enters the open EC. As a result, the head model has been found to be able to simulate OEs that better agree with the experimental data.

- Third, the head model developed from a living participant has made it possible to evaluate itself using the experimental data obtained on the participant. This is different from the previous models that were evaluated with the experimental data obtained on a group of participants.
- Fourth, the head model has allowed for evaluating the effects on the OE of various factors associated with the ear anatomy, the earplug, and the stimulation position. It thus gave access to quantify the respective contribution of each factor to the resulting OE. More precisely, it was used to investigate the variability of the OE induced by (i) the material properties of the EC surrounding tissues and (ii) the stimulation positions of the bone transducer.
- Lastly, it allowed for exploring how the measured sound pressures in the open and occluded ECs (thus the OE) are affected by the position of the microphone in the EC where the OE is evaluated. The latter is found to contribute partially to the difference between the experimental and simulated OEs obtained within the framework of this thesis. The results have also suggested that the measurement position of the sound pressure level in the EC may not be a contributor to the large variability of the experimental OEs in the literature.

5.1.2 Limitation and perspective

In this work, the OE of earplugs was investigated using a FE model of an entire human head developed based on the geometry of a participant's head. This specific head model does not represent a group of human subjects or an average human subject, but offers the possibility of using morphing techniques to deform the geometry of the head model and thus exploring the effect of anatomical changes on the OE.

The present FE head model could also be more realistic in terms of geometry as well as material properties of the biological tissues. Regarding the head geometry, it could consider more detailed anatomical structures in the head, for example, (i) by separating the different parts of

the skull, like the occipital, parietal, and frontal bones or by considering the sandwich structure of the bone, (ii) by distinguishing the muscles, fat, and skin from the ST, (iii) by considering the nasal cartilage, the eyeball. These were not done during this work considering the necessary time for the reconstruction, the resolution of the medical images, and the complexity of the model. The importance of including these anatomical complexities to predict the OE could be investigated through a sensitivity study. In addition, it can be helpful to redo the scan of the participant's head to have a clearer geometry of the left ear in particular the surrounding cartilagenous part. The transcranial transmission could then be investigated. Regarding the biological tissues, they are considered as isotropic linear elastic media with material properties taken from the literature instead of obtained on the participant due to the measurement difficulty and ethical issues. The measurements of these material properties were not carried out at body temperature. The head model does not consider the anisotropy, nonlinearity, visco-elasticity, prestress state and frequency dependence of the biological tissues due to a lack of data in the literature. Consequently, the mechanical coupling of the earplug in the EC could be affected, which influences thus the contribution of the earplug to the OE (Carillo, 2021). The ST could also be modeled as a hyper-elastic domain as the ST Poisson's ratio is supposed to be close to the theoretical limiting value 0.5 in the studied frequency range.

For the case of the occluded EC, the earplug inserted into the EC has been modeled in a simplified manner. In terms of geometry, (i) the protruding part of the earplug in the concha bowl is neglected; (ii) the circumferential boundary of the earplug is supposed to perfectly fit the shape of the EC walls, and (iii) the faces of the earplug in contact with the external environment and the occluded EC are supposed to be planar and normal to the curvilinear axis of the EC. A more realistic geometry of the earplug inserted into the EC could be obtained with the help of medical imaging techniques. In terms of material properties, the dependence on the compression rate which is spatially inhomogeneous and the dependence on the temperature are not considered.

The foam earplug could also be modeled as a porous and viscoelastic domain (Brummund *et al.*, 2014).

Another limitation of the FE head model is the expensive computational cost. This makes it challenging to further progress in validating and calibrating the FE head model, which requires an iterative process of comparing the model with the augmented ATF and the participant's head, revising the model if necessary, comparing again, until the model is validated. One solution could be to design a statistical surrogate model based on Gaussian processes (Gramacy, 2020) that replaces the FE head model, which economizes on expensive runs. The model could also be used to evaluate other acoustical indicators like the insertion loss and noise reduction of earplugs, keeping in mind that larger frequency ranges (i.e., 0.125 kHz – 8 kHz) should be considered, and consequently higher degrees of freedom and more computation time. Moreover, more numerical tests (e.g., investigation on the influence of the tissue material properties or of the sound radiation from the external ST) and experimental measurements on the participant of this project could be done in future work with different types of earplugs and insertion depths, in order to further evaluate the FE model.

5.2 Acoustic test fixture

In this work, a specially designed ATF, more precisely, an artificial head has been fabricated based on the same geometrical model as the FE head model. The artificial head was fabricated by a specialized company (True Phantom Solutions, Windsor, Canada) using artificial materials which mimic the biological tissues. It was used to evaluate the FE head model and was itself evaluated by the measurement of the OE on the participant whose head was scanned for constructing the geometrical head model.

5.2.1 Contribution

Unlike the commercial ATFs which are supposed not to consider the bone conduction through the head, this specially designed artificial head has allowed for considering the bone-conducted sound transmission through the head, and thus evaluating the OE of earplugs induced by a bone-conducted stimulation. Compared with the previous artificial ears designed and fabricated for assessing the OE of earplugs, this artificial head has provided more realistic EC vibration patterns. It also makes it possible to investigate the OE for different stimulation positions and other hearing protection devices (e.g., earmuff).

5.2.2 Limitation and perspective

The OE measured on human subjects decreases with frequency. The FE head model mentioned in Section 5.1 defined with the mechanical properties of biological tissues has reproduced the OE comparable with that measured on human subjects. However, the artificial head as well as the head model defined with the mechanical properties of the materials used for fabricating the artificial head presented a different tendency of OE with frequency. This probably or at least partially results from the differences between the mechanical properties of the materials used for fabricating the artificial head and the biological tissues, given that compared with the real head, the FE head model has the same simplifications in geometry as the artificial head. Future work could concentrate on choosing more appropriate materials for the artificial head in order to have an improved prediction of OE. This could begin with mechanical tests on urethane-based soft resins of different hardnesses (Benacchio *et al.*, 2020).

Besides, in this artificial head the eardrum as well as the middle and inner ears have been replaced by the bony tissue due to manufacturing challenges. An ongoing project within our research group proposes an artificial eardrum which mimics the acoustic impedance of a given

eardrum (Benacchio, Luan, Doutres & Sgard, 2022). Prospectively, this artificial eardrum could be integrated into the artificial head.

In addition, the temperature could also have an influence on the material properties and thus on the OE of earplugs (ANSI, 2020). No measurement has been done by heating the artificial head or earplugs in the present study. Further work could focus on including a heating system as well as built-in instrumentation (e.g., preamplifier, microphone, artificial eardrum) in the artificial head like commercial ATFs.

APPENDIX I

MATERIAL PROPERTIES OF THE SOFT TISSUES

Under the hypothesis of isotropic elastic material behavior, for characterizing the mechanical properties of solid materials, either Young's modulus E and Poisson's ratio ν or bulk modulus K and shear modulus G can be used. These parameters are related by the following equations:

$$G = \frac{E}{2(1+\nu)}, \tag{A I-1}$$

$$K = \frac{E}{3(1-2\nu)}. \tag{A I-2}$$

Besides, the following equation relates the speed of the longitudinal sound wave in a solid c_p to the Young's modulus E, density ρ, and Poisson's ratio ν (Kinsler, Frey, Coppens & Sanders, 2000):

$$c_p = \sqrt{\frac{E(1-\nu)}{\rho(1+\nu)(1-2\nu)}}. \tag{A I-3}$$

As mentioned in Section 1.4, the literature provides limited information concerning the ST material properties. According to the study of Taschke & Hudde (2006), the ST density ρ_{ST} is about 890 – 1170 kg/m^3.

At ultrasound frequencies (i.e., 10^6 – 10^7 Hz), the sound speed in the ST is within the range of 1400 m/s – 1600 m/s (Inagaki, Arai, Namekawa & Akiyama, 2018) and the ST Poisson's ratio is about 0.4 (Sarvazyan, 1975). Given that $c_{p,ST}$ = 1400 m/s, ν_{ST} = 0.4, and ρ_{ST} = 1030 kg/m^3, the value of E_{ST} estimated from Equation (A I-3) would be about 942 MPa. Then, the value of G_{ST} estimated from Equation (A I-1) would be about 336 MPa, and the value of K_{ST} estimated from Equation (A I-2) would be about 1570 MPa. While the value of K_{ST} seems to be within the range of literature data, the values of E_{ST} and G_{ST} tend to be larger than the values reported in the literature (Sarvazyan, 1975).

Table-A I-1 ST Young's modulus E_{ST}, shear modulus G_{ST}, and bulk modulus K_{ST} corresponding to different ST Poisson's ratios ν_{ST}

ν_{ST}	0.48	0.49	0.499	0.4999	0.49999
E_{ST} [MPa]	1.17	0.60	0.06	0.006	0.0006
G_{ST} [MPa]	0.40	0.20	0.02	0.002	0.0002
K_{ST} [MPa]	9.77	10.03	10.27	10.30	10.30

In the low frequency range concerned in the present study (i.e., below 1.0 kHz), the sound speed in the ST is within the range of 1 – 100 m/s (Sarvazyan, 1975; Blondé-Weinmann, Joubaud, Zimpfer, Hamery & Roth, 2022) and the ST Poisson's ratio is close to the theoretical limiting value of incompressible materials, namely 0.5 (Sarvazyan, 1975). Given that $c_{p,ST,max}$ = 100 m/s and ρ_{ST} = 1030 kg/m^3, Table I-1 shows the values of E_{ST}, G_{ST} and K_{ST} corresponding to different Poisson's ratios close to 0.5 respectively.

It is found that the value of G_{ST} estimated at ultrasound frequencies (i.e., 336 MPa) is 2 to 6 orders larger than those estimated at low frequencies (see Table-A I-1). According to Sarvazyan (1975), G may decrease by 3 – 5 orders from 10^6 to 10^2 Hz. Meanwhile, K_{ST} is decreased by about 150 times from ultrasound frequencies to low frequencies. As $c_{p,ST}$ and K_{ST} are proportional, for $c_{p,ST}$ lower than 100 m/s, K_{ST} would also be lower accordingly. However, the decrease of K_{ST} with frequency is in contradiction with the literature that K_{ST} is practically independent of the frequency (Sarvazyan, 1975) with less than one percent variation between the value measured from ultrasound in megahertz region and the static value (Sarvazyan *et al.*, 1995). At the moment, the author is not aware of other results in the literature which could explain this contradiction.

APPENDIX II

ACADEMIC ACHIEVEMENTS

This section lists my academic achievements during this doctorate.

Academic awards and honors obtained:

1. *Substance ÉTS* Grant for dissemination of research obtained in 2022 (amount $1 000).
2. Best student presentation award attributed by the *Canadian Acoustical Association* in October 2021 (amount $500).
3. Paper [1] featured on the cover of the November 2021 issue of *The Journal of the Acoustical Society of America*.

Papers published (or contributed to) in peer-reviewed scientific journals:

1. Xu, H., Sgard, F., Carillo, K., Wagnac, É., & de Guise, J. (2021). Simulation of the objective occlusion effect induced by bone-conducted stimulation using a three-dimensional finite-element model of a human head. *The Journal of the Acoustical Society of America*, 150(5), 4018-4030.
2. Carillo, K., Sgard, F., Xu, H., Guilloteau, A., Benacchio, S., Poissenot-Arrigoni, B., & Doutres, O. (2021). On the modeling of the objective occlusion effect induced by earplugs: Recent advances, challenges and perspectives. *Spectrum*, 38(2), 16-23.

Communications presented (or contributed to) in scientific conferences:

1. Xu, H., Sgard, F., Carillo, K., Wagnac, É., & De Guise, J. (2021). On the sound radiation of head tissues in the earcanal at low frequencies induced by a bone-conducted stimulation. *Acoustics Week in Canada 2021*.
2. Xu, H., Sgard, F., Carillo, K., Wagnac, É., & De Guise, J. (2020). A three-dimensional finite-element model of a human head for predicting the objective occlusion effect induced by earplugs. *The Journal of the Acoustical Society of America, 148(4), 2780-2780*.

3. Xu, H., Sgard, F., Wagnac, É., & De Guise, J. (2019). Development of an entire human head finite element model based on in-vivo medical images for investigation of sound transmission. *26th International Congress on Sound & Vibration (ICSV26)*, Montreal, Canada.
4. Sgard, F., Benacchio, S., Luan, Y., Xu, H., Carillo, K., Doutres, O., Nélisse, H., Wagnac, É., & De Guise, J. (2018). Vibroacoustic modeling of an in vivo human head wearing a hearing protection device using the finite element method. *11th European Congress and Exposition on Noise Control Engineering (Euronoise)*, Heraklion, Crete.

BIBLIOGRAPHY

ANSI. (1986). *Standard Specification for Octave-Band and Fractional-Octave-Band Analog and Digital Filters*. ANSI/ASA S1.11-1986. Washington D.C., USA: American National Standards Institute.

ANSI. (2020). *Methods for the Measurement of Insertion Loss of Hearing Protection Devices in Continuous or Impulsive Noise Using Microphone-in-Real-Ear or Acoustic Test Fixture Procedures*. ANSI/ASA S12.42-2020. Washington D.C., USA: American National Standards Institute.

Arezes, P. M. & Miguel, A. S. (2005). Individual perception of noise exposure and hearing protection in industry. *Human Factors*, 47(4), 683–692.

Auperrin, A., Delille, R., Lesueur, D., Bruyère, K., Masson, C. & Drazétic, P. (2014). Geometrical and material parameters to assess the macroscopic mechanical behaviour of fresh cranial bone samples. *Journal of Biomechanics*, 47(5), 1180-1185.

Benacchio, S., Doutres, O., Le Troter, A., Varoquaux, A., Wagnac, É., Callot, V. & Sgard, F. (2018). Estimation of the ear canal displacement field due to in-ear device insertion using a registration method on a human-like artificial ear. *Hearing Research*, 365, 16–27.

Benacchio, S., Doutres, O., Wagnac, É. & Sgard, F. (2020). *Conception d'oreilles artificielles réalistes dédiées à l'étude du confort acoustique et physique des protecteurs auditifs intra-auriculaires [Design of realistic artificial ears dedicated to the study of the acoustical and physical comfort of in-ear hearing protectors]* (Report n°R-1106). Montreal, Canada: IRSST.

Benacchio, S., Luan, Y., Doutres, O. & Sgard, F. (2022). *Influence de l'impédance tympanique sur la perte par insertion de protecteurs auditifs intra-auriculaires [Influence of tympanic impedance on the insertion loss of in-ear hearing protectors]*. Communication presented in 16ème Congrès Français d'Acoustique (CFA 2022), Marseille, France.

Berenger, J.-P. (1994). A perfectly matched layer for the absorption of electromagnetic waves. *Journal of Computational Physics*, 114(2), 185-200.

Berger, E. H. (1986). Methods of measuring the attenuation of hearing protection devices. *The Journal of the Acoustical Society of America*, 79(6), 1655–1687.

Berger, E. H. (2013). 'Calibrating' the insertion depth of roll-down foam earplugs. *Proceedings of Meetings on Acoustics (ICA 2013)*, 19, 040002.

Berger, E. H. & Kerivan, J. (1983). Influence of physiological noise and the occlusion effect on the measurement of real-ear attenuation at threshold. *The Journal of the Acoustical Society of America*, 74(1), 81–94.

Berger, E. H. & Voix, J. (2019). Hearing protection devices. In *The Noise Manual* (ed. 6). American Industrial Hygiene Association (AIHA).

Bicak, M. (2012). Biomedical Simulation Models of Human Auditory Processes. *Selected Papers Presented at MODSIM World 2011 Conference and Expo*.

Blondé-Weinmann, C., Joubaud, T., Zimpfer, V., Hamery, P. & Roth, S. (2022). Numerical and experimental investigation of the sound transmission delay from a skin vibration to the occluded ear canal. *Journal of Sound and Vibration*, 117345.

Bonnet, F. (2019). *Méthode de mesure individuelle de l'exposition sonore effective intra-auriculaire en milieu de travail [Method for individual measurement of effective in-ear sound exposure in the workplace]*. (Ph.D. thesis, École de technologie supérieure, Montreal, Canada).

Bonnet, F., Nélisse, H., Nogarolli, M. & Voix, J. (2020). Individual in situ calibration of in-ear noise dosimeters. *Applied Acoustics*, 157, 107015.

Borges, R. C., Costa, M. H., Naylor, P. A. & Ferreira, A. A. (2014). Impact of the vent size in the feedback-path and occlusion-effect in hearing aids. *2014 IEEE Biomedical Circuits and Systems Conference (BioCAS) Proceedings*, pp. 25–28.

Branda, E. (2012). Deep canal fittings: Advantages, challenges, and a new approach. *Hearing Review*, 19(4), 24–27.

Brummund, M. K., Sgard, F., Petit, Y., Laville, F. & Boutin, J. (2013). Implementation of a simplified, artificial external ear test fixture for measurement of the earplug induced auditory occlusion effect. *Proceedings of Meetings on Acoustics (ICA 2013)*, 19(1), 040005.

Brummund, M. K., Sgard, F., Petit, Y. & Laville, F. (2014). Three-dimensional finite element modeling of the human external ear: Simulation study of the bone conduction occlusion effect. *The Journal of the Acoustical Society of America*, 135(3), 1433-1444.

Brummund, M. K., Sgard, F., Petit, Y., Laville, F. & Nélisse, H. (2015). An axisymmetric finite element model to study the earplug contribution to the bone conduction occlusion effect. *Acta Acustica united with Acustica*, 101(4), 775-788.

Brummund, M. (2014). *Study of the occlusion effect induced by an earplug: Numerical modelling and experimental validation*. (Ph.D. thesis, École de Technologie Supérieure, Montreal, Canada).

Carillo, K. (2021). *On the objective occlusion effect induced by in-ear devices under bone-conducted stimulation: A theoretical investigation of the influence of the earcanal wall vibration and its spatial distribution*. (Ph.D. thesis, École de Technologie Supérieure, Montreal, Canada).

Carillo, K., Doutres, O. & Sgard, F. (2021a). Numerical investigation of the earplug contribution to the low-frequency objective occlusion effect induced by bone-conducted stimulation. *The Journal of the Acoustical Society of America*, 150(3), 2006–2023.

Carillo, K., Doutres, O. & Sgard, F. (2021b). Principle of an acoustical method for estimating the centroid position of the earcanal wall normal velocity induced by bone-conducted stimulation: Numerical evaluation. *Applied Acoustics*, 182, 108245.

Carillo, K., Doutres, O. & Sgard, F. (2020). Theoretical investigation of the low frequency fundamental mechanism of the objective occlusion effect induced by bone-conducted stimulation. *The Journal of the Acoustical Society of America*, 147(5), 3476-3489.

Carle, R., Laugesen, S. & Nielsen, C. (2002). Observations on the relations among occlusion effect, compliance, and vent size. *Journal of the American Academy of Audiology*, 13(01), 025–037.

Chan, J. C. & Geisler, C. D. (1990). Estimation of eardrum acoustic pressure and of ear canal length from remote points in the canal. *The Journal of the Acoustical Society of America*, 87(3), 1237–1247.

Chang, Y. & Stenfelt, S. (2019). Characteristics of bone-conduction devices simulated in a finite-element model of a whole human head. *Trends in Hearing*, 23, 2331216519836053.

Chang, Y., Kim, N. & Stenfelt, S. (2016). The development of a whole-head human finite-element model for simulation of the transmission of bone-conducted sound. *The Journal of the Acoustical Society of America*, 140(3), 1635–1651.

Chang, Y., Kim, N. & Stenfelt, S. (2018). Simulation of the power transmission of bone-conducted sound in a finite-element model of the human head. *Biomechanics and Modeling in Mechanobiology*, 17(6), 1741–1755.

Chung, K. (2004). Challenges and recent developments in hearing aids: Part II. Feedback and occlusion effect reduction strategies, laser shell manufacturing processes, and other signal processing technologies. *Trends in Amplification*, 8(4), 125–164.

Clavier, O. H., Wismer, M. G., Wilbur, J. C., Dietz, A. J. & O'Brien, W. D. (2010). Development and validation of a computational model of bone-conducted sound transmission for improved hearing protection design. *The Journal of the Acoustical Society of America*, 127, 1986–1986.

Conrad, S. & Rout, A. (2013). Perceived occlusion and comfort in receiver-in-the-ear hearing aids. *American Journal of Audiology*, 22(6), 283-290.

Cyr-Desroches, M.-O. (2021). *Développement d'une oreille artificielle simplifiée et réaliste pour quantifier l'effet d'occlusion objectif [Development of a simplified and realistic artificial ear to quantify the objective occlusion effect]*. (Master's thesis, École de technologie supérieure, Montreal, Canada).

Doutres, O., Sgard, F., Terroir, J., Perrin, N., Jolly, C., Gauvin, C. & Negrini, A. (2019). A critical review of the literature on comfort of hearing protection devices: Definition of comfort and identification of its main attributes for earplug types. *International Journal of Audiology*, 58(12), 824–833.

Gilman, S. & Dirks, D. D. (1986). Acoustics of ear canal measurement of eardrum SPL in simulators. *The Journal of the Acoustical Society of America*, 80(3), 783–793.

Gramacy, R. B. (2020). *Surrogates: Gaussian Process Modeling, Design, and Optimization for the Applied Sciences* (ed. 1). Chapman and Hall/CRC.

Grellmann, W., Berghaus, A., Haberland, E., Jamali, Y., Holweg, K., Reincke, K. & Bierögel, C. (2006). Determination of strength and deformation behavior of human cartilage for the definition of significant parameters. *Journal of Biomedical Materials Research*, 78A(1), 168-174.

Groenewold, M. R., Masterson, E. A., Themann, C. L. & Davis, R. R. (2014). Do hearing protectors protect hearing? *American Journal of Industrial Medicine*, 57(9), 1001–1010.

Hahn, K. S. (1985). *The effect of variation in ear canal skin parameters on the behavior of an ear-earplug model*. (Master's thesis, University of Toronto, Toronto, Canada).

Hansen, M. Ø. (1997). *Occlusion effects, Part I: Hearing aid users' experiences of the occlusion effect compared to the real ear sound level*. (Ph.D. thesis, Technical University of Denmark, Lyngby, Denmark).

Hansen, M. Ø. (1998). *Occlusion effects, Part II: A study of the occlusion effect mechanism and the influence of the earmould properties*. (Ph.D. thesis, Technical University of Denmark, Lyngby, Denmark).

Hu, F. Q. (1996). On absorbing boundary conditions for linearized Euler equations by a perfectly matched layer. *Journal of Computational Physics*, 129(1), 201–219.

Huizing, E. H. (1960). Bone conduction-the influence of the middle ear. *Acta Otolar*, 155.

IEC. (2010). *Simulators of human head and ear - Part 4: Occluded-ear simulator for the measurement of earphones coupled to the ear by means of ear inserts*. IEC 60318-4. Geneva, Switzerland: International Electrotechnical Commission.

Inagaki, K., Arai, S., Namekawa, K. & Akiyama, I. (2018). Sound velocity estimation and beamform correction by simultaneous multimodality imaging with ultrasound and magnetic resonance. *Applied Sciences*, 8(11), 2133.

ITU-T. (1996). *Telephone Transmission Quality – Artificial Mouth*. ITU-T P.51-1996. Geneva, Switzerland: International Telecommunication Union.

James, C. (2006). *Finite element modeling and exploration of double hearing protection systems*. (Master's thesis, Virginia Polytechnic Institute and State University, Blacksburg, USA).

Jones, B. & Nachtsheim, C. J. (2011). A class of three-level designs for definitive screening in the presence of second-order effects. *Journal of Quality Technology*, 43(1), 1-15.

Keidser, G., Carter, L., Chalupper, J. & Dillon, H. (2007). Effect of low-frequency gain and venting effects on the benefit derived from directionality and noise reduction in hearing aids. *International Journal of Audiology*, 46(10), 554–568.

Kiessling, J., Brenner, B., Jespersen, C. T., Groth, J. & Jensen, O. D. (2005). Occlusion effect of earmolds with different venting systems. *Journal of the American Academy of Audiology*, 16(04), 237–249.

Kim, N., Chang, Y. & Stenfelt, S. (2014). A three-dimensional finite-element model of a human dry skull for bone-conduction hearing. *BioMed Research International*, 2014, 519429.

Kinsler, L. E., Frey, A. R., Coppens, A. B. & Sanders, J. V. (2000). *Fundamentals of Acoustics* (ed. 4). John Wiley & Sons.

Kuk, F. K. (1991). Perceptual consequence of vents in hearing aids. *British Journal of Audiology*, 25(3), 163–169.

Kuk, F. K., Keenan, D. & Lau, C.-C. (2005). Vent configurations on subjective and objective occlusion effect. *Journal of the American Academy of Audiology*, 16(09), 747–762.

Lee, K. (2011). *Effects of earplug material, insertion depth, and measurement technique on hearing occlusion effect*. (Ph.D. thesis, Virginia Polytechnic Institute and State University, Blacksburg, USA).

Lim, J., Dobrev, I., Röösli, C., Stenfelt, S. & Kim, N. (2022). Development of a finite element model of a human head including auditory periphery for understanding of bone-conducted hearing. *Hearing Research*, 421, 108337.

Luan, Y., Cyr-Desroches, M.-O., Carillo, K., Doutres, O. & Sgard, F. (2022). Development and evaluation of an artificial ear for quantifying the objective occlusion effect. *Proceedings of the 24th International Congress on Acoustics (ICA 2022)*.

Maroudas, A., Muir, H. & Wingham, J. (1969). The correlation of fixed negative charge with glycosaminoglycan content of human articular cartilage. *Biochimica et Biophysica Acta*, 177(3), 492-500.

Mueller, H. G. (1994). CIC hearing aids: What is their impact on the occlusion effect? *The Hearing Journal*, 47(11), 29–30.

Mueller, H. G. (2003). There's less talking in barrels, but the occlusion effect is still with us. *The Hearing Journal*, 56(8), 10–12.

Nardi, C., Talamonti, C., Pallotta, S., Saletti, P., Calistri, L., Cordopatri, C. & Colagrande, S. (2017). Head and neck effective dose and quantitative assessment of image quality: A study to compare cone beam CT and multislice spiral CT. *Dentomaxillofacial Radiology*, 46(7), 20170030.

Nélisse, H., Le Cocq, C., Boutin, J., Voix, J. & Laville, F. (2013). Comparison of subjective and objective methods for the measurements of hearing protector devices attenuation and occlusion effect. *Proceedings of Meetings on Acoustics (ICA 2013)*, 19(1), 040004.

Nelson, D. I., Nelson, R. Y., Concha-Barrientos, M. & Fingerhut, M. (2005). The global burden of occupational noise-induced hearing loss. *American Journal of Industrial Medicine*, 48(6), 446–458.

Nielsen, C. & Darkner, S. (2011). The cartilage bone junction and its implication for deep canal hearing instrument fittings. *The Hearing Journal*, 64(3), 35–36.

Norris, J., Chambers, R., Kattamis, N., Davis, B. & Bieszczad, J. (2011). Effects of custom earplug design parameters on achieved attenuation. *Poster presentation at the annual meeting of the National Hearing Conservation Association*.

Peterson, J. & Dechow, P. C. (2003). Material properties of the human cranial vault and zygoma. *The Anatomical Record. Part A: Discoveries in Molecular, Cellular, and Evolutionary Biology*, 274(1), 785-797.

Prodanovic, S. & Stenfelt, S. (2020). Consequences of mastoidectomy on bone conducted sound based on simulations in a whole human head. *Otology & Neurotology*, 41(9), e1158–e1166.

Reinfeldt, S., Stenfelt, S. & Håkansson, B. (2013). Estimation of bone conduction skull transmission by hearing thresholds and ear-canal sound pressure. *Hearing Research*, 299, 19-28.

Réseau de santé publique en santé au travail. (2022). Faits saillants sur le bruit [Highlights on noise]. Retrieved from: https://www.santeautravail.qc.ca/documents/13275/220ea120-7d7b-4d5b-a385-00ad842a4862.

Saint-Gaudens, H., Nélisse, H., Sgard, F., Laville, F. & Doutres, O. (2019). Comparison of different excitations to assess the objective occlusion effect measured on human subjects. *Proceedings of the 26th International Congress on Sound and Vibration (ICSV26)*.

Saint-Gaudens, H., Nélisse, H., Sgard, F. & Doutres, O. (2022). Towards a practical methodology for assessment of the objective occlusion effect induced by earplugs. *The Journal of the Acoustical Society of America*, 151(6), 4086–4100.

Salvinelli, F., Maurizi, M., Calamita, S., D'alatri, L., Capelli, A. & Carbone, A. (1991). The external ear and the tympanic membrane a three-dimensional study. *Scandinavian Audiology*, 20(4), 253–256.

Sarvazyan, A. (1975). Low-frequency acoustic characteristics of biological tissues. *Polymer Mechanics*, 11(4), 594–597.

Sarvazyan, A., Skovoroda, A., Emelianov, S., Fowlkes, J., Pipe, J., Adler, R., Buxton, R. & Carson, P. (1995). Biophysical bases of elasticity imaging. In Jones, J. P. (Ed.), *Acoustical Imaging* (vol. 21, pp. 223-240). Springer.

Schroeter, J. & Poesselt, C. (1986). The use of acoustical test fixtures for the measurement of hearing protector attenuation. Part II: Modeling the external ear, simulating bone conduction, and comparing test fixture and real-ear data. *The Journal of the Acoustical Society of America*, 80(2), 505–527.

Sgard, F., Nélisse, H., Gaudreau, M.-A., Boutin, J., Voix, J. & Laville, F. (2010). *Étude de la transmission sonore à travers les protecteurs auditifs et application d'une méthode pour évaluer leur efficacité en milieu de travail - Partie 2: Étude préliminaire d'une modélisation par éléments finis [Study of the sound transmission through hearing protection devices and application of a method for evaluating their real efficiency in the workplace - Part 2: Preliminary study of finite element modeling]* (Report n°R-680). Montreal, Canada: IRSST.

Sgard, F., Viallet, G. & Nélisse, H. (2015). Using finite-element modelling to predict the effect of ear canal microphone positioning on the sound attenuation of hearing protectors. *Proceedings of the 22nd International Congress on Sound and Vibration (ICSV22)*.

Sgard, F., Nélisse, H., Laville, F., Petit, Y., Doutres, O., Voix, J., Brummund, M. K., Viallet, G., Boyer, S., Gaudreau, M.-A. et al. (2016). *Développement d'outils et de méthodes pour mieux évaluer et améliorer la protection auditive individuelle des travailleurs [Development of tools and methods to better assess and improve workers' personal hearing protection]* (Report n°R-901). Montreal, Canada: IRSST.

Sgard, F., Carillo, K. & Doutres, O. (2019). A 2D axisymmetric finite element model to assess the contribution of in-ear hearing protection devices to the objective occlusion effect. *INTER-NOISE and NOISE-CON Congress and Conference Proceedings*, 259, 2494-2505.

Shaw, E. & Stinson, M. (1981). Network concepts and energy flow in the human middle-ear. *The Journal of the Acoustical Society of America*, 69(S1), S43-S43.

Shaw, E. & Stinson, M. (1983). The human external and middle ear: Models and concepts. In *Mechanics of Hearing* (pp. 3–10). Springer.

Staab, W. J. (1996). Introduction to deep canal principles. *Seminars in Hearing*, 17(01), 3–19.

Standring, S. (2015). *Gray's Anatomy e-Book: The Anatomical Basis of Clinical Practice*. Elsevier Health Sciences.

Statistic Canada. (2015). Canadian Health Measures Survey Data User Guide: Cycle 3. Retrieved from: https://www150.statcan.gc.ca/n1/pub/82-003-x/2018008/article/00002-eng.htm.

Stenfelt, S. (2011). Acoustic and physiologic aspects of bone conduction hearing. *Implantable Bone Conduction Hearing Aids*, 71, 10–21.

Stenfelt, S. & Goode, R. L. (2005a). Bone-conducted sound: Physiological and clinical aspects. *Otology & Neurotology*, 26(6), 1245–1261.

Stenfelt, S. & Goode, R. L. (2005b). Transmission properties of bone conducted sound: Measurements in cadaver heads. *The Journal of the Acoustical Society of America*, 118(4), 2373–2391.

Stenfelt, S. & Prodanovic, S. (2022). Simulation of soft tissue stimulation–Indication of a skull bone vibration mechanism in bone conduction hearing. *Hearing Research*, 418, 108471.

Stenfelt, S. & Reinfeldt, S. (2007). A model of the occlusion effect with bone-conducted stimulation. *International Journal of Audiology*, 46(10), 595-608.

Stenfelt, S., Hato, N. & Goode, R. L. (2002). Factors contributing to bone conduction: The middle ear. *The Journal of the Acoustical Society of America*, 111(2), 947-959.

Stenfelt, S., Wild, T., Hato, N. & Goode, R. L. (2003). Factors contributing to bone conduction: The outer ear. *The Journal of the Acoustical Society of America*, 113(2), 902–913.

Stinson, M. R. & Lawton, B. (1989). Specification of the geometry of the human ear canal for the prediction of sound-pressure level distribution. *The Journal of the Acoustical Society of America*, 85(6), 2492-2503.

Stone, M. A., Paul, A. M., Axon, P. & Moore, B. C. (2014). A technique for estimating the occlusion effect for frequencies below 125 Hz. *Ear and Hearing*, 35(1), 49.

Surendran, S. & Stenfelt, S. (2022). The outer ear pathway during hearing by bone conduction. *Hearing Research*, 421, 108388.

Taschke, H. & Hudde, H. (2006). A finite element model of the human head for auditory bone conduction simulation. *Journal for Oto-Rhino-Laryngology, Head and Neck Surgery*, 68(6), 319-323.

Terroir, J., Perrin, N., Wild, P., Doutres, O., Sgard, F., Gauvin, C. & Negrini, A. (2021). Assessing the comfort of earplugs: Development and validation of the French version of the COPROD questionnaire. *Ergonomics*, 64(7), 912–925.

Tonndorf, J. (1966). Bone conduction studies in experimental animals. *Acta Oto-Laryngol.*, 213, 1–132.

Tonndorf, J. (1972). Bone conduction. In Tobias, J. (Ed.), *Foundations of Modern Auditory Theory* (pp. 197–237). New York: Academic Press.

Tufts, J. B., Chen, S. & Marshall, L. (2013). Attenuation as a function of the canal length of custom-molded earplugs: A pilot study. *The Journal of the Acoustical Society of America*, 133(6), EL446-EL451.

Vasil-Dilaj, K. A. & Cienkowski, K. M. (2011). The influence of receiver size on magnitude of acoustic and perceived measures of occlusion. *American Journal of Audiology*, 20(1), 61-68. doi: 10.1044/1059-0889(2010/09-0031).

Watson, N. A. & Gales, R. S. (1943). Bone-conduction threshold measurements: Effects of occlusion, enclosures, and masking devices. *The Journal of the Acoustical Society of America*, 14(4), 207–215.

WHO. (2021). Deafness and hearing loss. Retrieved from: https://www.who.int/news-room/fact-sheets/detail/deafness-and-hearing-loss.

Winkler, A., Latzel, M. & Holube, I. (2016). Open versus closed hearing-aid fittings: A literature review of both fitting approaches. *Trends in Hearing*, 20, 2331216516631741.

Zurbrügg, T., Stirnemannn, A., Kuster, M. & Lissek, H. (2014). Investigations on the physical factors influencing the ear canal occlusion effect caused by hearing aids. *Acta Acustica united with Acustica*, 100(3), 527-536.

Zwislocki, J. J. & Goodman, D. (1980). Absolute scaling of sensory magnitudes: A validation. *Perception & Psychophysics*, 28(1), 28–38.